



**NTNU – Trondheim**  
Norwegian University of  
Science and Technology

# Testing of Fibre Reinforced Concrete Structures

Shear Capacity of Beams with Openings

**Ane Marte Olimb**

Civil and Environmental Engineering

Submission date: June 2012

Supervisor: Terje Kanstad, KT

Co-supervisor: Giedrius Zirgulis, KT  
Elena Sarmiento, KT


Norwegian University of Science and Technology  
Department of Structural Engineering





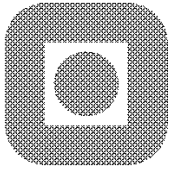
## MASTER THESIS 2012

SUBJECT AREA: Concrete structures	DATE: 11.06.2012	NO. OF PAGES: 102 (19)
--------------------------------------	---------------------	---------------------------

TITLE: <b>Testing of Fibre Reinforced Concrete Structures: Shear Capacity of Beams with Openings</b>  Prøving av fiberarmerte konstruksjoner: Skjærkapasitet av bjelker med utsparinger	
BY:  Ane Marte Olimb	

SUMMARY: This thesis treats the use of fibre reinforced concrete in beams with openings. Plain concrete beams with traditional reinforcement are compared to fibre reinforced beams. The FRC-recipe contains 1 volume % steel fibres. In addition to the full-scale beams there were cast cubes and standard beams to test the concrete's strength properties. The standard beams were cast and tested as described in NS-EN 14651 to find the residual tensile strength of the fibre reinforced concrete. The full-scale beams all have steel bar tensile reinforcement to ensure shear failure. 4 beam tests were carried out in a 4 point test rig and the beams were loaded until failure. The capacities were compared to theoretically calculated capacities based on design rules published by COIN.  The tests showed that by using 1 volume % steel fibres in the concrete mix the beams achieved a higher capacity than the beam with traditional shear reinforcement. This suggests that steel fibre reinforcement might be a good alternative to the traditional reinforcement. As the traditional reinforcement takes a large amount of time to fix on the construction site the FRC might be an economical solution. The calculations also gave quite good accordance to the real capacities. However, to find the capacity of the beam with only fibre reinforcement as shear reinforcement it might be necessary to develop a formula to allow calculation of a tensile trajectory which carries the shear force. The theoretical and measured values for the concrete's strength properties (compressive strength and residual tensile strength) proved to be quite different. The theoretical values were very conservative compared to the measured values, and it might be necessary to look closer into this in the future.
---

RESPONSIBLE TEACHER: Terje Kanstad
SUPERVISOR(S): Terje Kanstad, Belen Pina Fernandez, Elena Vidal Sarmiento and Giedrius Zirgulis
CARRIED OUT AT: Department of Structural Engineering



NORGES TEKNISK NATURVITENSKAPELIGE  
UNIVERSITET, NTNU  
Institutt for konstruksjonsteknikk

## **Master-oppgave i konstruksjonsteknikk VÅREN 2012**

**for**

**Ane Marte Olimb**

**Prøving av fiberarmerte betongkonstruksjoner:  
Skjærkapasitet av bjelker med utsparinger**

**Testing of fibre reinforced concrete structures:  
Shear capacity of beams with openings**

### **INTRODUCTION**

Fibre reinforcement replacing ordinary reinforcing bars is very interesting today due to economical reasons, need for rationalisation, and improved work conditions in the building and construction industry. The R&D activity internationally and in Norway has increased the last years and new types of fibres have been available at the markets. Furthermore several international pre-normative regulations have also been launched, and a proposal for Norwegian guidelines has been published.

This MSc thesis is connected to the research programme COIN, which is a center for research and innovation financed by the Norwegian Research council and the concrete industry through active partners. Sintef and NTNU, Department of structural engineering, are the research partners in this project

The principal aim of this Master's thesis is to use fibre reinforcement as a substitute for conventional bar reinforcement in shear problems, and the main focus is on shear problems in beams with circular openings.

## **COURSE**

The thesis includes a literature study which shall include relevant theory, and alternative design methods and guidelines.

The experimental part shall include testing of fibre reinforced beams with circular openings. And the evaluation of the results shall be related to current design methods, guidelines and previous results. Furthermore, alternative layouts for fibre reinforced concrete elements shall be compared with traditional layout, and the capacity, ductility, cracking load and crack pattern shall be investigated

## **GENERAL**

Supervisors:

Terje Kanstad, Elena Vidal Sarmiento, Belen Pina Fernandez and Giedrius Zirgulis.

The MSc thesis shall be finished within June 11<sup>th</sup> 2012.

Trondheim den 06.06.2012

Terje Kanstad

Professor

## Abstract

The thesis examines the use of fibre reinforced concrete in carrying structures. The basis of the project is shear capacity of beams with openings which is a very common structural element. It has been carried out full-scale tests of one reference beam and three beams with openings reinforced with different reinforcement combinations.

The first part of the report consists of a literature study based on earlier research and published material on fibre reinforced concrete and its use in carrying structures. Different fibres and their properties are described as well as the components in concrete and their effect. As of today there are no official set of rules for designing fibre reinforced structures, but there are several suggestions for rules which are described in the report. The most important set of rules for this project is made by COIN (Concrete Innovation Centre). The calculations done in the project are based on the COIN-report.

The concrete used in the tests were delivered by Unicon and the castings were done in two days, one casting with plain concrete (reference beam and one beam with openings with traditional shear reinforcement) and one casting with fibre reinforcement (Dramix 80/60). The fibre reinforced beams with openings consisted of one beam with a combination of fibre and traditional shear reinforcement and one with only fibres as shear reinforcement. The casting of the fibre reinforced concrete proved difficult as the fibres were lumping together and deteriorated the flowability. Therefore the FRC required a lot of work while being cast.

In addition to the full-scale beams standard beams and testing cubes were cast. These were later tested to establish the strength properties of the concrete. The tests showed that both the compressive strength and the residual tensile strength were higher than the theoretical values used in the pre-testing calculations, so post-testing calculations were carried out as well.

The full-scale beams were tested at the structural laboratory at NTNU. The testing was done in a rig with a four point testing set-up with two symmetrical loads. The beams were instrumented to measure the midspan vertical displacement as well as the crack openings beneath the openings and a computer registered the measured values. Both the fibre reinforced beams proved to have better capacity and ductility than the plain concrete beams. This indicates that steel fibre reinforcement is a good solution for shear reinforcement for beams with openings.

Most of the calculations done were in good accordance with the test results although they were a bit on the conservative side. The calculations for the beam with only fibre reinforcement were not very good, and post-testing calculations were done to find the width of a theoretical tensile trajectory based on the real capacity. All in all the tests showed that the use of FRC in beams with openings might be a good solution in the future. More research should be done on this subject to develop design rules for FRC beams with openings.

## Sammendrag

Denne masteroppgaven tar for seg bruken av fiberarmert betong i bærende konstruksjoner. Utgangspunktet for prosjektet er skjærkapasitet for bjelker med utsparinger, et svært vanlig konstruksjonselement. Den viktigste delen av oppgaven er utførelsen av fullskalatester av en referansebjelke og tre bjelker med utsparinger armert med ulike armeringskombinasjoner.

Første del av oppgaven består av et litteraturstudium basert på tidligere forskning og tidligere utgitt materiale om fiberarmert betong og bruken av dette i bærende konstruksjoner. Denne inneholder bl.a. beskrivelser av ulike fibre og deres egenskaper samt bestanddelene i betong og deres effekt. På nåværende tidspunkt finnes det ikke noe offisielt regelverk for dimensjonering av fiberarmerte konstruksjoner, men det fins flere forslag til slike regelverk og noen av disse er beskrevet i rapporten. Regelverket som er lagt til grunn for beregningene i oppgaven er foreslått av COIN (Concrete Innovation Centre).

Betongen brukt i testene ble levert av Unicon og støpingen skjedde i løpet av to dager. Den første dagen ble en referansebjelke og en bjelke med utsparing som kun hadde tradisjonell armering og andre dagen ble to bjelker med utsparinger med stålfiberarmering støpt (Dramix 80/60). Disse besto av en bjelke med en kombinasjon av fiber og tradisjonell skjærarmering og en bjelke med kun fibre som skjærarmering. Støpingen av fiberbetongen viste seg å være vanskelig på grunn av at fibre klumpet seg og forringet støpeligheten til betongen. Derfor krevde denne betongen mye bearbeiding under støpingen.

I tillegg til fullskalabjellekene ble standardbjelker og kuber støpt. Disse ble senere testet for å bestemme styrkeegenskapene til betongen. Testene viste at både trykkfastheten og rest strekkfastheten var høyere enn de teoretiske verdiene som ble brukt i beregningene utført før testingen. Dermed ble det utført nye beregninger etter testingen i tillegg.

Fullskalabjellekene ble testet ved konstruksjonslaboratoriet på NTNU. Testingen ble utført i en rigg med et firepunkts testoppsett med to symmetriske punktlaster. Bjellekene ble instrumentert for å måle den vertikale forskyvningen midt felts samt rissåpningene under utsparingene. En datamaskin registrerte verdiene underveis. Det viste seg at begge de fiberarmerte bjellekene hadde bedre kapasitet og duktilitet enn bjellekene av ren betong. Dette indikerer at stålfiberarmering er et godt alternativ for skjærarmering i bjelker med utsparinger.

De fleste beregningene som ble gjort stemte godt overens med testresultatene selv om de var litt konservative. Beregningene for den rent fiberarmerte bjelken var ikke spesielt bra og nye beregninger ble gjort for å finne bredden av en teoretisk strekkstav ved utsparingen basert på den reelle kapasiteten. Alt i alt viste testene at bruken av stålfiberarmering i bjelker med utsparinger kan være en god løsning for fremtiden. Mer forskning om dette temaet bør utføres for å utvikle et regelverk for fiberarmerte betongbjelker med utsparinger.

## Preface

This report is the end result of a master thesis written at the Department of Structural Engineering at the Norwegian University of Science and Technology (NTNU) the spring of 2012. COIN (Concrete Innovation Centre) is a part of SINTEF and has since 2007 cooperated closely with the department on the subject of innovation in the concrete industry. Research on fibre reinforced concrete is central in this work and the reason for this master thesis is this research.

The fact that this work could contribute to important research at a relatively early stage was very inspiring and was a driving force during the work with this thesis. It was also exciting to be able to combine the theoretical studies with practical work in the laboratory.

I would like to thank my supervisor, Terje Kanstad, for valuable guidance and advice during the work of this thesis. I would also thank the doctoral research fellows Belen Pina Fernandez, Elena Vidal Sarmiento and Giedrius Zirgulis for assistance with the casting, fresh concrete testing and the testing of standard beams and cubes. They were a great help.

Last but not least I must thank the staff in the laboratory at the department. Their assistance in the lab during a hectic time was invaluable. Special thanks are directed to Ove Loraas for assistance during the casting and Steinar Seehuus during the testing of the beams. It was their help that enabled the practical part of this project to be accomplished.

*Trondheim, 03.06.2012*

*Ane Marte Olimb*



## Table of contents

1 Introduction.....	1
2 Range of use today .....	2
3 Concrete technology .....	3
3.1 Cement .....	3
3.2 Aggregate .....	4
3.3 Chemical admixtures .....	5
3.4 Silica.....	6
4 Fibre types/properties.....	7
4.1 General requirements for the fibres .....	8
4.2 Steel fibres.....	8
4.3 Synthetic fibres.....	9
5 Mechanical properties.....	11
5.1 Orientation and distribution of fibres .....	11
5.2 Compressive strength.....	12
5.3 Tensile strength.....	12
5.3.1 Residual tensile strength .....	13
5.4 Shear properties.....	15
5.5 Moment properties .....	15
6 Calculation models .....	16
6.1 Moment capacity.....	16
6.1.1 COIN-report .....	16
6.1.2 Multi-layer force equilibrium .....	18
6.2 Shear Capacity .....	20
6.2.1 COIN-report .....	20
6.2.2 Technical Report.....	21
6.2.3 Model code.....	22
6.2.3 Beams with openings .....	22
6.3 Design forces .....	23
6.3.1 Vierendeel theory.....	23
7 Full-scale testing.....	25
7.1 American concrete institute.....	25
7.2 Full-scale tests in Norway.....	26
8 Testing methods .....	28

8.1 Pull-out test of single fibres.....	28
8.2 Beam tests.....	29
8.2.1 Norwegian sawn beam test.....	29
8.2.2 NS-EN 14651.....	30
8.3 Testing of compressive strength .....	35
9 Casting.....	37
9.1 Preliminary work .....	37
9.2 Materials.....	41
9.3 Fresh concrete testing.....	41
9.3.1 Methods .....	41
9.4 Casting and fresh concrete testing.....	44
9.4.1 1 <sup>st</sup> casting day (8 <sup>th</sup> of March).....	44
9.4.2 2 <sup>nd</sup> casting day (15 <sup>th</sup> of March).....	47
10 Testing of full-scale beams .....	52
10.1 Description of setup .....	52
10.2 Procedure .....	55
10.3 Test results .....	56
10.3.1 Stiffness of beams .....	57
10.3.2 Beam A .....	61
10.3.3 Beam B.....	64
10.3.4 Beam C.....	68
10.3.5 Reference beam .....	72
11 Calculations of shear capacity .....	75
11.1 Pre-testing calculations .....	75
11.1.1 Reference beam .....	75
11.1.2 Beam A .....	75
11.1.3 Beam B.....	76
11.1.4 Beam C.....	76
11.2 Post testing calculations.....	78
11.2.1 Shear capacity .....	78
11.2.2 Calculation of tensile trajectory for beam C.....	78
11.2.3 Calculation of tensile trajectory for beam B .....	80
12 Discussion.....	82
12.1 Comparison of calculations and test.....	82

---

12.2 Comparison of the beams .....	83
13 Conclusions and suggestions for further work.....	84
13.1 Conclusions.....	84
13.2 Suggestions for further work.....	84
13 References.....	86
Annex.....	88

## List of figures

Figure 1: Example of aggregate grading curve (Gossila, 2005) .....	4
Figure 2: Typical fibre geometry (Löfgren, 2005) .....	9
Figure 3: Example of synthetic fibres (Elasto Plastic Concrete) .....	10
Figure 4: Example of synthetic fibres (Elasto Plastic Concrete) .....	10
Figure 5: Different distributions of discontinuous fibres (Löfgren, 2005).....	11
Figure 6: Behaviour of concrete and FRC in compression (Löfgren, 2005) .....	12
Figure 7: Distribution of stress and strain for a rectangular cross-section of FRC in bending (COIN, 2011).....	16
Figure 8: Distribution of stress and strain for a rectangular cross-section of reinforced FRC in bending (COIN, 2011) .....	17
Figure 9: Multi-layer model (Døssland, 2008).....	18
Figure 10: Illustration of the Vierendeel model and the distribution of forces .....	23
Figure 11: Storm water detention facility (Brodowski, et al., 2010) .....	25
Figure 12: Arch unit for stream crossing (Brodowski, et al., 2010).....	25
Figure 13: Setup for round panel slab test (Destrée, 2010).....	26
Figure 14: Finished FRC house (Døssland, 2008).....	26
Figure 15: Slab 2 after testing (Døssland, 2008) .....	26
Figure 16: Principle drawing of pull-out test of single fibres (Thorenfeldt, 2006).....	28
Figure 17: Setup of the Norwegian sawn beam test (Thorenfeldt, 2006) .....	29
Figure 18: Plate element for sawing out test beams .....	30
Figure 19: Wall element for sawing out test beams .....	30
Figure 20: Test setup for the NS-EN 14651-test (Standard Norge, 2005) .....	31
Figure 21: Casting of a NS-EN 14651-test beam (Standard Norge, 2005).....	31
Figure 22: Standard beam in testing rig .....	32
Figure 23: Load-deflection curves for the reference beams .....	33
Figure 24: Mean load-deflection curve for the reference beams .....	33
Figure 25: Load-deflection curves for the SFRC beams.....	34
Figure 26: Failures of a cubic test specimen (Standard Norge, 2009).....	36
Figure 27: Reinforcement for beam A while being fixed .....	37
Figure 28: Reinforcement for beam A after being put into the mould.....	37
Figure 29: Reinforcement for beam B while being fixed.....	38
Figure 30: Reinforcement for beam C after being put into the mould.....	38
Figure 31: Drawing of the reinforcement in beam A .....	38
Figure 32: Drawing of the reinforcement in beam B.....	39
Figure 33: Drawing of the reinforcement in beam C.....	39
Figure 34: Drawing of the reinforcement in the reference beam.....	40
Figure 35: Slump test.....	42
Figure 36: 4C Rheometer.....	42
Figure 37: Close-up of the 4C Rheometer .....	42
Figure 38: Geometry of the LCPC-box (Roussel, 2007) .....	43
Figure 39: Flow of concrete in the LCPC-box (Roussel, 2007).....	43
Figure 40: Air content measure, FTS-B 2020 apparatus.....	44
Figure 41: Slump test 1.....	44

Figure 42: Slump test 2.....	44
Figure 43: Hopper used for casting .....	45
Figure 44: The casting process .....	45
Figure 45: The beams after casting .....	45
Figure 46: Beam A after removing the formwork .....	46
Figure 47: The beams piled for hardening .....	46
Figure 48: 4C Rheometer-test 1 .....	46
Figure 49: LCPC-box test 1.....	47
Figure 50: Chute for pouring concrete .....	48
Figure 51: Casting of the SFRC beams .....	49
Figure 52: Lumping of steel fibres .....	49
Figure 53: Beams piled for hardening .....	49
Figure 54: Beams piled for hardening .....	49
Figure 55: 4C Rheometer-test 2 .....	50
Figure 56: Measuring the slump.....	50
Figure 57: LCPC-box test 2.....	51
Figure 58: Measuring the spread length .....	51
Figure 59: Test setup for full-scale beams.....	52
Figure 60: Beam B in the testing rig .....	53
Figure 61: Placement of LVDTs.....	53
Figure 62: Two modes of shear failure at openings (Mansur, et al., 1999) .....	54
Figure 63: Calculation of real crack opening .....	54
Figure 64: Drawing of cracks on the beam.....	55
Figure 65: Force-displacement curves for all the beams .....	56
Figure 66: Stiffness of the beams .....	57
Figure 67: Unit dummy load method .....	58
Figure 68: Load-displacement curve for beam A .....	61
Figure 69: Initial cracking, beam A .....	62
Figure 70: Crack development, beam A .....	62
Figure 71: Crack development, beam A .....	62
Figure 72: Close to failure, beam A .....	62
Figure 73: Beam A after failure .....	63
Figure 74: Crack openings for northern opening in beam A .....	63
Figure 75: Crack openings for southern opening in beam A.....	64
Figure 76: Load-displacement curve for beam B.....	65
Figure 77: Initial cracking, beam B .....	66
Figure 78: Crack development, beam B .....	66
Figure 79: Crack development, beam B .....	66
Figure 80: Close to failure, beam B .....	66
Figure 81: Beam B after failure .....	67
Figure 82: Crack openings for northern opening in beam B .....	67
Figure 83: Crack openings for southern opening in beam B.....	68
Figure 84: Load-displacement curve for beam C.....	69
Figure 85: Initial cracking, beam C .....	70
Figure 86: Crack development, beam C .....	70

Figure 87: Crack development, beam C .....	70
Figure 88: Close to failure, beam C .....	70
Figure 89: Beam C after failure.....	71
Figure 90: Crack openings for northern opening in beam C .....	71
Figure 91: Crack openings for southern opening in beam C .....	72
Figure 92: Load-displacement curve for the reference beam.....	73
Figure 93: Initial cracking, reference beam.....	73
Figure 94: Crack development, reference beam.....	73
Figure 95: Close to failure, reference beam.....	74
Figure 96: The reference beam after failure .....	74
Figure 97: Vertical tensile zone near opening.....	77
Figure 98: Angled tensile zone near opening.....	77
Figure 99: Crack angle for beam C.....	79

## List of tables

Table 1: Main Ingredients of Cement.....	3
Table 2: Physical properties of some fibres (Löfgren, 2005).....	7
Table 3: Partial safety factor for FRC.....	22
Table 4: Results of the NS-EN 14651 test for the reference beams.....	33
Table 5: Results of the NS-EN 14651 test for the SFRC beams .....	34
Table 6: Results from the testing of cubic test specimens.....	36
Table 7: Specifications for the fibres (Bekaert, 2005).....	41
Table 8: Results of 4C Rheometer-test 1.....	46
Table 9: Results of LCPC-box test 1 .....	47
Table 10: Density results 1 .....	47
Table 11: Air content result 1 .....	47
Table 12: Results from 4C Rheometer-test 2 .....	50
Table 13: Results from LCPC-box test 2.....	50
Table 14: Density results 2 .....	51
Table 15: Air content results 2 .....	51
Table 16: Stiffness of the beams .....	57
Table 17: Crack registration for beam A.....	61
Table 18: Crack registration for beam B.....	65
Table 19: Crack registration for beam C.....	69
Table 20: New capacity for beam B and C.....	78
Table 21: Summary of test and calculation results .....	82

## Symbols and abbreviations

### Abbreviations

ACI	American concrete institute
CMOD	Crack mouth opening displacement
EC2	Eurocode 2
EHS	Environment, Health and Safety
FRC	Fibre reinforced concrete
LVDT	Linear variable differential transformer
NSBT	Norwegian sawn beam test
SCC	Self compacting concrete
SFRC	Steel fibre reinforced concrete

### Latin upper case letters

$A_o$	Area above opening
$A_s$	Area of tensile reinforcement bar
$A_s'$	Area of compressive reinforcement bar
$A_{sv}$	Cross-sectional area of shear stirrup
$A_u$	Area beneath opening
$C_{Rd,c}$	Factor
$F$	Load
$F_j$	Load corresponding with $CMOD = CMOD_j$ ( $j=1,2,3, \dots$ )
$F_{max}$	Total load capacity
$F_o$	Axial force over opening
$F_u$	Axial force beneath opening
$I_o$	Moment of inertia for uncracked upper flange
$I_u$	Moment of inertia for uncracked lower flange
$I_{u,riss}$	Moment of inertia for cracked lower flange
$M$	Moment
$M_{Rd}$	Moment capacity
$M_{Rd,test}$	Trial moment capacity
$N$	Axial force
$S$	Tensile force
$S_a$	Tensile force in reinforcement bars
$S_f$	Tensile force in fibre reinforced concrete
$T$	Compressive force
$T_c$	Compressive force in concrete
$T_{500}$	Time until slump reaches a diameter of 500 mm
$V$	Shear force
$V_{Ed}$	Design shear force
$V_o$	Shear force over opening
$V_{Rd}$	Shear capacity
$V_{Rd,c}$	Shear capacity
$V_{Rd,cf}$	Shear contribution from fibre reinforcement
$V_{Rd,ct}$	Shear contribution from concrete
$V_{wd}$	Shear contribution from stirrup
$V_u$	Shear force beneath opening



*Latin lower case letters*

$b$	Width of cross-section
$b_w$	Width of web
$d$	Effective depth
$d'$	Torque arm
$f_c$	Compressive strength for concrete
$f_{cd}$	Design concrete compressive cylinder strength
$f_{ck}$	Characteristic concrete compressive cylinder strength
$f_{ctk}$	Tensile strength for plain concrete
$f_{ftd,res2.5}$	Design residual tensile strength
$f_{ftk,res2.5}$	Characteristic residual tensile strength at CMOD = 2.5 mm
$f_{R,j}$	Residual flexural strength at CMOD = CMOD <sub>j</sub> (j = 1,2,3, ... )
$f_{Rk,3}$	Characteristic residual flexural strength at CMOD = 2.5 mm
$f_{yd}$	Design yield stress of steel bar reinforcement
$f_{yk}$	Characteristic yield stress of steel bar reinforcement
$f_{ywd}$	Design yield stress of stirrups
$h$	Height of cross-section
$k$	Factor
$k_f$	T-section flange factor
$k_1$	Factor
$l$	span length
$n_f$	Number of fibres
$n_l$	Number of layers
$s$	Standard deviation
$s$	Stirrup spacing along longitudinal axis
$v_f$	Volume fraction of fibres
$y_i$	Distance from layer i to centroid axis
$y_s$	Distance from tensile reinforcement to centroid axis
$y_s'$	Distance from compressive reinforcement to centroid axis
$z$	Inner torque arm
$\emptyset$	Diameter of steel bar

*Greek letters*

$\alpha$	Fibre orientation factor
$\gamma_f$	Partial safety factor
$\gamma_m$	Material coefficient
$\eta_0$	Capacity factor
$\theta$	Crack angle
$\rho$	Density
$\rho$	Fibre area ratio
$\rho_l$	Factor
$\sigma_{c,i}$	Stress in layer i
$\sigma_{cp}$	Axial stress in concrete
$\sigma_{fk, average}$	Average stress in all fibres
$\sigma_s$	Stress in tensile reinforcement bar
$\sigma_s'$	Stress in compressive reinforcement bar
$\tau_{fd}$	Design value of shear strength contribution from steel fibres
$\varphi$	Angle of tensile trajectory

## 1 Introduction

The background for this report is that the building industry of today experiences a falling recruitment of skilled labour in addition to requirements of continuous efficiency improvements. This opens for research in more efficient construction methods and has led to an increased interest in fibre reinforced concrete. The reason for this is that iron fixing is a very time-consuming activity on a building site and if fibre reinforced concrete may fully or partially replace the traditional reinforcement this work will be smaller. In addition to reducing work time the EHS on the building site may be improved as the iron fixing is a heavy work and may cause work injuries and early retirement for the workers. Another benefit is that the FRC can allow more complex geometry of casting moulds.

In this master thesis written at the Department of Structural Engineering at NTNU the object is to look into the use of fibre reinforced concrete in load carrying structures. A very common structural element is beams with openings to allow air vents etc through, and this type of beam is the main focus of this thesis. Earlier experiments has showed that steel fibres can have a good effect on shear capacity and in this project there have been conducted experiments to inquire into whether this will be efficient for beams with openings as well.

The report starts with a literature study to illustrate the different properties and behaviours of fibre reinforced concrete. As the use of FRC in carrying structures is at the research stage there are several different propositions for designing methods and some of these are described in this section. The most important proposition from Norway is made by COIN (Concrete Innovation Centre) and it is their suggestion that will be emphasized in this thesis.

The main part of the thesis describes the laboratory tests that were carried out. Four beams were cast and tested in the lab. The beams consisted of one reference beam without openings and three beams with openings. The three beams with openings had different types of reinforcement to compare. The details of the experiments are described in the report along with calculations and discussions about the results.

## 2 Range of use today

In Norway today there is no commercial use of fibre reinforced concrete in carrying structures, and the use of fibres is mainly limited to slabs on the ground, sprayed concrete in tunnels and such. Usually the use of fibres is meant to counteract cracking caused by shrinkage or temperature variations.

The fibre reinforcement has a great potential to be used in combination with traditional reinforcement to reduce the amount of reinforcement bars in many kinds of structural elements. In some cases the fibre reinforcement might be able to replace the traditional reinforcement completely. A reason for the lack of use of fibre reinforced concrete in carrying structures is that there is of today no specified set of design guidelines (Døssland, 2008). There is a lot of research going on around the world on this subject and there will in all likelihood be an approved set of rules available in a few years time.

Another reason for the lack of use of FRC in carrying structures is that the fibres have been very expensive and it has not been economically favourable to use them. The last few years there have been a decline in the access of trained labour as well as the cost of said labour has increased. Roughly 40% of the cost for the superstructure for a concrete building is caused by the labour (Löfgren, 2005). This makes the fibre reinforcement more desirable because of its decreasing of the amount of work to be done before casting.

### 3 Concrete technology

Concrete is a composite material, and consists of several different constituent parts. These parts are cement, water, aggregate (sand and stone) and usually one or more special additives to ensure that the concrete has the desired properties.

#### 3.1 Cement

Cement is a hydraulic binding agent, which means that it's a binding agent that hardens when water is added. The cement type that is used today is called Portland cement, because of its colour which is similar to the colour of stone from the island of Portland. Specifications to the Portland cement are described in the Norwegian standard. The cement is mainly consisting of four minerals which constitute 90-95% of the blend. These are made up of oxides of calcium (Ca), silicon (Si), aluminium (Al) and iron (Fe). In addition to the "main minerals" the cement contains small amounts of oxides of manganese (Mn), sulphur (S), potassium (K) and sodium (Na) (Gjerp, et al., 2004).

The main minerals in the blend influence its properties like heat generation, development of strength, the final strength and its durability. These properties may be controlled by changing the proportionality of the main minerals. Even though the rest of the minerals make up a small part of the cement, these can have important effects on the cement's properties as well. The potassium- and sodium oxides (the alkalis) are important. They can make the cement harden faster and make it expand. Table 1 shows the main ingredients of the cement:

**Table 1: Main Ingredients of Cement**

Name	Chemical formula	Symbol
Tricalcium silicate	$3\text{CaO}\cdot\text{SiO}_2$	$\text{C}_3\text{S}$
Dicalcium silicate	$2\text{CaO}\cdot\text{SiO}_2$	$\text{C}_2\text{S}$
Tricalcium aluminate	$3\text{CaO}\cdot\text{Al}_2\text{O}_3$	$\text{C}_3\text{A}$
Tetracalcium aluminate ferrite	$4\text{CaO}\cdot\text{Al}_2\text{O}_3\cdot\text{Fe}_2\text{O}_3$	$\text{C}_4\text{AF}$

When the different minerals in the cement react with water there will be heat generation. As a result of this it is important to keep the concrete damp while hardening to avoid dehydration and cracking.

### 3.2 Aggregate

The aggregate in the concrete consists of sand and stone and makes up 60-70% of the concrete volume. As this is the largest part of the concrete the properties of the aggregate may greatly influence the properties of the concrete. Even though there can be specific requirements to the aggregate in a special blend, there are certain general requirements that should always be followed:

- Should not be porous
- Should not be efflorescent, micaceous or buttery or have schistose structure.
- Should not contain sulphates (alum slate), silicates (phyllite, flint, opal) or chlorides (sand from earlier littoral zones)
- Should not contain much humus, mud and clay.

(Gjerp, et al., 2004)

The aggregate is often evaluated by its material grading, grain shape and superficial structure. The material grading means the distribution of different grain sizes in the aggregate. It is desirable to have a good distribution of the grain sizes, that the amount of each size is approximately the same. This will lead to few hollows and a low air content in the concrete which is an advantage as large air content will reduce the strength of the concrete. If the hollows between the aggregate particles are small the amount of cement adhesive necessary to bind them together is small. However, if the distribution is too good the concrete can be a bit hard to work with. Figure 1 shows an example of a aggregate grading curve.

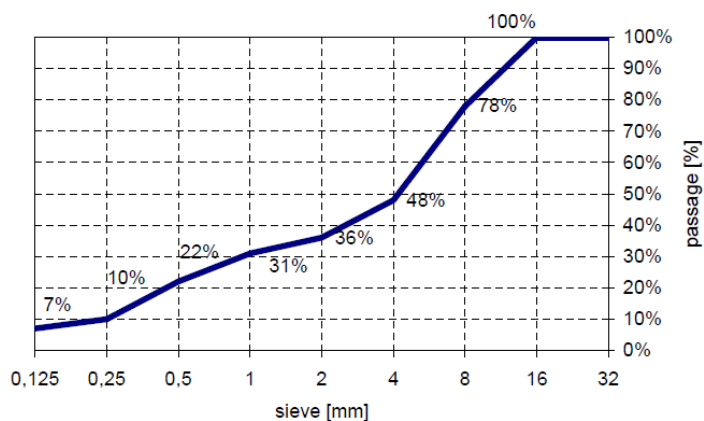


Figure 1: Example of aggregate grading curve (Gossila, 2005)

The grain shape and superficial structure means how the shapes of the grains are. Natural aggregate (sand, gravel and pebbles) is often rounded and smooth, while human made aggregate like crushed stone has sharp edges and rough surface. Usually these parameters are important for filling compounds for road construction, but there are rarely requirements for these properties for concrete.

### 3.3 Chemical admixtures

The chemical admixtures are additives that are added to the fresh concrete to give it desired properties either in fresh or hardened condition. These additives were to a large degree developed in the 70's and 80's and today virtually all concrete blends contain some amount of additives. The most important categories of chemical admixtures are described below. (Gjerp, et al., 2004)

#### *Plasticizers*

The plasticizers are the most usual additives and are added to increase the workability of the fresh concrete so that it's easier to cast, without having to add more water and thereby reduce the concrete's capacity. This happens because the plasticizers reduce the water's surface tension, thus reducing the friction between the components in the mix, and the thickness of the water film around the aggregate grains is reduced and releases water. The plasticizers belong to two categories; plasticizers and superplasticizers. The plasticizers are based on a material called lignosulfonate which originates from the wood processing industry. At high dosages the plasticizer may have a retarding side effect. This means that the concrete dries slower and this is not always desirable.

The superplasticizers usually have a better plasticizing effect than the regular plasticizers (12-40% water reducing effect against only 8% for plasticizers). A positive side of the superplasticizers is that they have fewer deteriorious effects, e.g. the retarding effect is smaller. They have a short working period (1/2-3/4 hour), but can be added several times without having negative effect on the concrete strength. On the downside it must be mentioned that they are quite expensive.

#### *Retarders*

Retarders restrain the hydration of the cement by forming a slowly dissolving membrane around the cement grains. They are used when it's desirable to delay the solidification time of the concrete. As examples this may be desirable for long transportation, to elongate the concrete's processing time in the casting frame or when casting in warm weather to avoid fast solidification. As the plasticizers have retarding as a side effect, the retarders have plasticizing as a side effect.

#### *Accelerators*

The effect of the accelerators is quickening of the hardening process. These additives are relatively rarely used in Norway. It may be necessary with accelerators when casting in the winter to obtain early removal of the casting frame and frost resistance, and when producing prestressed concrete. A problem when using accelerators is that the accelerated hardening process may produce a lot of heat. This can then cause the concrete to crack, increase the concrete's potential for shrinkage or lessen the strength of the hardened concrete.

### *Air entrainments*

The air entrainments bind many small and evenly distributed air bubbles into the cement when the concrete is mixed. The point with this may be to enhance the frost resistance of the concrete, because the air bubbles allow water in the concrete to expand without cracking the concrete. Another advantage given by high air content is that the air bubbles enhance the concrete's castability. The problem is that high air content will reduce the strength of the concrete by 5% per each % of added air. (Gjerp, et al., 2004)

### *Other*

In addition to the most usual chemical admixtures which are described above, there are other additives that are used. These can be additives for casting under water which prevent washing out of the concrete, pumping aids to improve the pumpability by making the concrete more cohesive or bonding agents when casting together old and new concrete. The additives can also be added to improve the aesthetics of the concrete, e.g. pigments to add colour.

### **3.4 Silica**

Silica fume is a by-product from the production of silicon and ferrosilicon alloys. The silica particles are very small, about 1/100 of the size of the cement particles and 1-5/1000 mm. This gives them a very large surface per volume. It is normal to add 5% of the cement weight of silica. The silica is not hydraulic by itself, but under given conditions it can react with the calcium hydroxide from the water-cement reaction to make compounds. These compounds are similar to the ones from the cement-water reactions, and are called pozzolans. (Gjerp, et al., 2004)

When added to the concrete mixture the silica will bind a lot of water because of its large surface area. This will make the fresh concrete more viscous and stiff as the inner cohesion is increasing. The result is that the concrete needs more energy to be spread into the formwork, but it also decreases the possibility of separation. It is generally necessary to use superplasticizers for workability when silica is added.

## 4 Fibre types/properties

There are many different types of fibres that can be used in fibre reinforced concrete. Manufacturers make fibres out of steel, polymers and basalt, among others. Historically there have also been used many types of fibres of natural origin in buildings. One of these is asbestos. Asbestos was used as reinforcement in fibre cement wallboards (eternite or asbestos cement) in the middle of the last century. This is forbidden today because the substance is carcinogenic (Riksantikvaren, 2009).

The fibres of interest in this thesis are the ones mentioned above; steel, polymer and basaltic fibres. Steel fibres are the most used and best examined out of these, and it's this type that will be used in the experiments in this thesis. Different fibres and their most important properties are listed in table 2.

Table 2: Physical properties of some fibres (Löfgren, 2005)

Type of Fibre	Diameter [µm]	Specific gravity [g/cm <sup>3</sup> ]	Tensile strength [MPa]	Elastic modulus [GPa]	Ultimate elongation [%]
<b>Metallic</b>					
Steel	5-1 000	7.85	200-2 600	195-210	0.5-5
<b>Glass</b>					
E glass	8-15	2.54	2 000-4 000	72	3.0-4.8
AR glass	8-20	2.70	1 500-3 700	80	2.5-3.6
<b>Synthetic</b>					
Acrylic (PAN)	5-17	1.18	200-1 000	14.6-19.6	7.5-50.0
Aramid (e.g. Kevlar)	10-12	1.4-1.5	2 000-3 500	62-130	2.0-4.6
Carbon (low modulus)	7-18	1.6-1.7	800-1 100	38-43	2.1-2.5
Carbon (high modulus)	7-18	1.7-1.9	1 500-4 000	200-800	1.3-1.8
Nylon (polyamide)	20-25	1.16	965	5.17	20.0
Polyester (e.g. PET)	10-8	1.34-1.39	280-1 200	10-18	10-50
Polyethylene (PE)	25-1 000	0.96	80-600	5.0	12-100
Polyethylene (HPPE)	-	0.97	4 100-3 000	80-150	2.9-4.1
Polypropylene (PP)	10-200	0.90-0.91	310-760	3.5-4.9	6-15.0
Polyvinyl acetate (PVA)	3-8	1.2-2.5	800-3 600	20-80	4-12
<b>Natural - organic</b>					
Cellulose (wood)	15-125	1.50	300-2 000	10-50	20
Coconut	100-400	1.12-1.15	120-200	19-25	10-25
Bamboo	50-400	1.50	350-50	33-40	-
Jute	100-200	1.02-1.04	250-350	25-32	1.5-1.9
<b>Natural - inorganic</b>					
Asbestos	0.02-25	2.55	200-1 800	164	2-3
Wollastonite	25-40	2.87-3.09	2 700-4 100	303-530	-



## 4.1 General requirements for the fibres

For the fibres to work efficiently in a concrete mix, the following criteria must be fulfilled (Löfgren, 2005):

- The fibres must have a tensile strength much higher than that of the matrix (two or three orders).
- The bond between the matrix and the fibres must have a strength of at least the same order as that of the matrix.
- The fibres' elasticity modulus must be at least three times larger than that of the matrix.
- The fibres must have a ductility high enough to prevent fracturing of the fibres due to abrasion or bending.
- The Poisson ratio and the coefficient of thermal expansion of the fibres should be about the same order as that of the matrix. If the Poisson ratio of the fibres is much larger than that of the matrix, it may lead to debonding due to lateral contraction of the fibres.
- In addition, the fibres must be durable and able to withstand the alkaline environment in the concrete matrix.

## 4.2 Steel fibres

Steel fibre is the fibre type with the most extensive use. In table 2 we can see that the steel fibres has a tensile strength between 200 and 2600 MPa, but typically the fibres that are used have a tensile strength typically 2-3 times that of traditional reinforcement. They have typical diameters from 0.5 to 1 mm and length between 25 and 60 mm (The Concrete Society, 2007). The fibres are classified after which basic materials they are produced from (COIN, 2011):

I: Cold-drawn wire

II: Cut sheet

III: Melt extracted

IV: Shaved cold drawn wire

V: Milled from blocks

The steel fibres may have different shapes, usually with deformed ends to ensure good bonding. The most usual design is with end hooks. An important issue is that the bond between the fibres and the concrete needs to be ductile. Therefore it's better if the structure fractures when the fibres gets pulled out of the concrete, rather than by fracturing of the fibres themselves. E.g. There will be very good bonding between the concrete and wave shaped fibres, but that also means that it will be very difficult to pull these fibres out of

the concrete. This may lead to fracture in the structure when the fibres fracture, and we get a brittle fracture. Because of this, the wave shape is not necessarily a good design even though there is a very good bonding between fibre and matrix. The fibres with end hooks can be gradually deformed and get pulled out of the concrete, and will give a more ductile fracturing. This type will be used in the following experiments. Figure 2 shows typical steel fibre designs.

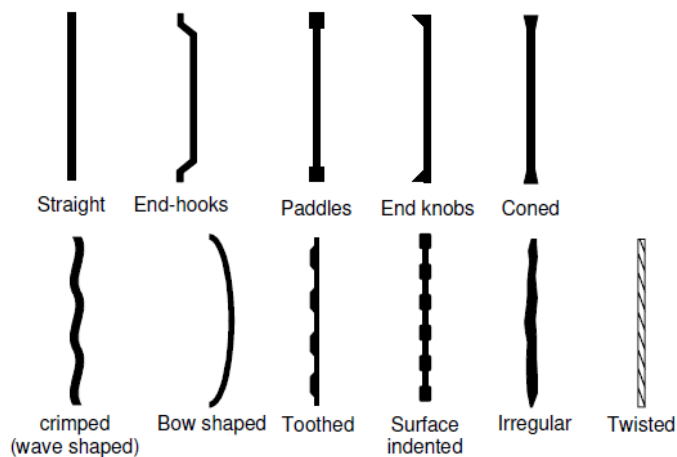


Figure 2: Typical fibre geometry (Löfgren, 2005)

As with other reinforcement, the steel fibres will not become active until crack openings of a certain size appears. Even so, the steel fibres need smaller CMOD (Crack mouth opening displacements) to gain full strength than the fibres made of polymers.

The steel fibres have a disadvantage when it comes to the aesthetic prospect. Since fibres get spread out in the matrix some of them will be at the surface of the structure. These might rust so that the surface gets discoloured by rust stains.

### 4.3 Synthetic fibres

Synthetic fibres for concrete are made from a wide range of organic polymers, and there is an increasing amount of examples where these are used in practice. Earlier these fibres have not been very good for post cracking load capacity for concrete as the polymers often have very high Poisson's ratio which result in poor bonding. However, recent interest in polymer fibres has resulted in research and development of materials with E-modulus up to 10 000 MPa and production techniques that enables the manufacturers to create fibres with good anchoring mechanisms.

The synthetic fibres are usually divided into two classes:

- Class I: Micro fibres
  - o Class Ia: Micro fibres < 0.30 mm in diameter, mono-filamented
  - o Class Ib: Micro fibres < 0.30 mm in diameter, fibrillated
- Class II: Macro fibres > 0.30 mm in diameter

(The Concrete Society, 2007)

The Class I micro fibres have been used since the mid 80s as a means to modify the properties of fresh concrete. Their primary goal is to control plastic shrinkage cracking. They may also affect the bleeding of the concrete and more recently they are used to reduce spalling of concrete exposed to fire. However, their contribution to load-bearing capacity post cracking is insignificant.

The Class II macro fibres has similar dimension as steel fibres used in concrete structures. These provide the concrete with some post cracking load-bearing capacity when added in large enough doses (up to about 1.35% of the volume). They are mainly used to increase the residual flexural strength in concrete.

The synthetic fibres have the advantage compared to steel fibres that they have a very high resistance to acidic and alkaline environment and thus do not require concrete cover to protect against corrosion. This also gives FRC with synthetic fibres a better aesthetical surface than FRC with steel fibres as the steel fibres at the surface will corrode and discolour the concrete when exposed to outdoor weather. An important negative aspect to the synthetic fibres is that they will soften at elevated temperatures and melt at about 150-160°C, thus losing all their mechanical properties. This limits their use in structures where there is a risk of fire.

Figure 3 and 4 shows examples of synthetic fibres



**Figure 3: Example of synthetic fibres (Elasto Plastic Concrete).**



**Figure 4: Example of synthetic fibres (Elasto Plastic Concrete).**

## 5 Mechanical properties

Concrete is a quite brittle material with very little tensile strength, so to use concrete in structures it is necessary to improve its tensile qualities. The traditional way of doing this is adding steel bars with high yield strength to take the tensile forces in the structure element. Another way to improve the tensile strength of concrete is to add reinforcement fibres. This might enhance the concrete's toughness, ductility and energy absorption under impact and increase the post crack capacity when added in sufficient quantity. The fibres can act in different ways, but mainly in two mechanisms: They can stop micro cracks from developing into larger cracks either from external loads or from drying shrinkage. Secondly, after cracking the fibres that span the cracks that have formed will give the concrete a residual load bearing capacity. With enough fibres this capacity may be considerable, but the fibres may influence the casting qualities of the fresh concrete.

### 5.1 Orientation and distribution of fibres

The orientation of fibres in FRC is important for the capacity and mechanical performance. For randomly dispersed fibres the placement depend on the method of adding fibres, the casting equipment used and the fresh concrete properties among others. A problem when casting fibre reinforced concrete is that the fibres may clot together and prevent a good flow of the concrete. This can cause a less fortunate dispersing of the fibres. Another problem that may occur is separation, which can cause the steel fibres to sink to the bottom of the formwork. Figure 5 shows different distribution of discontinuous fibres.

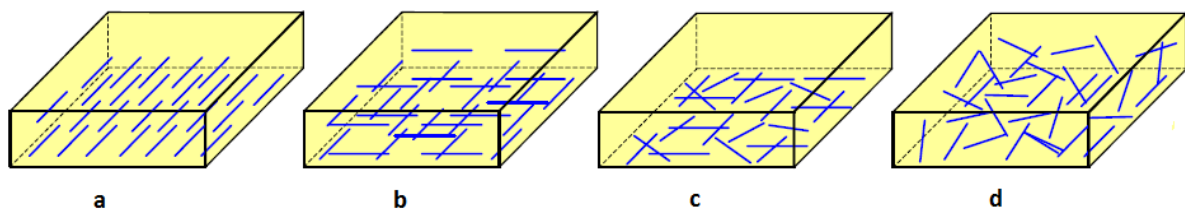


Figure 5: Different distributions of discontinuous fibres (Löfgren, 2005)

- a) Biased 1-D fibre orientation
- b) Biased 2-D fibre orientation
- c) Plane random fibre orientation
- d) Random fibre orientation

(Löfgren, 2005)

The fibres are most effective when they are normal to the cracks and the crack occurs at the middle of the fibre. This will not happen for all fibres in most FRC structural elements, and it's important to allow for this when designing. The theoretical formula for residual tensile strength given in the COIN-report allows for this and is described in section 5.3.1 *Residual tensile strength*.

## 5.2 Compressive strength

In the stress-strain relation for concrete in compression the concrete has got an almost linear response up to about 30% of the compressive strength. After this a gradual softening happens up to the concrete compressive strength, where the stress-strains relation exhibits a strain softening until failure by crushing. The main explanation of the concrete's macroscopic behaviour during compressive failure is proposed by Neville (1997). This explanation states that there are interfaces between the aggregate and the hardened cement paste, and that in these interfaces micro cracks develop even at smaller load levels. These cracks develop through the weakest part of the concrete (the cement is less strong and stiff than the aggregate for normal-strength concrete, but in high-strength concrete these are more equal), and eventually result in crushing. (Löfgren, 2005)

When fibres are added to the concrete it becomes more ductile and increase the resistance against longitudinal crack growth. The effect of fibres on concrete compressive strength is highly dependent of the fibre type, their size and properties, the amount of fibres added and the properties of the matrix. The main rule is that conventional steel fibres in moderate dosages (<1%) do not affect the concrete's properties before maximum stress has been reached, it may, however, increase the failure strain and the strain at crack localisation. This is illustrated in figure 6. Still, it's possible to increase the compressive strength with higher dosages and with microfibers. (Löfgren, 2005)

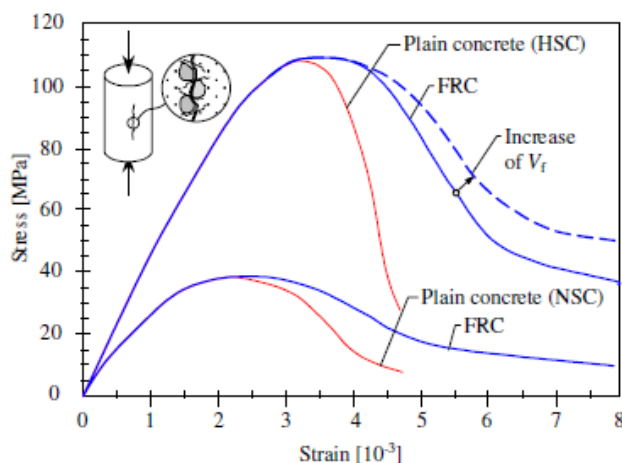


Figure 6: Behaviour of concrete and FRC in compression (Löfgren, 2005)

## 5.3 Tensile strength

The important effect fibres have on concrete tensile strength is on the tensile fracture behaviour. In normal concrete the tensile load carrying abilities of the concrete will decrease a lot after crack widths of about 0.3 mm. The FRC will be able to carry considerable loading after cracking. (Löfgren, 2005)

After the initial cracking has started, the fibres across the cracks will often be able to carry more load than other weak zones in the matrix. Therefore new cracks will continue to form in the brittle matrix. When many cracks have formed the fibres will have plastic deformations by being drawn out of the concrete matrix. The ultimate failure will happen when the fibres get completely drawn out of the concrete. This way the FRC will have a much more ductile behaviour than regular concrete, and will have some residual capacity after the stress-strain diagram has reached its peak.

### 5.3.1 Residual tensile strength

What's special about the fibre reinforced concrete is that after cracking the concrete still has a relatively stable tensile strength with increasing crack widths. This is called the residual tensile strength. The residual tensile strength is denoted as  $f_{ftk,res2.5}$  and is defined as resulting tensile force resultant per area unit for a crack through the concrete at 2.5 mm crack opening.

The residual flexural strength for FRC is decided from the bending moment in standardized testing beams at the relevant crack width while assuming linear stress distribution over the height of the cross-section. As this is not corresponding to the real stress distribution, this variable is not used directly in the design rule but is used as a means to calculate the residual tensile strength. The residual tensile strength is defined as 0.37 times the characteristic residual flexural strength:

$$f_{ftk,res2.5} = 0.37f_{Rk,3}$$

The characteristic residual flexural strength is found from the residual flexural strength by the following formula:

$$f_{Rk,i} = f_{R,i} - ks$$

$f_{R,i}$  is the residual flexural strength

$s$  is the standard deviation from the testing series

$k$  is a factor that is set to 1.7 as described in NS-EN 14651, see chapter 8.2.2. *NS-EN 14651*.

(COIN, 2011)

Another way of calculating the residual tensile strength is by a theoretical formula. For this formula it is assumed that the fibres keep their original direction after cracking.

$$f_{ftk,res2.5} = \eta_0 \cdot v_f \cdot \sigma_{fk,average}$$

$f_{ftk,res2.5}$  is the theoretical residual tensile strength

$\eta_0$  is a capacity factor which indicates how much of the fibre forces are effective normal to the crack plane.

$v_f$  is the volume fraction of fibres

$\sigma_{fk,average}$  is the average stress in all fibres crossing the crack, measured by pull-out test of single fibres.

(Døssland, 2008)

The capacity factor  $\eta_0$  may be assumed to be 1/3 for 3-D random fibre orientation. If the fibre orientation is documented by experiments the capacity factor may be calculated from the following relation:

$$\eta_0 = \frac{4}{3} \cdot \alpha - \frac{1}{3} \quad \text{for } 0.5 < \alpha < 0.8$$

$$\eta_0 = \frac{2}{3} \cdot \alpha \quad \text{for } 0.3 < \alpha < 0.5$$

And the fibre orientation factor ( $\alpha$ ) is calculated as follows:

$$\alpha = \frac{\rho}{v_f} = \frac{n_f \cdot A_f}{A_c \cdot v_f}$$

$\rho$  is the fibre area ratio

$n_f$  is the number of fibres

$A_f$  is the cross-sectional area for one fibre

$A_c$  is the area of the relevant part of the concrete cross-section

(COIN, 2011)

### *Calculation of theoretical residual tensile strength*

Based on earlier experiments the average stress for fibres crossing crack will be set to  $\sigma_{fk,average} = 500$  MPa (Døssland, 2008). There was no time to carry out pull-out tests during this thesis and assumed values are therefore used. As there was no way to calculate the fibre orientation factor ( $\alpha$ ) without a fibre count, the capacity factor is set to  $\eta_0 = 1/3$  as that was recommended for a random 3-D fibre orientation. Having used these assumptions the theoretical residual tensile strength is calculated as follows:

$$f_{ftk,res2.5} = \eta_0 \cdot v_f \cdot \sigma_{fk,mid} = \frac{1}{3} \cdot 0.01 \cdot 500 = \underline{\underline{1.67 \text{ MPa}}}$$

## 5.4 Shear properties

In regular concrete the shear forces are transferred across a crack by interlocking of the aggregate and friction. For FRC the fibres are activated when the cracks occur and the shear force is transferred by the fibres across the cracks. After cracking the fibres start being pulled out and provide a ductile behaviour of the concrete and significant toughening behaviour. Earlier experiments has indicated that the fibres have a great effect on the shear capacity and can increase the capacity up to 60% of the compressive capacity for regular concrete with low or moderate dosages of fibres. For high-strength concrete with  $40 \text{ kg/m}^3$  steel fibres the increase has been measured up to 100% of the compressive capacity. This is because the fibres act as dowels between the crack surfaces and therefore increase the capacity quite significantly. The effect increases with higher fibre volume fractions (Löfgren, 2005).

## 5.5 Moment properties

The fibres in FRC do also have a large impact on the moment capacity. The increase in moment capacity is highly dependent on the amount of fibres and the fibre type. When the concrete has cracked the tensile zone may still carry a stress equal to the residual tensile strength. Simplified the tensile zone may be characterized as a uniform stress distribution with the stress equal to the design residual tensile strength. This residual tensile strength may work together with the regular reinforcement if the latter is present. The fibres will also reduce the crack width of the moment cracks by spreading the moment to several smaller cracks.



## 6 Calculation models

### 6.1 Moment capacity

For fibre reinforced concrete that is subjected to moment, parts of the concrete cross-section can carry tensile forces after cracking. According to the COIN-report (COIN, 2011), the tensile zone can for simplicity be characterized by a uniform stress distribution with a tensile stress equal to the design residual tensile strength,  $f_{ftd,res 2,5}$ .

When calculating the moment and axial capacities of FRC we can assume that Navier's hypothesis is applicable (that plane cross-sections remain plane) and that the compression zone for the FRC and the stress-strain properties for the conventional reinforcement is as described in EC2.

#### 6.1.1 COIN-report

##### *Moment capacity for FRC*

For FRC without conventional bar reinforcement we can simplify by assuming that the residual tensile strength,  $f_{ftd,res 2,5}$ , works over a height  $0,8h$ , and that the inner moment arm is  $0,5h$ . Figure 7 shows the distribution of stress and strain for a FRC cross-section subjected to bending (COIN, 2011).

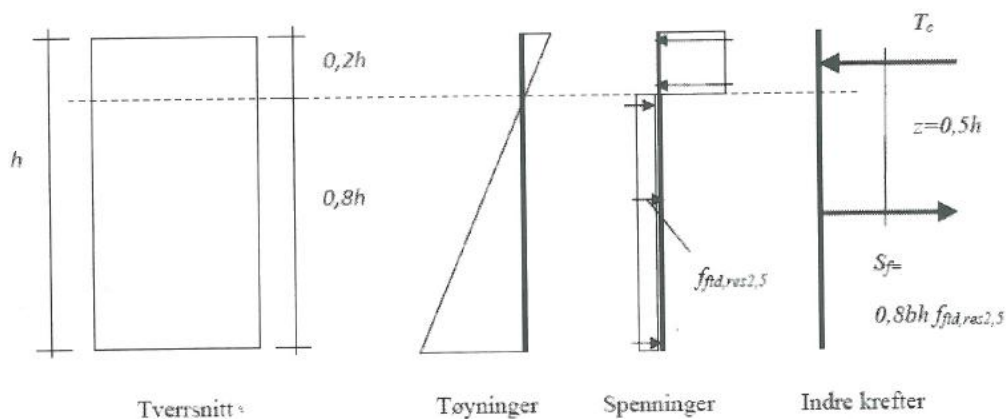


Figure 7: Distribution of stress and strain for a rectangular cross-section of FRC in bending (COIN, 2011)

Then the moment capacity for a rectangular cross-section is:

$$M_{Rd} = 0,4 \cdot f_{ftd,res 2,5} \cdot b \cdot h^2$$

However, for FRC with characteristic residual tensile strength,  $f_{ftk,res 2,5}$ , larger than  $2.5 \text{ N/mm}^2$ , the compression zone height must be calculated by axial equilibrium, as described in the next section.

### Moment capacity for reinforced FRC

For FRC with additional steel bar reinforcement, the moment capacity must be calculated based on the following principles (COIN, 2011):

- It must be proven that the structural element carries the design load by both the fibre reinforcement and the bars.
- The work diagram of the conventional reinforcement is assumed to follow the description in EC2 (3.2.7).
- The compressive zone of the concrete must be characterized as given in EC2 (3.1.7).
- The tensile capacity of the FRC can be included as shown in figure 8, with a constant stress over the tensile zone.
- When calculating the capacity, the height of the compressive zone must be determined by axial equilibrium:  $T_c = S_f + S_a$

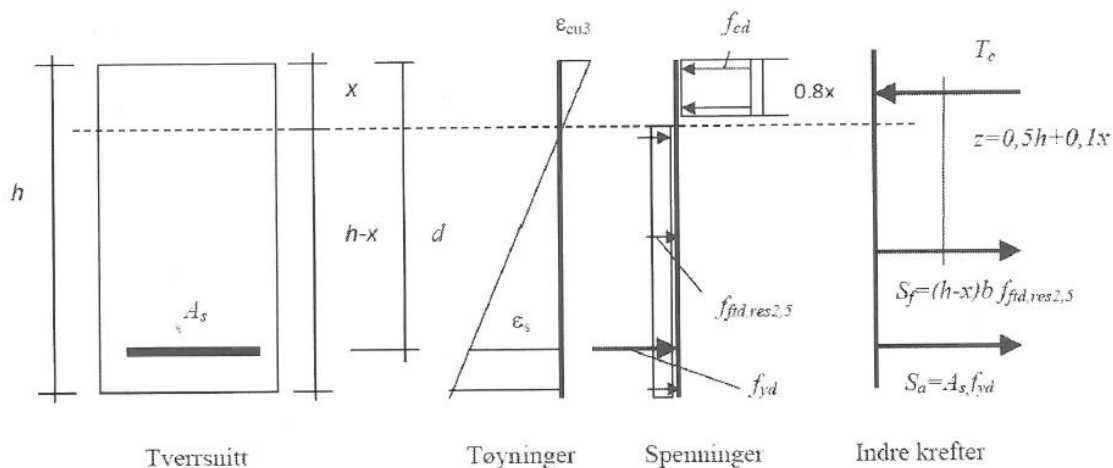


Figure 8: Distribution of stress and strain for a rectangular cross-section of reinforced FRC in bending (COIN, 2011)

When all these principles are fulfilled the moment capacity can be calculated by using moment equilibrium about the compressive resultant as following:

$$M_{Rd} = S_f(0,5h + 0,1x) + S_a(d - 0,4x)$$

For structural elements with reliability class 2, 3 or 4 it must be shown in addition that the conventional reinforcement can carry the bending moments and axial forces without contribution from the fibre reinforcements. In such calculations all material coefficients may be set as  $\gamma_m = 1.0$ .

### 6.1.2 Multi-layer force equilibrium

Another method for estimation of the moment capacity for a beam is the multi-layer force equilibrium method. As in the previous methods, the rules from EC2 is applicable for the compressed part of the concrete and the conventional reinforcement, but the concrete in tension follow other rules because of the contribution of the fibres.

The model consists of dividing the cross-section in a known number of layers connected by springs. The strain across the cross-section is assumed to be linearly distributed, and the tensile stress in the concrete can usually be assumed to be constant and equal to  $f_{ft, res 2.5}$ . See figure 9 for illustration (Døssland, 2008).

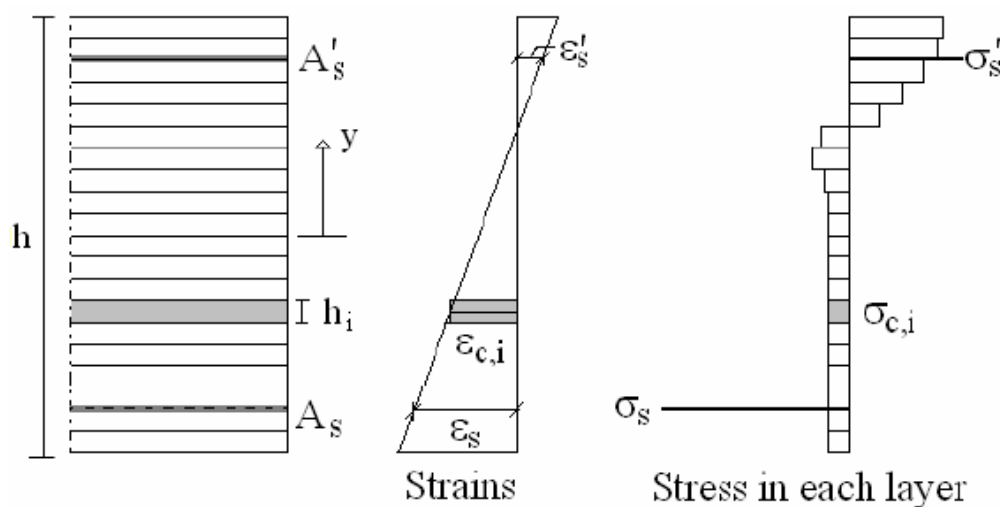


Figure 9: Multi-layer model (Døssland, 2008)

By assuming arbitrary strains in the top and bottom of the cross-section, the whole strain distribution can be established. It's important to choose strains that give the correct moment capacity. Reasonable choices may be 3.5‰ for the compressive strain, and the COIN-report establishes that for FRC the maximum strain at the tension edge should be less than  $3/h$ ‰ for a cross-section subjected to bending (COIN, 2011).

When the strain distribution of the cross-section is established, the stresses for each layer can be calculated. When the stresses are known, the moment capacity may be found by force and moment equilibrium of the cross-section:

$$N = \sum \left( \sigma_{c,i} \cdot b \cdot \frac{h}{n_l} \right) + \sigma_s \cdot A_s - \sigma'_s \cdot A'_s$$

$$M = \sum \left( \sigma_{c,i} \cdot b \cdot \frac{h}{n_l} \cdot y_i \right) + \sigma_s \cdot A_s \cdot y_s + \sigma'_s \cdot A'_s \cdot y'_s$$

Where:

$\sigma_{c,i}$  is the stress in layer  $i$

$b$  is the width of the cross-section

$h$  is the height of the cross-section

$n_l$  is the number of layers

$\sigma_s$  is the stress in the conventional tensile reinforcement

$A_s$  is the area of the tensile reinforcement

$\sigma'_s$  is the stress in the conventional compressive reinforcement

$A'_s$  is the area of the compressive reinforcement

$y_i$  is the distance from layer  $i$  to the centroid axis of the concrete cross-section

$y_s$  is the distance from the tensile reinforcement to the centroid axis of the concrete cross-section

$y'_s$  is the distance from the compressive reinforcement to the centroid axis of the cross-section

## 6.2 Shear Capacity

One of the fields where steel fibres have proved efficient is increasing of the shear capacity. Therefore it might be possible to replace the traditional shear reinforcement with fibres. This would be quite labour-saving on a construction site, as the complex work of binding the shear reinforcement will be unnecessary. Polymer fibres have proven to have small effect for the shear capacity (COIN, 2011).

### 6.2.1 COIN-report

For elements made of fibre reinforced concrete the COIN-report generally use the formula for shear capacity without shear reinforcement from EC2 as a basis. Then there is an addition for the contribution from the fibre reinforcement. This gives the following general formula for shear capacity in fibre reinforced concrete (COIN, 2011):

$$V_{Rd,c} = V_{Rd,ct} + V_{Rd,cf}$$

$$V_{Rd,ct} = [C_{Rd,c} k (100 \rho_l f_{ck})^{\frac{1}{3}} + k_1 \sigma_{cp}] b_w d \geq (v_{min} + k_1 \sigma_{cp}) b_w d$$

$$V_{Rd,cf} = 0,6 \cdot f_{ftd,res2,5} b_w h$$

$$C_{Rd,c} = \frac{0,18}{\gamma_C}$$

$$\rho_l = \frac{A_s}{b_w d} \leq 0,02 \text{ where } A_s \text{ is the area of tensile flexural reinforcement}$$

$b_w$  is the width of the web

$d$  is the effective depth

$$\sigma_{cp} = \frac{N_{Ed}}{A_c} \leq 0,2 f_{cd}$$

$N_{Ed}$  is the axial force due to load or pre-stress

$$k = 1 + \sqrt{200/d} \leq 2 \text{ (} d \text{ in mm)}$$

$f_{ftd,res2,5}$  is design residual tensile strength.

In this thesis, it will be of more use to employ  $f_{ftk,res2,5}$ , the characteristic value of the residual tensile strength than using the design value. This is because it's interesting to compare the real capacity to the calculations, so it will be impractical to calculate conservatively.

As the fibres don't have any effect on the maximum shear capacity, this can be calculated the same way as shown in EC2 (Standard Norge, 2004):

$$V_{Ed} \leq 0,5 b_w d v f_{cd}$$

$$v = 0,6 \left[ 1 - \frac{f_{ck}}{250} \right]$$

## 6.2.2 Technical Report

For beams with shear stirrups in addition to longitudinal reinforcement and fibre reinforcement, Technical Report no. 63 gives the following formula as a suggestion:

$$V_{Rd,c} = [C_{Rd,c} k (100 \rho_l f_{ck})^{\frac{1}{3}} + k_1 \sigma_{cp} + v_{fd}] b_w d + V_{wd}$$

Where:

$$v_{fd} = 0,7 k_f k \tau_{fd}$$

$k_f$  is a factor taking into account the contribution of flanges in a T-section:

$$k_f = 1 + n \left( \frac{h_f}{b_w} \right) \left( \frac{h_f}{d} \right) \leq 1,5$$

$$n = \frac{b_f - b_w}{h_f} \leq 3 \text{ and } n \leq 3 b_w / h_f$$

$\tau_{fd}$  is the design value of the increase in shear strength due to steel fibres:

$$\tau_{fd} = 0,12 f_{Rk4} \approx 0,12 R_{e,3} f_{ctk,fl}$$

$f_{Rk,4}$  is the residual flexural strength at a crack width of 3.5 mm.

$f_{ctk,fl}$  is the characteristic flexural strength of plain concrete

$V_{wd}$  is the contribution of the stirrups to shear strength:

$$V_{wd} = \left( \frac{A_{sw}}{s} \right) 0,9 d f_{ywd}$$

$s$  is the stirrup spacing along the longitudinal axis.

$f_{ywd}$  is the design yield stress of the stirrups

If there are no longitudinal reinforcement bars for flexure the equation is not valid. For such structures it is suggested to use the following formula:

$$V_{Rd} = 0,35 k^{3/2} f_{ck}^{1/2} b_w d$$

$k$  is as defined in last section.

(The Concrete Society, 2007)

### 6.2.3 Model code

In FIB's Model code, there are two formulas for shear capacity; one for fibre reinforced concrete beams with neither tensile reinforcement nor shear reinforcement, and one for beams with fibre reinforcement and tensile reinforcement. (The International Federation for Structural Concrete, 2010)

#### *Beams without tensile reinforcement and shear reinforcement*

For beams with only fibre reinforcement, the capacity formula is given as a limit value of the principal stress,  $\sigma_1$ . By this follows that the axial and shear stresses must be converted to principal stress to control the capacity.

$$\sigma_1 \leq \frac{f_{Ftuk}}{\gamma_F}$$

$f_{Ftuk}$  is the characteristic value of the ultimate residual tensile strength of the fibre reinforced concrete.

$\gamma_F$  is the partial safety factor for the FRC, and may be found in the Model code table 5.6-1 (see table 3).

**Table 3: Partial safety factor for FRC**

Material	Partial Safety factors
FRC in compression	As plain concrete
FRC in tension (limit of linearity)	As plain concrete
FRC in tension (residual strength)	$\gamma_F = 1.5$

#### *Beams without shear reinforcement*

The formula Model code uses for shear capacity in fibre reinforced concrete with traditional tensile reinforcement is quite similar to the one used in the COIN-report. Both formulae use the EC2-formula for shear capacity for regular concrete as a basis, but they incorporate the contribution from the fibre reinforcement in different ways.

$$V_{Rd,F} = \left[ \frac{0,18}{\gamma_c} \cdot k \cdot (100 \cdot \rho_1 \cdot (1 + 7,5 \cdot \frac{f_{Ftuk}}{f_{ctk}})) \cdot f_{ck} \right]^{\frac{1}{3}} + 0,15 \cdot \sigma_{cp} \cdot b_w \cdot d$$

(The International Federation for Structural Concrete, 2010)

### 6.2.3 Beams with openings

For the beams with openings there are no new standard as of today for calculating after Eurocode. For FRC beams with openings there has been very little work done that can be found. In this report the calculations have been done on the basis of the COIN-report as this is the Norwegian suggestion to new calculation rules. The calculations are based on a truss theory.

## 6.3 Design forces

### 6.3.1 Vierendeel theory

In this report beams made of fibre reinforced concrete with openings will be particularly emphasized, and in that context it is usual to find the design shear forces by use of Vierendeel theory. This is a calculation method that can be used on most concrete beams with openings. According to *Betongelementboka bind C* certain conditions must be present for the Vierendeel theory to be applicable: (Betongelementforeningen, 2006)

- The length of the opening is small compared to the span of the beam
  - The beam webs on both sides of the opening can be assumed to have infinite bending stiffness compared to the flanges.
  - Moment and shear force is determined from design forces by the centre of the opening, and is assumed constant over the length of the opening.
  - The inflection point is by the centre of the opening.
- (Betongelementforeningen, 2006)

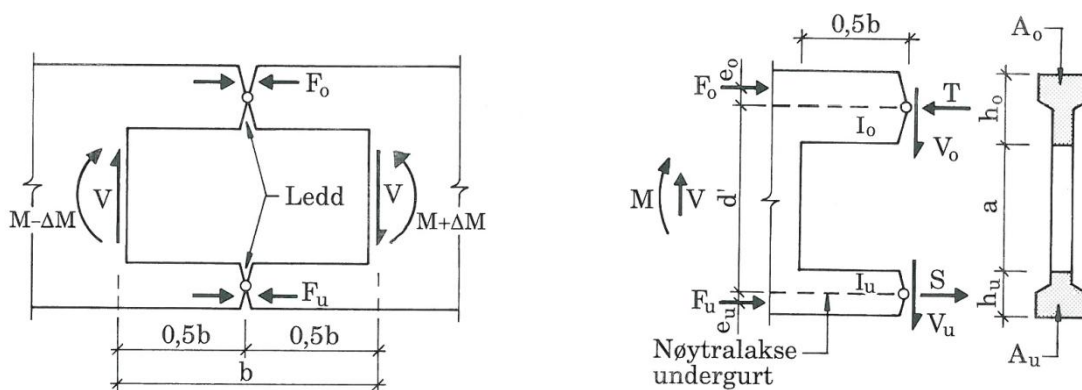


Figure 10: Illustration of the Vierendeel model and the distribution of forces

The basis of the Vierendeel theory is that we assume that the beam parts around the opening is considered to be a Vierendeel truss, with the parts over and under the opening working as flanges. The shear force will be distributed to the upper and lower flanges, depending on the stiffness relation. Figure 10 illustrates the Vierendeel theory.

The tensile force is found by means of moment equilibrium:

$$S \cdot d' = M + F_o \cdot e_o - F_u(d' + e_u)$$

$$S = \frac{M}{d'} + \frac{F_o \cdot e_o}{d'} - F_u(1 + \frac{e_u}{d'})$$

The compressive force is found by axial equilibrium:

$$T = S + F_o + F_u$$



By comparing  $S$  to certain limits, the state of cracking in which the beam is may be decided. When this has been established the design shear force in the upper and lower flanges can be calculated:

$$\text{Fully cracked if:} \quad S \geq 0,5A_u\sqrt{f_{ck}} \rightarrow \begin{cases} V_o = V \\ V_u = 0 \end{cases}$$

$$\text{Partly cracked if:} \quad 0 < S < 0,5A_u\sqrt{f_{ck}} \rightarrow \begin{cases} V_o = V \cdot I_o / (I_o + I_{u,riss}) \\ V_u = V - V_o \end{cases}$$

$$\text{Not cracked if:} \quad S < 0 \quad \begin{cases} V_o = V \cdot I_o / (I_o + I_u) \\ V_u = V - V_o \end{cases}$$

$I_o$  – Moment of inertia for uncracked upper flange

$I_u$  – Moment of inertia for uncracked lower flange

$I_{u,riss}$  – Moment of inertia for cracked lower (tensile) flange (Stadium II moment of inertia). Calculated as described under.

$$\text{Relative height of compression zone: } \alpha = \sqrt{(\eta\rho)^2 + 2\eta\rho} - \eta\rho, \quad \eta = \frac{E_s}{E_{cm}}, \quad \rho = \frac{A_s}{bd}$$

$$\text{Stadium II Moment of inertia: } I_c = \frac{1}{2} \cdot \alpha^2 \left(1 - \frac{\alpha}{3}\right) bd^3$$

(NTNU, 2010)

## 7 Full-scale testing

As of today fibre reinforced concrete is not used in carrying structures commercially. This is mostly because there are no existing official design rules or guidelines available. As these are being worked out there have been a multitude of full-scale experiments carried out in different countries. These help giving an idea of how the fibre reinforcement will work in commercial structural use in the future.

### 7.1 American concrete institute

The American concrete institute has published a series of articles treating this subject. One of these articles describes an extensive study on FRC in buried structures. The testing consisted of full-scale, in-place load tests on precast buried arch structures cast from steel fibre reinforced concrete. All the structures had a fibre content equal to or less than 1% of the volume. The experiments gave very good results, as the ductility of the SFRC allowed the structure to take advantage of soil-structure interaction. The structures proved efficient and economical, and the maximum load they could carry was more than double the required load from AASHTO Standard Specifications for Highway Bridges. The report concludes that the product is a cost effective alternative to box culverts, corrugated metal pipes and plastic detention vaults. (Brodowski, et al., 2010)

Figure 11 and 12 shows the tested structures during the installation at the testing site.



**Figure 11: Storm water detention facility**  
(Brodowski, et al., 2010)



**Figure 12: Arch unit for stream crossing**  
(Brodowski, et al., 2010)

Another article publicised by ACI describes full-scale tests of free suspended elevated slabs. Two identical full-scale tests were carried out with SFRC suspended slabs. The slabs had spans of 3.10 m in each direction, span-depth ratio of 20 and  $45\text{kg/m}^3$  steel fibres. The two tests were independent of each other, one carried out in Belgium and the other in Australia, but they had similar results. The results showed that the slabs had a completely ductile rupture process with deformations along yield lines. The ultimate load appeared to be 3-4 times the initial crack loading and the slabs never punched out before yielding in flexure.

The yield line moment intensity was confirmed by the lab tests with round panel slabs with centre point load which were carried out by ACI. The plates tested had spans of 1500 mm and 2000 mm and thicknesses of respectively 150 and 200 mm. The conclusions of the tests were that the SFRC slabs worked to satisfaction and are a good replacement for slabs with traditional structural reinforcement. Figure 13 shows the test setup for the round slabs. (Destrée, 2010)

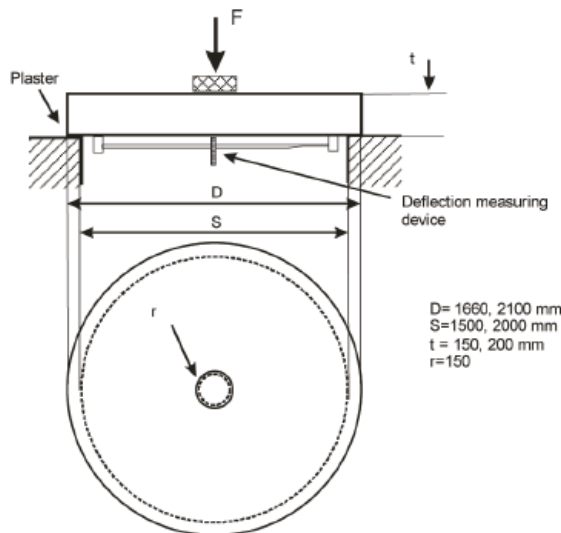


Figure 13: Setup for round panel slab test (Destrée, 2010)

## 7.2 Full-scale tests in Norway

In 2004 the Norwegian Defence Estate Agency built a village of concrete houses in the Rena military training camp. One of these houses was completely made out of steel fibre reinforced concrete and full-scale experiments were carried out on the slabs in the building. A concentrated load was applied on the three slabs which had different reinforcement combinations; slab 1 had traditional steel bar reinforcement, slab 2 had a combination of a minimum of reinforcement bars and fibres and slab 3 had only steel fibre reinforcement. Figure 14 shows the finished SFRC house and figure 15 shows slab 2 after loading.



Figure 14: Finished FRC house (Døssland, 2008)



Figure 15: Slab 2 after testing (Døssland, 2008)

The loading was stopped before the ultimate loading so as not to cause irreparable damage to the building. From the tests it became apparent that 0.8 vol. % of fibres was more than enough to replace all traditional reinforcement. In addition the FRC slab exhibited a satisfactory ductility as the load was increased a long period of time after initial cracking at large deformations. All slabs showed refined crack patterns. The testing showed that fibres may be a good replacement for traditional bar reinforcement for slabs with relatively short spans. The only difficulties that were experienced were that some blocking of the fibres happened during the casting, which made the casting time consuming. (Døssland, 2008)

## 8 Testing methods

### 8.1 Pull-out test of single fibres

The strength of the fibre reinforced concrete is dependent on the bonding between fibre and concrete, and this again is dependent on the fibre and concrete properties as well as the length of embedment. Therefore it's important to have a good testing method to find bond strength for typical combinations between concrete and fibre types, and to what extent the bonding strength depend on the different parameters.

The principle of the test is that one fibre is cast partly into a concrete cylinder, centric and normal to one of the cylinder's end faces. The specimen is then placed into a tensile testing machine with a clamping system for the concrete cylinder and a gripping device for the protruding fibre. A tensile force is applied with a controlled deformation speed, so the fibre is pulled out. Then the relation between loading and slippage is monitored and the stress in the fibre may be calculated at certain slippage measures. These values are then plotted into a curve similar to regular stress-strain curves (Thorenfeldt, 2006). Figure 16 shows a principle drawing of the test.

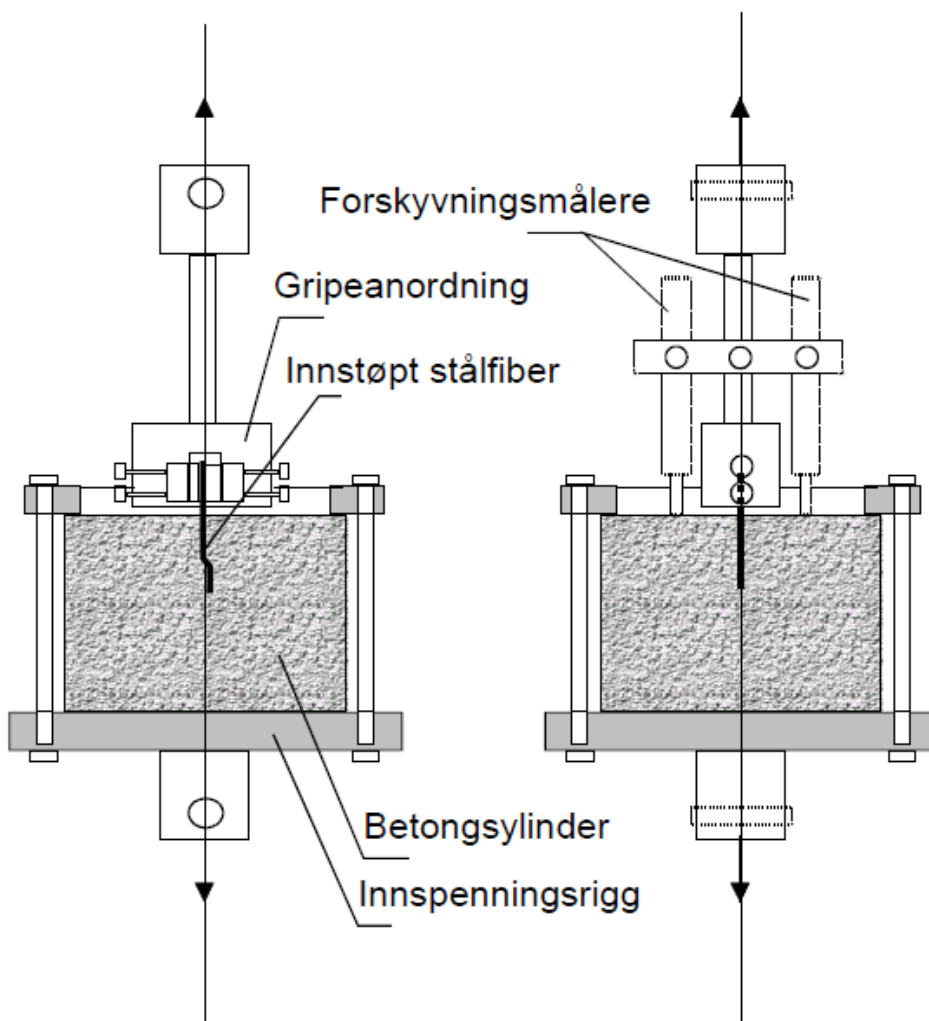


Figure 16: Principle drawing of pull-out test of single fibres (Thorenfeldt, 2006)

## 8.2 Beam tests

### 8.2.1 Norwegian sawn beam test

The Norwegian sawn beam test is a way of finding the residual flexural strength for steel fibre reinforced concrete. The test specimen is subjected to a bending moment by means of roller bearers, and the load is applied with a controlled deformation speed. The test specimen is subjected to moment by two point loads symmetrically placed on the testing beam. The load-deflection relation is registered, and the residual flexural strength by first cracking and the equivalent residual tensile strength by given deflections are calculated.

The testing is performed in a testing machine with accuracy according to NS-EN 12390-4. The testing machine must be able to apply deflection with a constant rate. The load is applied by a rig consisting of a standard beam with two bearing rollers and a load distributing beam with two rollers. One of the bearing rollers must be fixed, the others must be able to roll freely and also be able to rotate about an axis parallel to the test specimen's axis to compensate for possible warping. All the rollers are made out of massive steel with diameter between 20 and 40 mm, and ought to be at least 10 mm longer than the test specimen's width.

Deflection measuring devices is mounted on each side of the beam, although measuring on only one side is acceptable too. Load and deflection should be registered in a computer program.

The test set up is shown in figure 17 (Thorenfeldt, 2006)

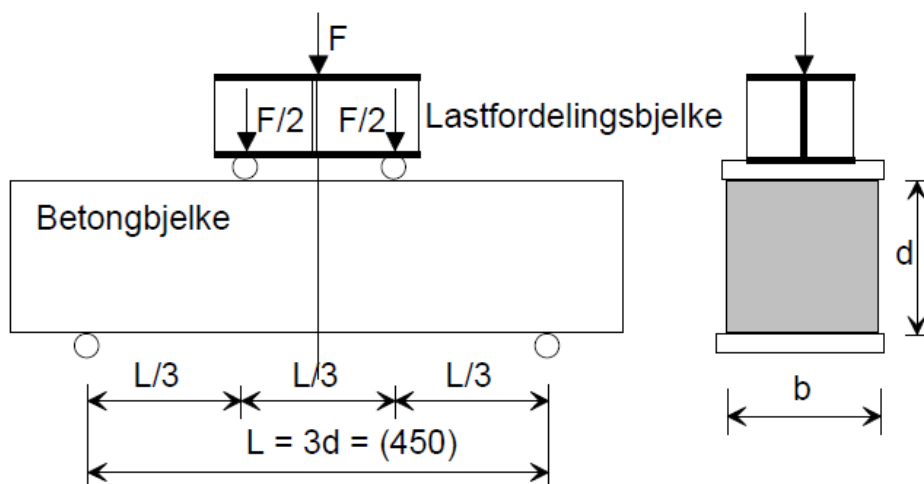


Figure 17: Setup of the Norwegian sawn beam test (Thorenfeldt, 2006)

The test specimens are made by casting plates or wall elements as a panel with dimensions 600x600x150 mm. Three beams with dimensions 150x150x600 mm are then sawn from each panel. The outer 75 mm on each side of the panel is not used. Figures 18 and 19 show the panels from which the testing beams are sawn. The plate elements are cast from the upper end of the central beam while the mould is lying as in the paper plane. The wall elements are

cast from the left hand top corner, and the mould is standing on the bottom end (Thorenfeldt, 2006).

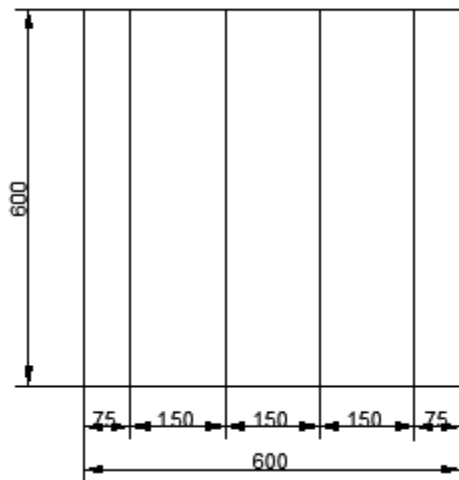


Figure 18: Plate element for sawing out test beams

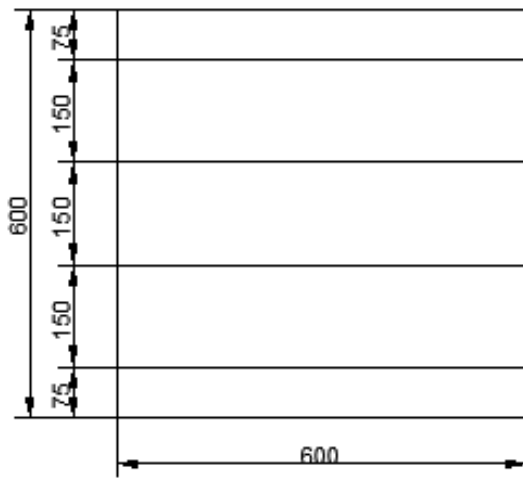


Figure 19: Wall element for sawing out test beams

For the NSBT the cracking of the concrete will happen somewhere between the two point loads. The position of the crack is registered. The main objective of the NSBT is to find the FRC's residual flexural tensile strength, but can also be used to compare different concrete recipes. The advantage with this test is that the casting is done as in real structures, and it's possible to document the in-situ flexural tensile strength. That can be done by using residue concrete that is sawn out of real structures, e.g. windows sawn out from a cast concrete wall (Sandbakk, 2011).

### 8.2.2 NS-EN 14651

As opposed to NSBT the test described in NS-EN 14651 uses only one point load in the middle of the test specimen to create bending moment. The objective of the test is as for NSBT to find the residual flexural tensile strength for the concrete, and create a load-deflection curve.

The test set up is similar to that of NSBT, with two bearer rollers where one of them is free to rotate about its axis. However there is only one roller for the load on top of the beam. This is in the centre of the span, and the roller here must also be able to rotate about its axis. The testing beam also has a notch sawn into it in the bottom of the beam midspan. The set up for this test is shown in figure 20 (Standard Norge, 2005).

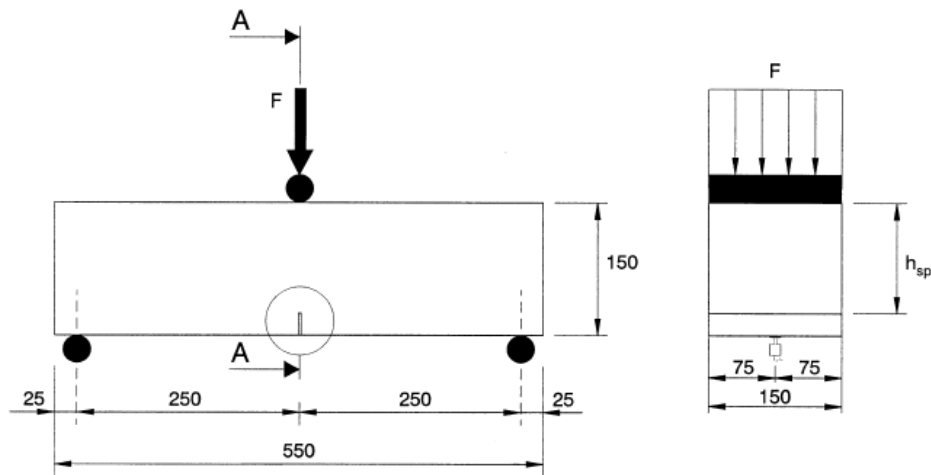


Figure 20: Test setup for the NS-EN 14651-test (Standard Norge, 2005)

The test specimen is a concrete prism with width and height both 150 mm and a length between 550 and 700 mm. The mould should be filled as showed in figure 21 until 90% full, and then compacted while being topped and levelled off. The size of (1) should be twice that of (2) (Standard Norge, 2005). Fibre reinforced SCC does not need compacting.

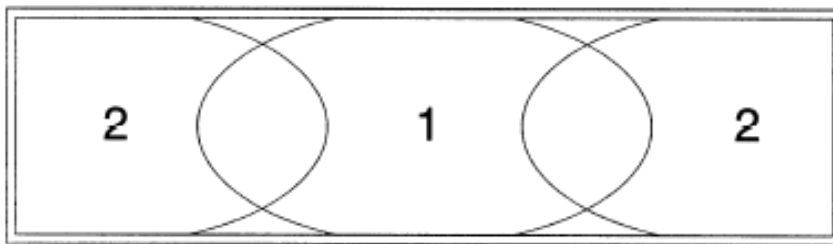


Figure 21: Casting of a NS-EN 14651-test beam (Standard Norge, 2005)

The notch is made by wet sawing the test specimen. It must be sawn through the width at mid-span on the underside of the prism. The width of the notch should be equal to or smaller than 5 mm, and the depth of the notch 25 mm  $\pm$  1 mm. The test specimen must be cured according to NS-EN 12390-2 for a minimum of 3 days after sawing until maximum 3 h before testing (at 28 days).

For the NS-EN 14651 the cracking of the concrete always happens at mid-span due to the notch, as it is at this point the cross-section is the smallest and the bending stresses are the largest. This gives an expected flexural tensile stress at cracking that is larger than the one found in NSBT. The test gives a Load-CMOD curve (Crack Mouth Opening Displacement), but the standard gives a formula for the relation between deflection and the CMOD (Standard Norge, 2005).

$$\delta = 0,85 \cdot CMOD + 0,04$$



The standard also gives a formula for calculating the residual flexural strength, which can then be used to calculate the residual tensile strength:

$$f_{R,j} = \frac{3 \cdot F_j \cdot l}{2 \cdot b \cdot h_{sp}^2}$$

$f_{R,j}$  is the residual flexural strength corresponding with  $CMOD=CMOD_j$  ( $j=1,2,3,4$ )

$F_j$  is the load corresponding with  $CMOD=CMOD_j$

$l$  is the span length [mm]

$b$  is the width of the specimen [mm]

$h_{sp}$  is the distance between the tip of the notch and the top of the specimen [mm]

### **Results from NS 14651-tests**

The NS 14651- test was carried out for 3 standard beams from the concrete mix without fibres and 6 from the fibre reinforced concrete. The results from these tests are presented in the following sections. Figure 22 shows a standard beam in the testing rig.

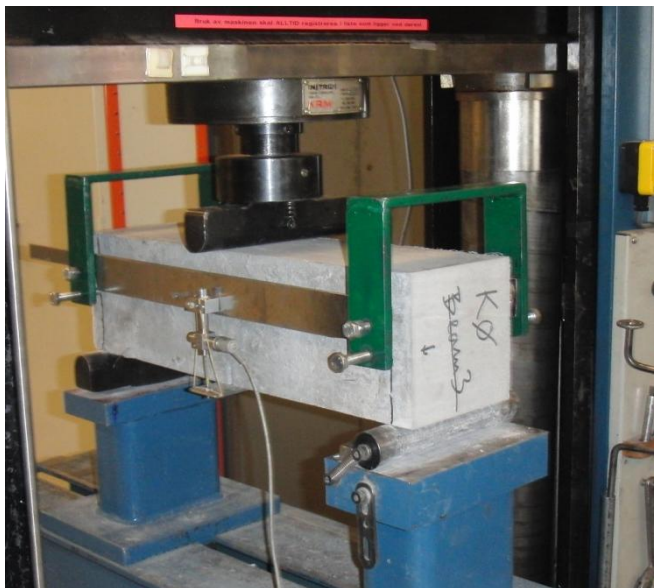


Figure 22: Standard beam in testing rig

#### **Test 1 – concrete without steel fibres**

These results are from the standard beams without fibres which were cast the 8<sup>th</sup> of March. They were tested in week 11. As the reference beams haven't got any fibres there's no residual tensile strength, so only the load-deflection curves and the maximal load is registered. Figure 23 and 24 shows the curves for load-deflection curves each of the beams and the mean curve respectively. The summarized results are shown in table 4. The full overview may be seen in annex 1.

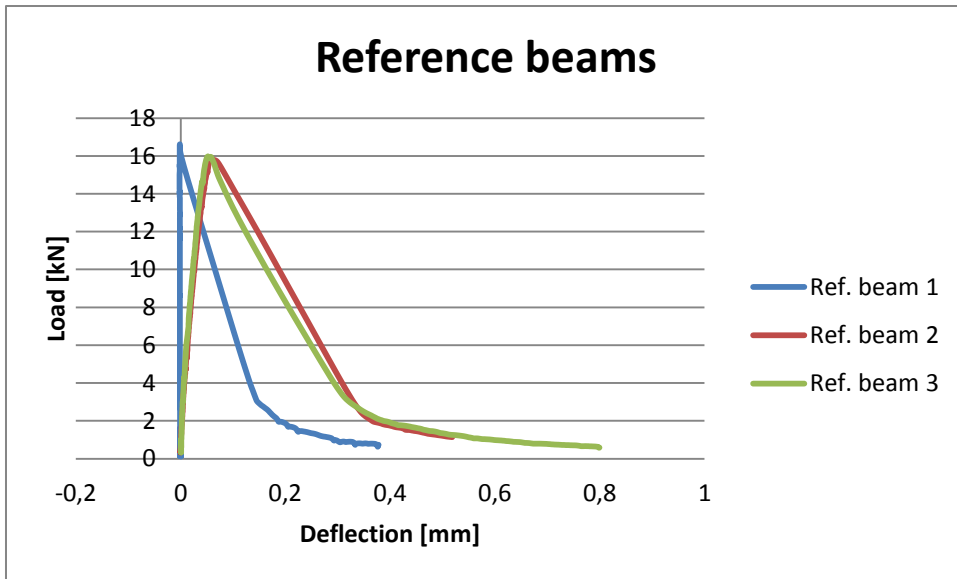


Figure 23: Load-deflection curves for the reference beams

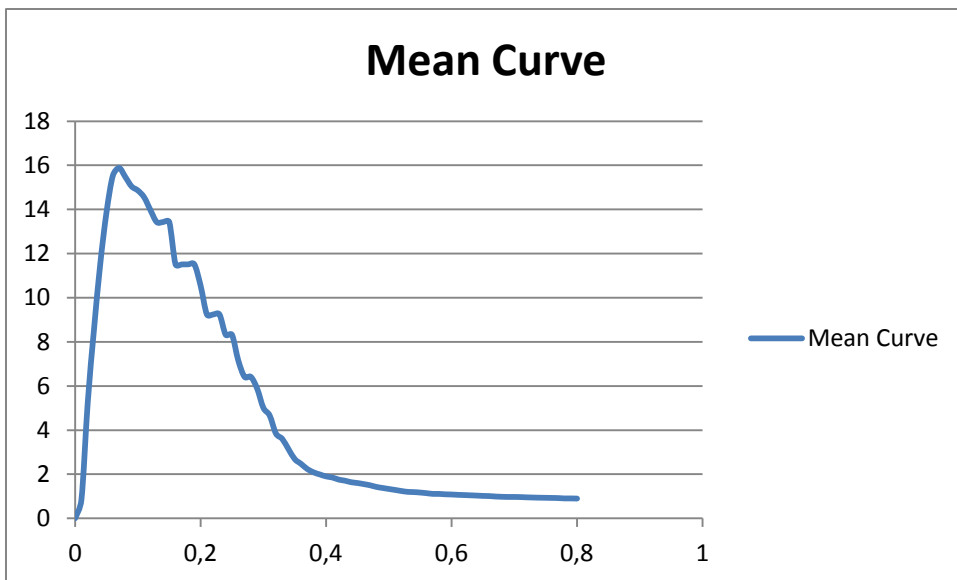


Figure 24: Mean load-deflection curve for the reference beams

Table 4: Results of the NS-EN 14651 test for the reference beams

Summarized						
	Ref_1	Ref_2	Ref_3	Mean value	CoV	
Average Width, b	150,6	150,6	151,35	<b>150,9</b>	mm	0,3%
Average height, h	125,35	125,35	121,65	<b>124,1</b>	mm	1,7%
Length, L	500	500	500	<b>500,0</b>	mm	0,0%
$F_L$	16,6	15,9	16,0	<b>16,2</b>	kN	2,4%

### Test 2 – steel fibre reinforced concrete

The steel fibre reinforced standard beams were cast the 15<sup>th</sup> of March. As the reference beams they were tested in week 11. For these the residual flexural strength is calculated.

Figure 25 shows the resulting load-deflection curves for the beams and table 5 shows the mean values for the calculated residual flexural strength. The full overview may be seen in annex 2.

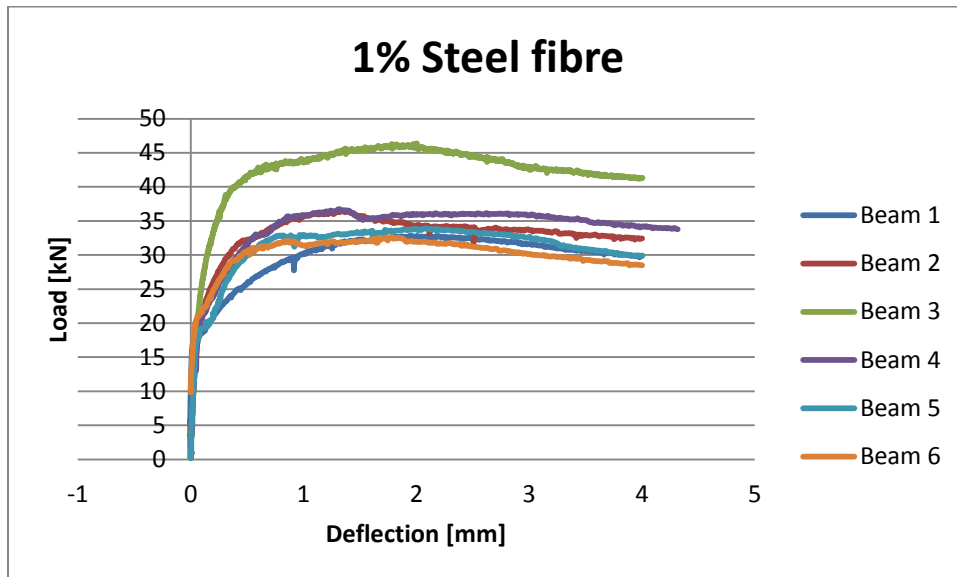


Figure 25: Load-deflection curves for the SFRC beams

Table 5: Results of the NS-EN 14651 test for the SFRC beams

Summarized			
	Mean value	Unit	CoV
Average Width, b	152,0	mm	1,1%
Average high, h	134,0	mm	11,2%
Length, L	383,7	mm	52,5%
$F_L$	20,3	kN	12,6%
$f_{ct,L}^f$	6,4	N/mm <sup>2</sup>	12,5%
$f_{R,1}$	10,3	N/mm <sup>2</sup>	24,3%
$f_{R,2}$	11,8	N/mm <sup>2</sup>	17,9%
$f_{R,3}$	11,7	N/mm <sup>2</sup>	18,8%
$f_{R,4}$	11,3	N/mm <sup>2</sup>	16,7%

As described in chapter 5.3.1 *Residual tensile strength*, the residual tensile strength may be calculated from the residual flexural strength. As  $f_{R,3}$  is calculated for CMOD = 2.5 mm this is the relevant number for the calculation.

$$f_{Rk,3} = f_{r,3} - ks = f_{r,3} - k \cdot \sqrt{CoV} = 11.7 - 1.7 \cdot \sqrt{0.188 \cdot 11.7} = 9.18$$

$$f_{ftk,res2.5} = 0.37 f_{Rk,3} = 0.37 \cdot 9.18 \frac{N}{mm^2} = \underline{\underline{3.40 \frac{N}{mm^2}}}$$

This is quite a bit higher than 1.67 N/mm<sup>2</sup> as found by theoretical calculation in chapter 5.3.1 *Residual tensile strength* and used in the calculations in chapter 11.1 *Pre-testing calculations*.

But as these calculations are pre-testing that is one of the elements of uncertainty. The number calculated here will be used in the post-testing calculations.

### Discussion

Generally it's clear that the fibre reinforced concrete had a higher capacity than the reference beams, which was to be expected as the reference beams have no reinforcement whatsoever. The mean value of the  $F_L$  load for the reference beams was 16.2 kN, while for the FRC beams it was 20.3 kN.  $F_L$  is defined as the maximum load in the interval  $CMOD < 0.05$ , corresponding to  $\delta < 0.08$ .

For both tests all the beams had a similar behaviour. For the plain concrete beams beam 1 turned out to have a bit less ductile behaviour than the two others, and has hardly any deformations until maximum load is reached. But apart from that the three beams act very similarly with almost the same maximum load and corresponding curves after the top has been reached. The reason for the variation may be irregularities in the shape or the sawn notch in the beam.

The FRC beams had a quite different behaviour than the plain beams. They are much more ductile and maintain a good capacity after the maximum load is reached. Here as well the six beams act similarly with the exception of beam 3 which reach a maximum load of about 10 kN more than the rest. As the rest of the beams have very corresponding behaviour it might be a good idea to omit beam 3 in calculations of capacity. The reason for the difference may be irregularities in shape or notch as for the plain beams, but for the FRC beams it may also be that beam 3 happened to have a more beneficial distribution of the fibres than the other beams.

### 8.3 Testing of compressive strength

A way of finding the compressive strength of concrete is to test it according to NS-EN 12390. The principle of this test is to load a specified test piece in a compression testing machine until failure. The largest load is registered and is used to calculate the compressive strength of this particular concrete. The test piece should be a cube, a cylinder or a core. In this thesis cube specimens were used. The load should be subjected perpendicular to the direction of the casting and should be applied by a constant rate of  $0.6 \pm 0.2$  MPa/s until failure. Then the compressive strength is calculated as follows:

$$f_c = \frac{F}{A_c}$$

$f_c$  is the compressive strength, in MPa

$F$  is the maximum load at failure, in N

$A_c$  is the cross-sectional area of the specimen on which the compressive force acts

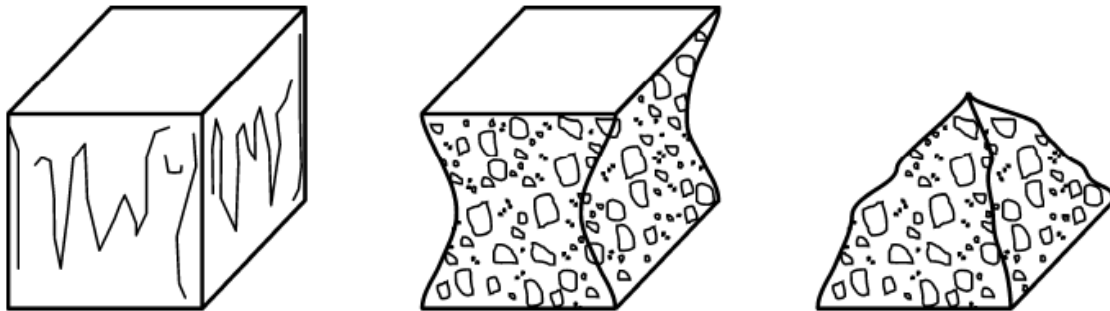


Figure 26: Failures of a cubic test specimen (Standard Norge, 2009)

Figure 26 shows the desired failures of a cubic test specimen.

### Results from cube test

During casting 6 cubes were cast each of the casting days and were later tested. The results from the tests are shown in table 6.

Table 6: Results from the testing of cubic test specimens

Compressive strength (MPa)						
Reference cubes (plain concrete)						
C1	C2	C3	C4	C5	C6	Average
51,0	50,5	51,5	51,5	50,5	48,0	50,5
Steel fibre cubes						
C1	C2	C3	C4	C5	C6	Average
63,0	64,5	63,5	62,0	62,5	63,5	63,2

This is the cube compressive strength for the concrete, and the cylinder compressive strength should therefore be calculated as this is the usual design value. From interpolation from table 3.1 in EC2 (Standard Norge, 2004) the following values are calculated:

Plain concrete:  $f_{ck} = 40.5$  MPa

SFRC:  $f_{ck} = 52.3$  MPa

As shown the real compressive strength of the concrete proved to be quite a bit higher than the assumed  $f_{ck} = 35$  MPa. This is to be expected as the strength of concretes with assumed equal strengths may have different strengths in reality. Therefore the safety rules for concrete require that a low limit is assumed to make the chance of failure as low as is reasonable.

## 9 Casting

The concrete for the testing beams were delivered by Unicon, so there haven't been any trial castings or developing of recipes for this project. Therefore the laboratory work in phase one consisted of binding of reinforcement steel, fresh concrete testing and casting.

### 9.1 Preliminary work

Before the casting was to be carried through some preliminary work had to be done. The reinforcement had to be set up and bound together and the formwork had to be built.

For the beams without fibre reinforcement, the reinforcement was regular with wide stirrups along the length. To make the openings in the beams, a plastic tube with 140 mm diameter was cut in appropriate lengths and put into the formwork. Figure 27 and 28 show the reinforcement for the beam with openings without fibre before and after being put into the formwork. Notice the plastic tubes.



Figure 27: Reinforcement for beam A while being fixed



Figure 28: Reinforcement for beam A after being put into the mould

For the FRC beams the stirrups were made slimmer to make it easier for the fibres to spread evenly throughout the beam. The openings were made the same way as the first time. For the slim reinforcement to be able to stand straight in the formwork, it was bound to each side of the top by steel wire. Figure 29 and 30 show the slim reinforcement before and after being put into the formwork, and the steel wire binding the reinforcement.



Figure 29: Reinforcement for beam B while being fixed



Figure 30: Reinforcement for beam C after being put into the mould

The detailed reinforcement plans for each beam can be seen in figure 31 to 34. For all the beams there is  $2\phi 20$  bars as tensile reinforcement at the bottom of the beam and  $1\phi 20$  as longitudinal reinforcement in top of the beam.

#### Beam A

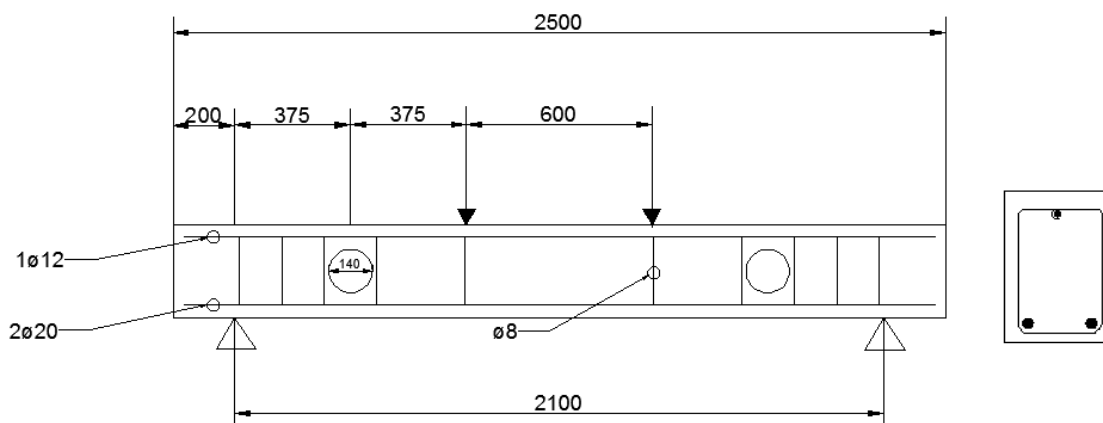


Figure 31: Drawing of the reinforcement in beam A

Beam A is reinforced with 10  $\phi 8$  stirrups with varying distance from about 135 mm near the bearers to 600 in the middle. Between the two loads there will be no shear force and therefore no need for reinforcement. The most important reinforcement stirrups are the ones placed beside the openings, as they must “lift” the shear force over the opening. The shape of the reinforcement is the regular wide stirrups.

## Beam B

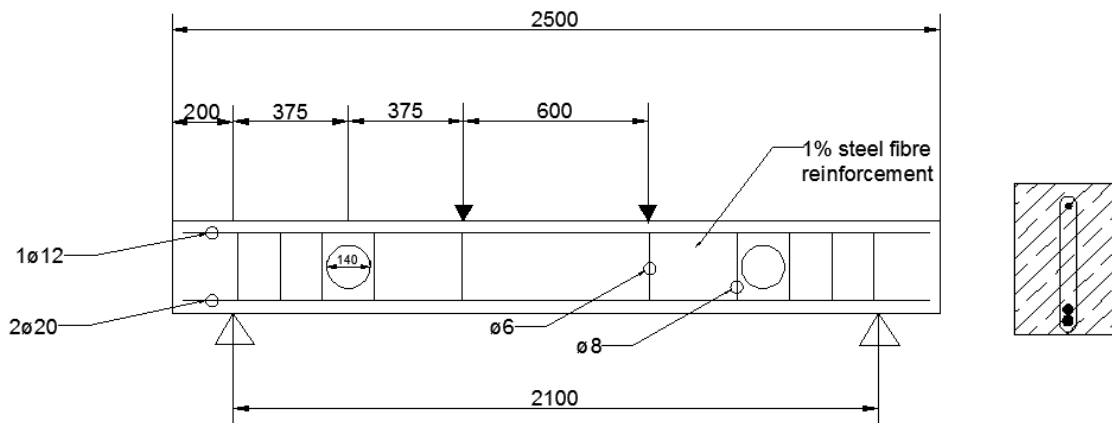


Figure 32: Drawing of the reinforcement in beam B

Beam B has the same number and placement of the reinforcement stirrups, but these are  $\varnothing 6$  stirrups instead of  $\varnothing 8$ . The stirrups beside the openings are still  $\varnothing 8$  to enable “lifting” of the shear force. This beam also has 1 % steel fibre reinforcement of the type Dramix 80/60 delivered by Bekaert. Because of the fibres in the concrete mix the shape of the reinforcement is made slimmer to allow better flowing of the fibres.

## Beam C

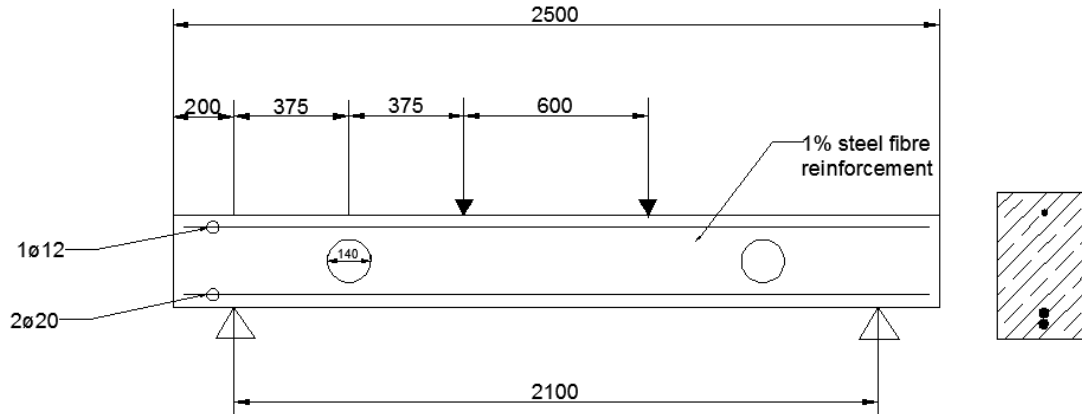


Figure 33: Drawing of the reinforcement in beam C

Beam C had from a strength perspective no traditional shear reinforcement, as all the shear force was meant to be taken by the steel fibre reinforcement. To enable the casting of the beam, however, it was necessary to include some stirrups to ensure that the longitudinal reinforcement were in the right place. These installation stirrups were made of  $\varnothing 6$  bars, but they were placed outside the bearers and between the loads as to ensure that they had as little effect as possible on the strength of the beam. As for beam B the reinforcement bars were placed in centre of the width of the cross section to allow the fibre flow.



## Reference beam

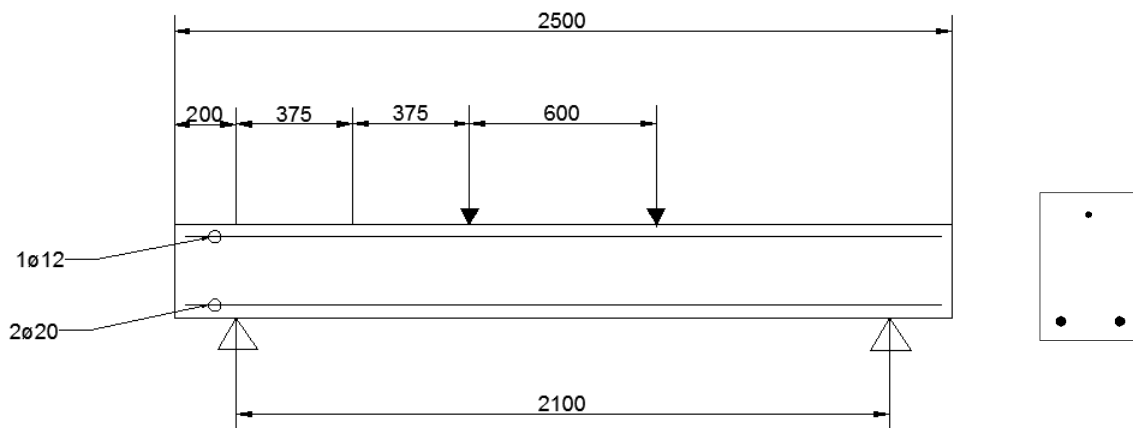


Figure 34: Drawing of the reinforcement in the reference beam

The reference beam does not have openings or steel fibre reinforcement. It was reinforced with the same longitudinal reinforcement as the rest of the beams but had no shear reinforcement. As beam A the reinforcement was placed in the traditional “wide” way, with the 2Ø20 bars placed in each of the bottom corners of the cross-section. As in beam C it was necessary to have installation stirrups to keep the longitudinal reinforcement bars in place. These were made of Ø6 bars and placed in the same way as for beam C to avoid them giving shear strength to the beam.

## 9.2 Materials

The concrete used in the casting was delivered by Unicon and was a C35 concrete. The recipes used are found in annex 3.

The fibres mixed into the concrete the 15<sup>th</sup> of March was from Bekaert and the type was Dramix 80/60. These fibres are steel fibres with end hooks with a length of 60 mm and performance class 80. The specifications for the fibres are shown in table 7

**Table 7: Specifications for the fibres (Bekaert, 2005)**

Name	Bekaert Dramix RC-80/60-BN
Material	Steel
Tensile yield strength	Minimum 1050 MPa
E-modulus	210 000 MPa
Length	60 mm
Diameter	0.75 mm
Surface	Round, smooth with end hooks
Fibres/kg	4600

The full product datasheet may be found in annex 4.

## 9.3 Fresh concrete testing

The fresh concrete was subjected to several tests to establish different properties of the concrete mix.

### 9.3.1 Methods

#### *Slump test*

Before starting the casting, it's important to control whether the fresh concrete has the desired properties for the casting. It is essential that the concrete will be able to spread out and fill all parts of the casting frame. To check this we use a slump test. It consists of filling a standardized cone with fresh concrete, and then lift it carefully straight upwards. When the concrete stops spreading the diameter is measured to see if it is close to what is desired.

Figure 35 shows the standard cone and the process of filling it. It is important to fill from different angles to get an even distribution of the cement paste and the aggregate stones.



Figure 35: Slump test

### *4C Rheometer*

The 4C Rheometer is a more standardized version of the slump test. There is a machine that lifts the cone, and the glass plate on which the concrete spreads has a rough surface, and is lit from underneath. The spreading of the concrete is recorded by a camera, and the information is sent to a computer programme that calculates yield stress, plastic viscosity and  $T_{500}$ . The spreading must be measured manually and written into the programme before it can make all the calculations.

Figure 36 and 37 show the 4C Rheometer.



Figure 36: 4C Rheometer

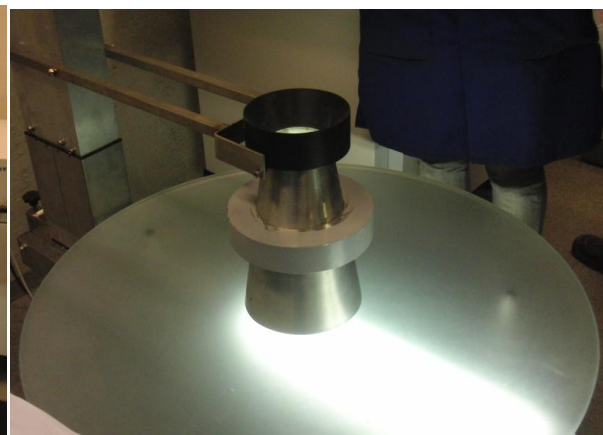


Figure 37: Close-up of the 4C Rheometer

### *LCPC-box test*

The LCPC-box test is a simple way to control the workability of self compacting concrete (SCC). The test consists of pouring a known amount of concrete (6 litres), into a standard box. The dimensions of the LCPS-box can be seen in figure 38 (Roussel, 2007). The concrete

should be poured into the box from one of the ends, and the whole amount of concrete should be poured out in a near constant speed during a period of 30 seconds.

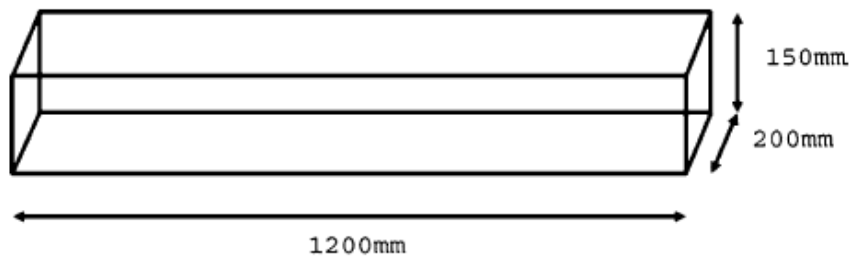


Figure 38: Geometry of the LCPC-box (Roussel, 2007)

After the concrete has been poured into the box, the height  $h_0$  by the pouring end, the length of the spreading on each side and the maximum spreading length should be measured. The shape after the concrete has stopped flowing should be something like the shape in figure 39.



Figure 39: Flow of concrete in the LCPC-box (Roussel, 2007)

### Density check

The density is measured by weighing a container of known volume before filling it with concrete, and then weighing it again, thus finding the weight of the concrete. The container used here could contain 8L. When knowing the volume and the weight of the concrete, the density can be calculated using the following formula:  $\rho = \frac{m}{V}$ .

### Air content

To measure the air content of the concrete an apparatus called FTS - B 2020 is used. The container used in the density check was the same container as the one used in the air content measurements. An air- and watertight lid with a measuring device is clamped on top of the container, and a thin layer of water is filled into the container to form as a piston on top of the concrete when the pressure in the container is heightened. The concrete is compressed, and the measured volume change is equal to the air content. Figure 40 shows the FTS-B 2020 apparatus.



Figure 40: Air content measure, FTS-B 2020 apparatus

## 9.4 Casting and fresh concrete testing

### 9.4.1 1<sup>st</sup> casting day (8<sup>th</sup> of March)

The first casting day the beams without fibre reinforcement were cast, the reference beam without openings and the beam with openings with regular tension and shear reinforcement. The concrete truck from Unicon arrived at 10 in the morning, and a slump test was carried out to establish that the concrete had the desired properties. The initial slump test only measured 36 cm in diameter after the spreading had stopped. This showed that the concrete was much too dry, and more superplasticizer (see chapter 3.3 *Chemical admixtures* for details) had to be added before the casting could proceed. The second slump test gave a spreading diameter of 55 cm, which is acceptable. Figure 41 and 42 shows the first slump test where the concrete was too dry, and the second, after the superplasticizer was added.



Figure 41: Slump test 1

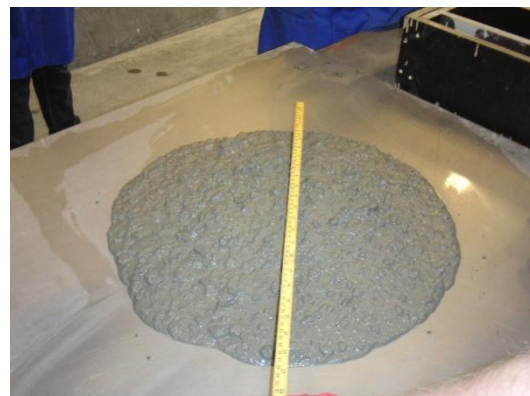


Figure 42: Slump test 2

The casting was carried out satisfactory, and the beams came out as planned. The only potential source of error was that one of the openings in the beam was placed a little too high up, which may decrease the capacity of that beam end. In addition to the large beams 3 standard beams (500 mm) and 6 testing cubes were cast to test the concrete's material properties.

Figure 43 shows the concrete truck and the hopper used to fill the formwork and figure 44 shows the casting in progress (the photo is not of a beam described in this report, but in a parallel master thesis, which was cast simultaneously). Figure 45 shows the beams after finishing the casting.



Figure 43: Hopper used for casting



Figure 44: The casting process



Figure 45: The beams after casting

The 9<sup>th</sup> of March the casting frames were removed, and the concrete beams were covered in wet burlap sacks and put aside for hardening for 4 weeks. Figure 46 and 47 show the beams.



Figure 46: Beam A after removing the formwork



Figure 47: The beams piled for hardening

While the beams were being cast, the fresh concrete tests described above were carried out, and the results are described below.

4C Rheometer:

Table 8: Results of 4C Rheometer-test 1

Time of test	<i>kl.1020</i>
Manually measured spread for correction	<b>55</b>
Yield stress (Pa)	<b>55</b>
Plastic viscosity (Pa·s)	<b>76</b>
Name of the video file (.avi)	83sirianemarte

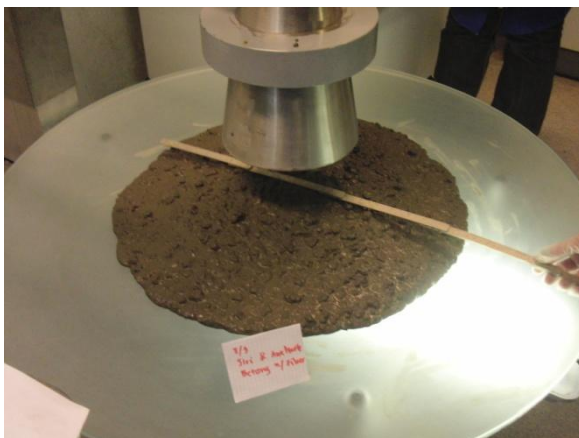


Figure 48: 4C Rheometer-test 1

## LCPC-box:

Table 9: Results of LCPC-box test 1

Time of test	<i>kl.1035</i>
Mass of bucket filled with 6L concrete (g)	<b>14455</b>
Mass of empty bucket, with residual concrete (g)	<b>769,3</b>
Lateral wall spread length 1 (cm)	<b>48</b>
Lateral wall spread length 2 (cm)	<b>51</b>
Maximum spread length (cm)	<b>51</b>
Height at start boundary, h0 (cm)	<b>8</b>



Figure 49: LCPC-box test 1

## Density

Table 10: Density results 1

Time of test	<i>kl. 1047</i>
Mass of concrete (g)	19901
Volume of the container, V (L)	8
Density (kg/m <sup>3</sup> )	<b>2487,6</b>

## Air content

Table 11: Air content result 1

Time of test	<i>kl.1053</i>
Air content (%)	<b>3 %</b>

9.4.2 2<sup>nd</sup> casting day (15<sup>th</sup> of March)

The second casting day the two FRC beams with openings were to be cast, one with a combination of shear reinforcement and fibres and one with only fibres and tensile reinforcement. The concrete truck from Unicon arrived at 10.45 in the morning, and as last time a slump test was carried out to establish if the concrete's workability was satisfactory.



The spreading of the concrete only reached 37.5 cm, and more superplasticizer had to be added to make it more self compacting. 0.3 litre superplasticizer was added to the blend, before it was tested again. This time the spreading reached about 50 cm, still a bit too little but by adding more superplasticizer we would risk separation of the concrete.



**Figure 50: Chute for pouring concrete**

The plan for casting the FRC beams with the dapped ends (the other master thesis), were to start by filling the ends and keep them closed off by plates that were then to be lifted 10 cm to allow the concrete to flow along the bottom of the beam. The concrete would then be filled into the middle. Figure 50 shows the chute that allowed the concrete to pour into both ends of the beam. However, as this method was tried on the first beam it became apparent that the concrete had too little flowability to allow this, and the concrete flowed over the edges of the formwork. Therefore the rest of the beams had to be cast from the middle. This too proved difficult due to the fibres' tendency to lump up and stop the flow, and the concrete had to be worked on continuously to make it flow all the way to the edges. Especially by the openings there were difficulties, and it required some work to get all the beams cast. As the last time 6 standard beams and 6 testing cubes were cast as well. Figure 51 and 52 shows the casting process, as is shown the concrete had to be worked on continuously to be distributed well.



Figure 51: Casting of the SFRC beams



Figure 52: Lumping of steel fibres

The beams came out seemingly as desired, but it's hard to know whether the fibres were distributed in a satisfactory way as the concrete were flowing so poorly. As with the last casting, the holes were a bit uneven and that makes a potential source of error. Figure 53 and 54 show the finished beams piled for hardening.



Figure 53: Beams piled for hardening



Figure 54: Beams piled for hardening

The fresh concrete tests from the 2<sup>nd</sup> casting gave the following results:

#### 4C Rheometer

Table 12: Results from 4C Rheometer-test 2

Time of test	11:05
Manually measured spread for correction	520
Yield stress (Pa)	75
Plastic viscosity (Pa·s)	60
Name of the video file (.avi)	Hanna

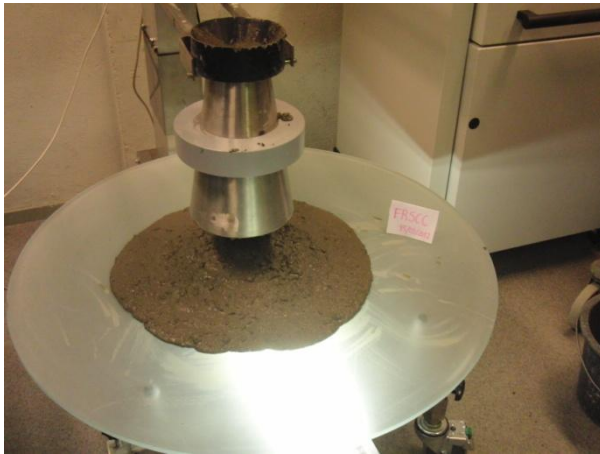


Figure 55: 4C Rheometer-test 2



Figure 56: Measuring the slump

#### LCPC-box

Table 13: Results from LCPC-box test 2

Time of test	11:15
Mass of bucket filled with 6L concrete (g)	14079
Mass of empty bucket, with residual concrete (g)	974,2

Lateral wall spread length 1 (cm)	45
Lateral wall spread length 2 (cm)	45,5
Maximum spread length (cm)	45,5
Height at start boundary, h0 (cm)	7,5



Figure 57: LCPC-box test 2



Figure 58: Measuring the spread length

## Density

Table 14: Density results 2

Time of test	11:25
Mass of concrete (g)	19400
Volume of the container, V (L)	8
<b>Density (kg/m<sup>3</sup>)</b>	<b>2425,0</b>

## Air content

Table 15: Air content results 2

Time of test	11:30
<b>Air content (%)</b>	<b>2,1</b>

## 10 Testing of full-scale beams

### 10.1 Description of setup

The objective of the tests is to examine how the fibre reinforcement influences the shear capacity of beams with openings. The goal is to get a shear fracture at the openings on one of the sides of the beam, to be able to get comparable results from each of the testing beams.

Four beams were to be tested; one reference beam without openings and three with openings, one with traditional stirrup reinforcement, one with a combination of stirrups and fibre reinforcement, and one with only fibres as shear reinforcement. All beams had traditional longitudinal reinforcement which was doubled compared to the necessary amount to ensure that the beam would break in shear and not in moment. Details of the reinforcement in each beam may be found in chapter 9 *Casting*.

The test was carried out as a four point test with symmetrical loading, with two equal loads applied on top of the beam with an internal distance of 600 mm. This gave the ends with the openings the same amount of load. The test setup is demonstrated in figure 59.

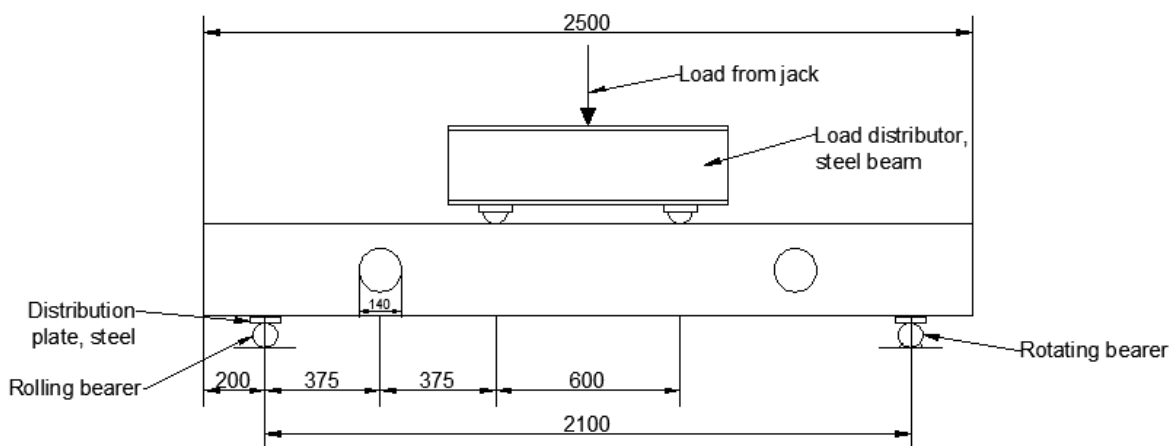


Figure 59: Test setup for full-scale beams

As shown in the figure the bearers are located 200 mm from each side of the beam. The bearers are made from steel pipes where the right one is welded to the foundation to allow rotation of the beam but not displacement whereas the left steel pipe bearer is allowed to roll freely on its foundation. This simulates a freely supported beam and prevents axial forces from appearing. The load distributing steel beam on top is made from two channel sections welded together, and is supported by two freely rolling solid steel half cylinders. These allow the load to be equally distributed as two symmetrical point loads. The cylinders are placed on top of fibre plates with small steel plates on top. The fibre plates will compensate for inaccuracies in the surface of the concrete beam. The steel beam and the cylinders give the beam an additional loading of 50 kg (0.5 kN) which may be of interest

when calculating. The load is applied by a hydraulic jack that can cause up to 1000 kN load. The photo in figure 60 shows beam B after being installed into the testing rig.



Figure 60: Beam B in the testing rig

The test also required sensors to measure displacement in different areas of the beam. There was a deflection gauge placed underneath in the middle of the beam to measure the deflection midspan. For the beams with openings there were installed LVDTs (linear variable differential transformer) beneath each opening on each side of the beam, four LVDTs in total. These were going to measure the crack-openings around the holes as the beams were expected to break there. As the fracture would happen both over and under the opening it was desirable to have LVDTs over the openings as well, but there weren't more available in the laboratory. Figure 60 shows how the LVDTs were placed and figure 62 shows possible fracture patterns for the beam.

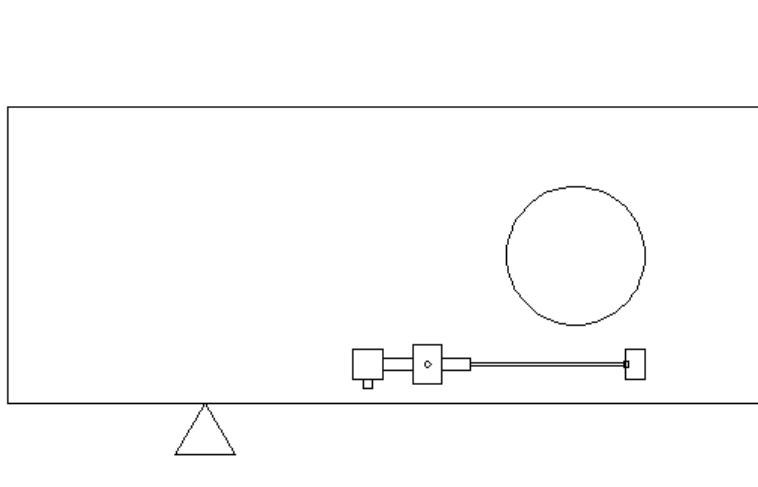


Figure 61: Placement of LVDTs

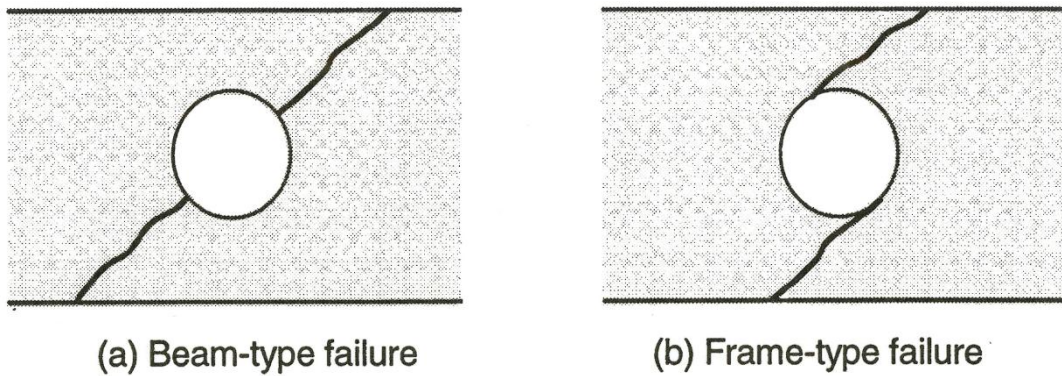


Figure 62: Two modes of shear failure at openings (Mansur, et al., 1999)

As the LVDTs are placed horizontal and the cracks will be angled the registered values has to be recalculated to describe the real crack openings. The formula is shown beneath and figure 63 illustrates the calculation.

$$\frac{w}{w^*} = \sin \varphi \rightarrow w = w^* \cdot \sin \varphi$$

Where  $w^*$  is the registered value and  $w$  is the real crack opening.  $\varphi$  is the crack angle.

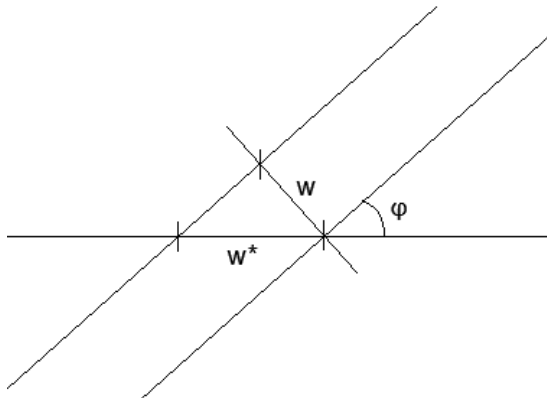


Figure 63: Calculation of real crack opening

## 10.2 Procedure

The test specimens are loaded with a constant displacement from the jack at 3 mm/min or 0.05 mm/s. At fairly regular intervals the jack is stopped to enable checking and drawing of cracks. In the start of each test the machine was stopped at every 20 kN load interval, and near the end the intervals were reduced to 10 kN. When the jack was stopped the load level would decrease a bit as the beam yielded a little, and that can be seen quite clearly in the resulting diagrams. However, this does not affect the results much. Figure 64 shows an example of drawing of the cracks. The cracks are numbered after in which interval they formed.

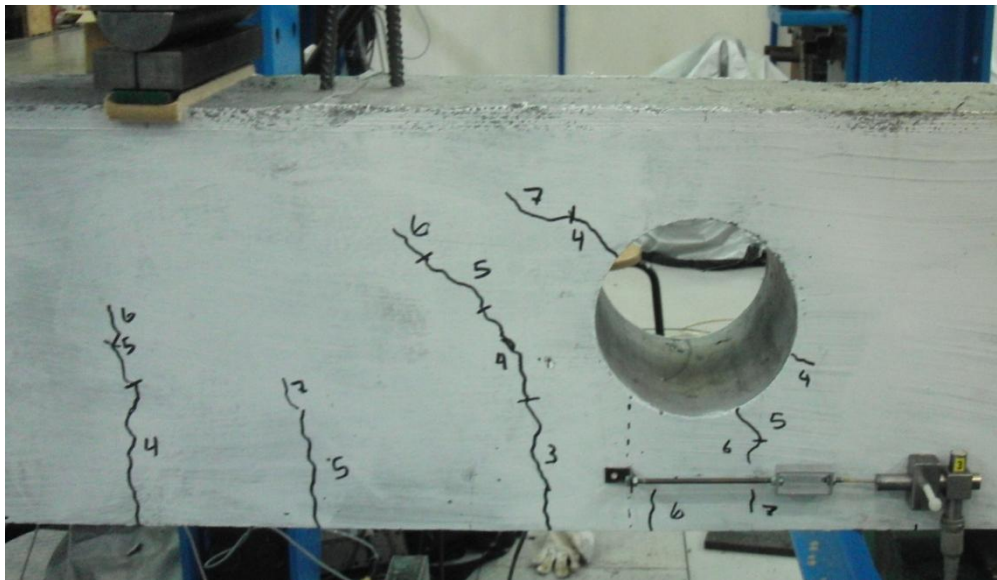


Figure 64: Drawing of cracks on the beam

The figure also shows the transformer described over, glued beneath the opening. The four transformers and the deflection gauge glued underneath the beam measured the displacement on the various places and this was registered by the computer.



### 10.3 Test results

The testing curves from all the full-scale beam tests are shown in figure 65. The diagram shows the force-displacement curves. Details from each of the tests is described in the following sections

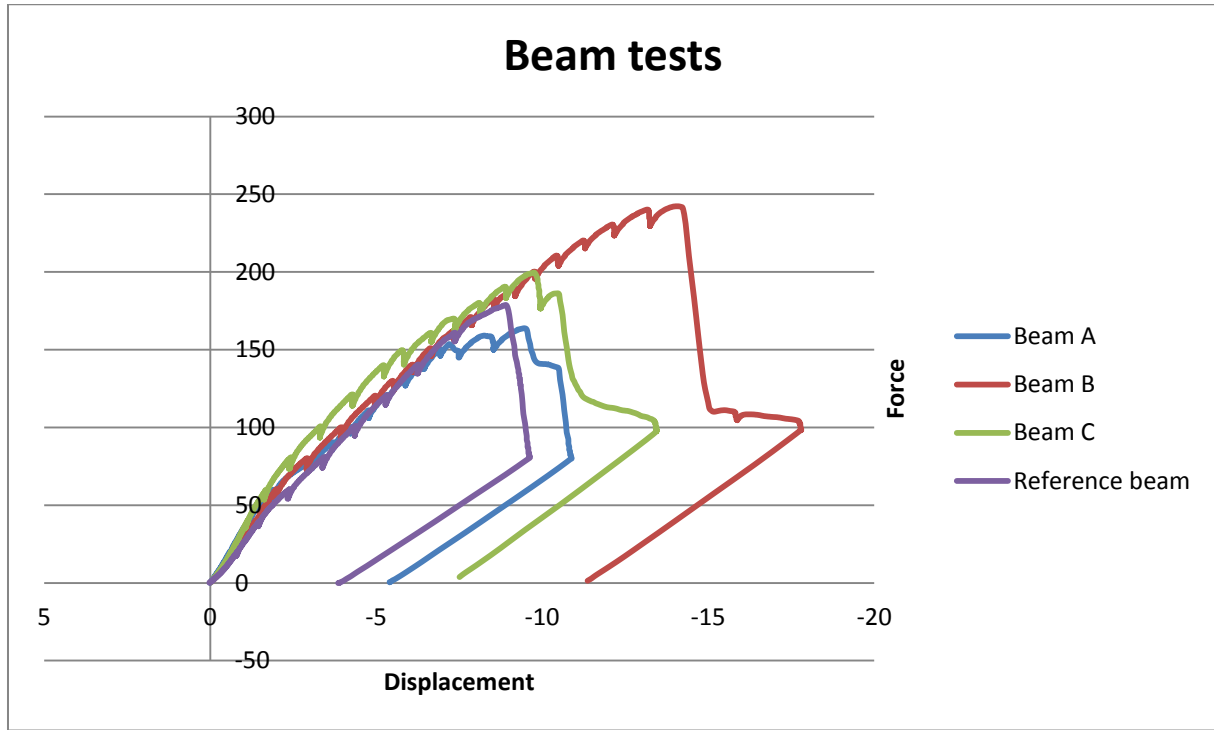


Figure 65: Force-displacement curves for all the beams

From this combined diagram it's evident that the behaviour of the beams up to fracturing is quite similar for all four beams. They follow nearly the same almost straight curve to start with, but they fail at different force levels, and the two fibre reinforced beams have some residual strength after fracture has occurred.

The small drops in the curves are due to pausing of the machine to register cracking.

### 10.3.1 Stiffness of beams

To compare the stiffness of the beams the straight parts of the force-displacement curves are shown in figure 66. The stiffness may be calculated as the slope of a straight line from zero to a deflection of about 2.5 mm. The deflection is measured halfway between the bearers of the beam. As the curve shows, the stiffness is similar for all the beams. In table 16 the stiffness of each beam is calculated.

Table 16: Stiffness of the beams

Beam A	28.31 kN/mm
Beam B	28.71 kN/mm
Beam C	31.72 kN/mm
Ref.beam	24.40 kN/mm

The calculated stiffness for the beams seems a bit illogical. For beams with traditional reinforcement the reinforcement bars should not have any influence of the stiffness, but the fibres in FRC should have some effect. Therefore it's a bit unexpected that beam A and beam B has got about the same stiffness while beam C has got a bit higher. The expected result would be that beam B and C had about the same stiffness which was a bit higher than that of beam A. Another strange result is that the reference beam has got so much lower stiffness than beam A as neither of them has got fibre reinforcement. A possible explanation for this is that there are some irregularities in the concrete and the fibre distribution that causes weaknesses in some of the beams.

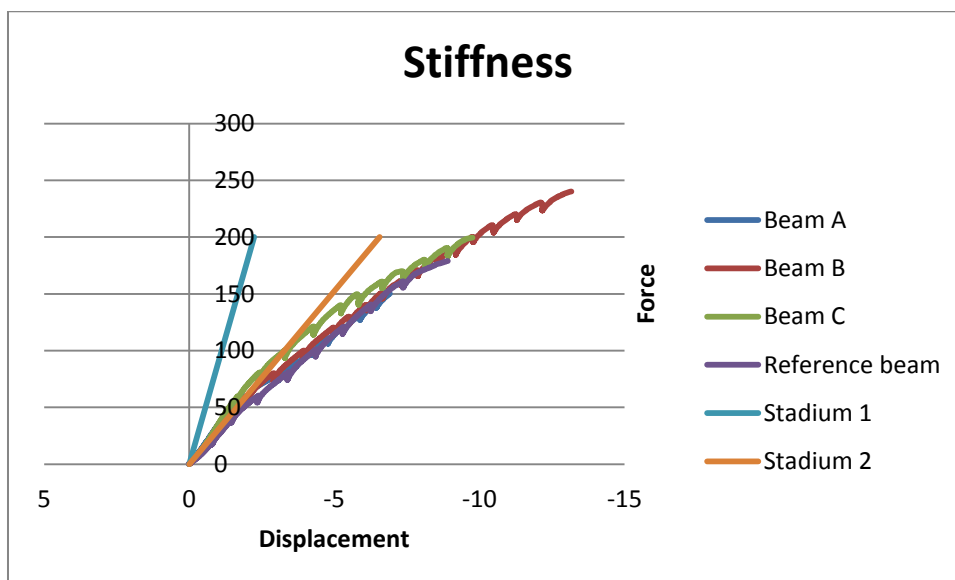


Figure 66: Stiffness of the beams

### Theoretical stiffness

As a means of comparison the theoretical stiffness for stadium 1 (uncracked cross-section) and 2 (cracked cross-section) are calculated. The real stiffness should be between the two, probably closest to the stadium 2 calculation.

Figure 67 shows the real moment diagram for the beam ( $M_0$ ) and the moment diagram for the beam loaded with a unit load  $\tilde{P} = 1$  ( $M_1$ ). By using the unit dummy load method the displacement midspan can be found.

$$a = 750 \text{ mm}$$

$$L = 2100 \text{ mm}$$

$$E_c = 34\,000 \text{ N/mm}^2 \text{ (Standard Norge, 2004)}$$

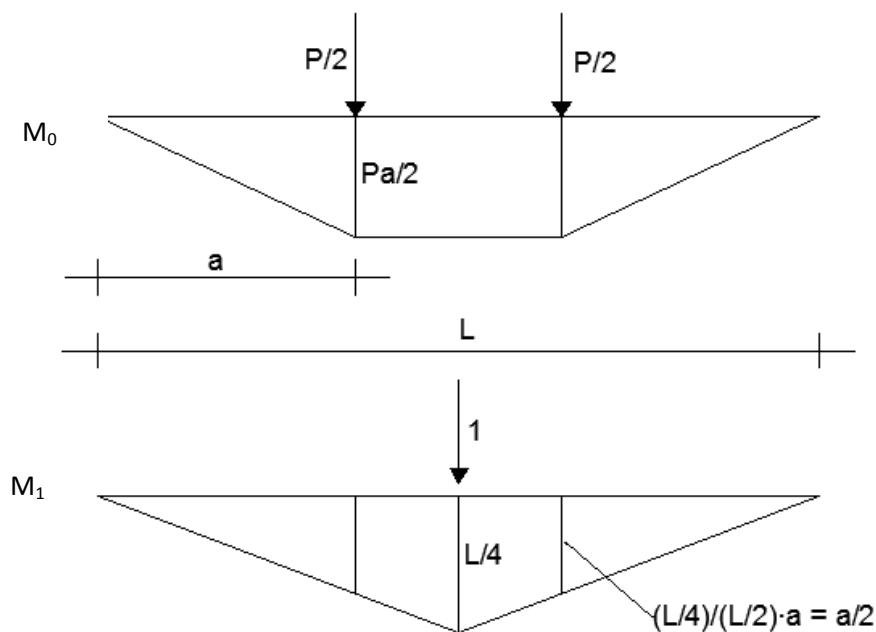


Figure 67: Unit dummy load method

$$\delta = \int_0^L \frac{M_0 M_1}{EI} dx = \frac{Pa}{2EI} \cdot 2 \left[ \frac{1}{3} \cdot 1 \cdot \frac{a}{2} \cdot a + \frac{1}{2} \cdot \left( \frac{a}{2} + \frac{L}{4} \right) \cdot 1 \cdot \left( \frac{L}{2} - a \right) \right]$$

$$\delta = \frac{P}{EI} \cdot 750 \cdot \left[ \frac{1}{6} \cdot 750 \cdot 750 + \frac{1}{2} \cdot 900 \cdot 300 \right] = \frac{P}{EI} \cdot 1.7156 \cdot 10^8 \text{ mm}^3$$

### Stadium I:

For stadium I the moment of inertia is calculated by the standard mechanical formula:

$$I_I = \frac{1}{12} \cdot b \cdot h^3 = \frac{1}{12} \cdot 200 \cdot 300^3 = 450 \cdot 10^6 \text{ mm}^4$$

$$EI_I = 34\,000 \cdot 450 \cdot 10^6 = 1.53 \cdot 10^{13} \text{ Nmm}^2$$

Setter P = 200 kN:

$$\delta = \frac{200 \cdot 10^3 N}{1.53 \cdot 10^{13} \frac{N}{mm^2}} \cdot 1.7156 \cdot 10^8 mm^3 = \underline{2.24 mm}$$

$$k = \frac{P}{\delta} = \frac{200 kN}{2.24 mm} = \underline{89.3 \frac{kN}{mm}}$$

Stadium II:

For stadium II the moment of inertia is calculated with the formulas described in chapter 6.3.1 *Vierendeel theory*.

$$\eta = \frac{E_s}{E_c} = \frac{200\,000 MPa}{34\,000 MPa} = 5.882, \quad \rho = \frac{A_s}{bd} = \frac{628.3 mm^2}{200 mm \cdot 260 mm} = 0.012$$

$$\eta\rho = 0.0711$$

$$\alpha = \sqrt{(\eta\rho)^2 + 2\eta\rho} - \eta\rho = \sqrt{0.0711^2 + 2 \cdot 0.0711} - 0.0711 = 0.31259$$

$$I_{II} = \frac{1}{2} \alpha^2 \left(1 - \frac{\alpha}{3}\right) b \cdot d^3 = \frac{1}{2} \cdot 0.31259^2 \left(1 - \frac{0.31259}{3}\right) \cdot 200 \cdot 260^3$$

$$I_{II} = 153.84 \cdot 10^6 mm^4$$

$$EI_{II} = 34\,000 \cdot 153.84 \cdot 10^6 = 5.23 \cdot 10^{12} Nmm^2$$

Setter P = 200 kN:

$$\delta = \frac{200 \cdot 10^3 N}{5.23 \cdot 10^{12} \frac{N}{mm^2}} \cdot 1.7156 \cdot 10^8 mm^3 = \underline{6.56 mm}$$

$$k = \frac{P}{\delta} = \frac{200 kN}{6.56 mm} = \underline{30.48 \frac{kN}{mm}}$$

The calculated results are drawn into the diagram in figure 66 as a light blue and an orange line. Even though the stadium II stiffness ended up quite close to the measured value, the calculation results were a bit unexpected. The measured stiffness should have been somewhere between the stadium I and stadium II stiffness, and closest to the stadium II stiffness. In the calculations both stiffnesses ended up higher than the measured values. A possible source of error is that the value for the E-modulus is found in Eurocode 2 rather than measured and calculated. The E-modules in EC2 is a bit too high compared to the real E-modules calibrated after Norwegian conditions. By using the formulae from NS3473 the E-modulus will probably be in better accordance with the tests (Standard Norge, 2003).

Steel fibre reinforced concrete:

$$E_{c,f} = 9500 \cdot f_{ck}^{0.3} = 9500 \cdot 52.3^{0.3} = 31\,137 MPa \approx 31\,100 MPa$$

Plain concrete:

$$E_{c,f} = 9500 \cdot f_{ck}^{0.3} = 9500 \cdot 40.5^{0.3} = 28\,838 MPa \approx 28\,800 MPa$$

The  $f_{ck}$ -values are the values found from the experiments described in chapter 8.3 *Testing of compressive strength*.

By using these values we get the following results:

**SFRC:**

Stadium I:  $\delta_1 = 2.45 \text{ mm} \rightarrow k_1 = 81.6 \text{ kN/mm}$

Stadium II:  $\delta_1 = 7.18 \text{ mm} \rightarrow k_1 = 27.9 \text{ kN/mm}$

**Plain concrete:**

Stadium I:  $\delta_1 = 2.65 \text{ mm} \rightarrow k_1 = 75.5 \text{ kN/mm}$

Stadium II:  $\delta_1 = 7.74 \text{ mm} \rightarrow k_1 = 25.8 \text{ kN/mm}$

As is shown this gives better results than the first calculation. The stadium II stiffness is smaller than the calculated values except for the reference beam. But as this result was very incongruous compared to the rest there is reason to believe that the measurements from this beam is wrong or that the beam had an irregularity that decreased its stiffness.

### 10.3.2 Beam A

Beam A was reinforced by traditional stirrups, like the ones commonly used in these beams in buildings today. It had extra stirrups near the openings to help “lift” the shear force over the opening.

The force-displacement curve for beam A is shown in figure 68. As can be seen the curve is almost straight up to about 140 kN, where the failure commences. There is also a slight change of slope at about 50 kN which may be the result of the cracking, and the load bearing changing from concrete to reinforcement. The ultimate failure happens at 163.8 kN, and the capacity drops dramatically from here without much increase in displacement. The machine was stopped at almost 11 mm displacement and the load was removed, as can be seen in the graph.

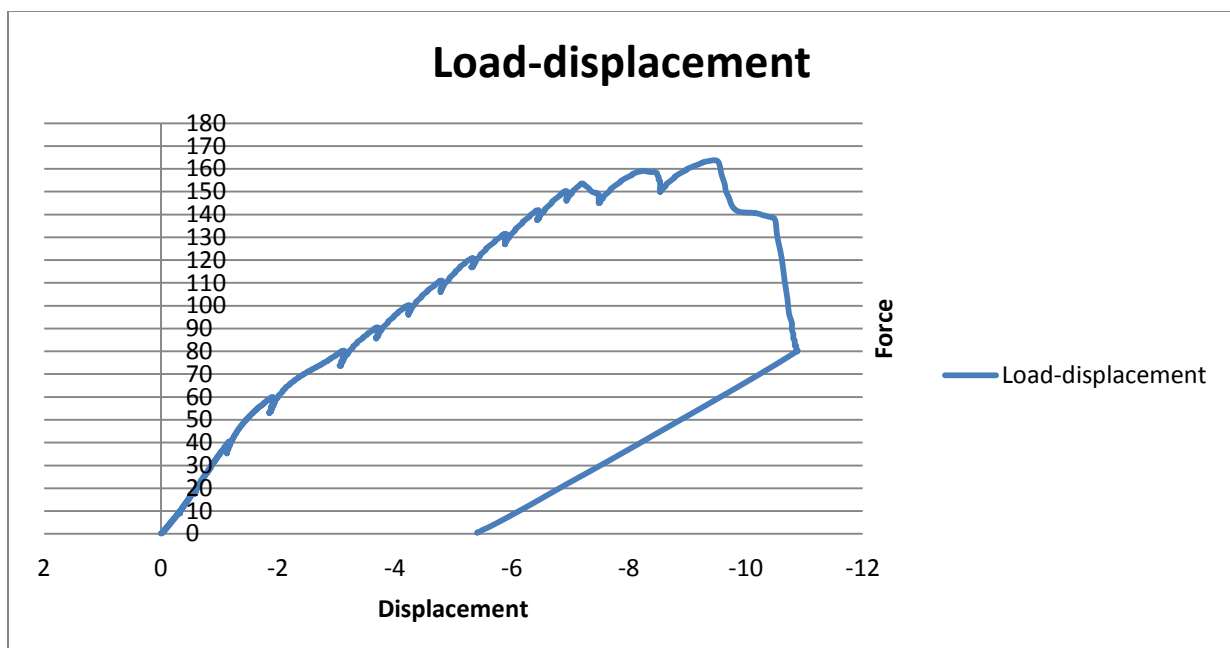


Figure 68: Load-displacement curve for beam A

The following notes in table 17 were made during the testing, for each time the cracks were registered. At each load level when the jack was stopped the cracks were drawn on to the beam to make them more visible and to see which cracks formed when. Figure 69 to 72 shows some of the crack development and figure 73 shows the beam after failure.

Table 17: Crack registration for beam A

Load level	Force	Comments
1	10 kN	No cracking
2	20 kN	No cracking
3	40 kN	Cracks starting to appear
4	60 kN	Development of existing cracks and some new cracking.
5	80 kN	Much more cracks, very visible shear cracking
6	90 kN	Not much development

<b>7</b>	100 kN	Not much development
<b>8</b>	110 kN	Deeper cracks
<b>9</b>	120 kN	Deeper cracks
<b>10</b>	130 kN	Deeper cracks and some new ones
<b>11</b>	140 kN	Development
<b>12</b>	150 kN	Development
<b>13</b>	160 kN	Close to failure



Figure 69: Initial cracking, beam A



Figure 70: Crack development, beam A



Figure 71: Crack development, beam A



Figure 72: Close to failure, beam A

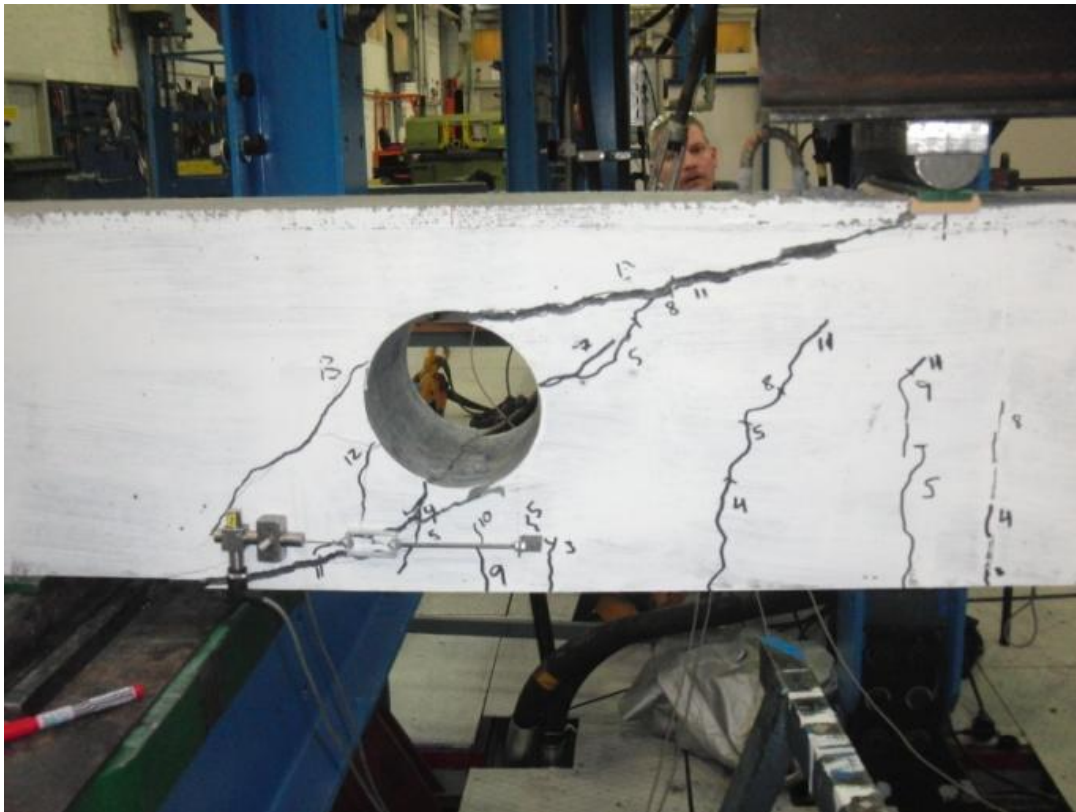


Figure 73: Beam A after failure

The transducers on the beams registered the shear cracking around the openings. The transformers were placed on each side of the beam as the cracking is likely to be different from one side to the other. Figure 74 and 75 shows the cracking by the opening in the north and south respectively. According to EC2 table NA.7.1N (Standard Norge, 2004) the crack width limit for serviceability limit state for regular structures are set to 0.3 mm and that must be taken into consideration when designing structures.

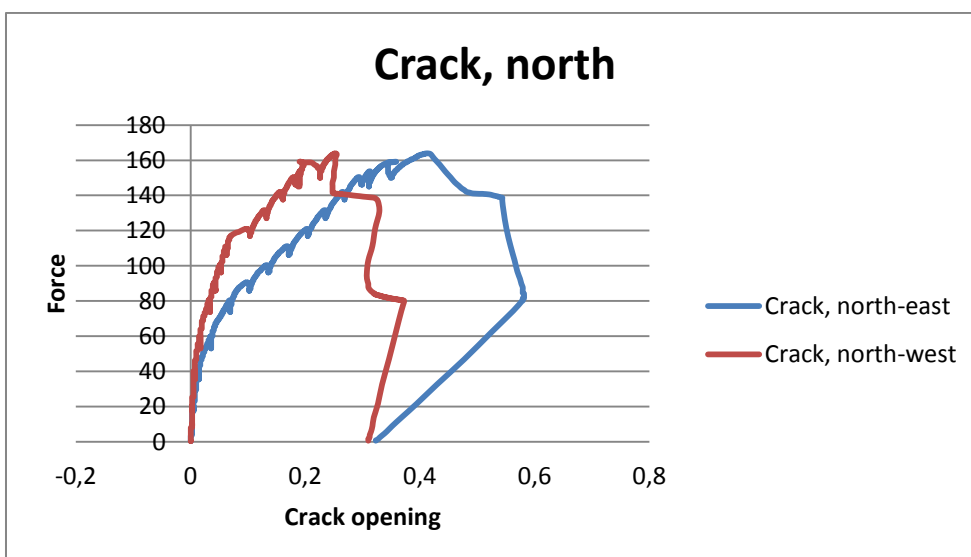


Figure 74: Crack openings for northern opening in beam A



As shown in the diagram in figure 74 the cracks formed in a quite similar way on both sides although they formed quicker and became larger on the east side than west. They follow almost the same pattern up to about 30 kN loading. The largest crack opening at failure is 0.41 mm. This seems a bit low when comparing to the lower cracks in figure 73. From this photo it appears that the upper cracks are larger than the lower ones after failure, and it would be desirable to have LVDTs here as well. The cracks on both sides of the beam became larger than 0.3 mm, and therefore a beam like this would perhaps need to be designed according to SLS. The north-east crack reached the limit at about 150 kN while the north-west crack reached it at about 140 kN although this side had passed the maximum load before this point. For the southern opening the cracks on either side followed the same pattern up to almost 60 kN. Here the two sides don't reach the 0.3 mm limit at the same load. The west side reached about 152 kN while the east side never reached the limit.

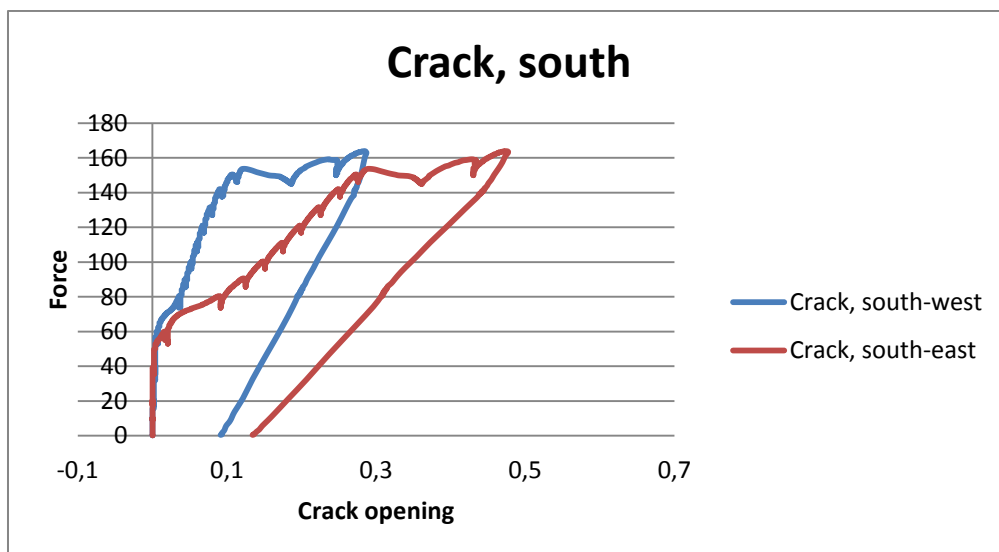


Figure 75: Crack openings for southern opening in beam A

### 10.3.3 Beam B

Beam B was reinforced by traditional stirrups in addition to fibre reinforcement, and is therefore likely to have the highest capacity. As in Beam A there were extra stirrups near the openings to “lift” the shear force over the opening.

The force-displacement curve for beam B is shown in figure 76. As can be seen the curve is almost straight all the way to breaking. There is, as for beam A, slight change of slope at a lower level, this time at about 60 kN. This is probably the result of the cracking, and the load bearing changing from concrete to reinforcement. The definite break happens at 242.2 kN, and the capacity drops dramatically from here without much increase in displacement down to about 110 kN. Here the curve levels out and the beam has a residual capacity between 105 and 110 kN. The machine was stopped at almost 18 mm displacement and the load was removed, as can be seen in the graph.

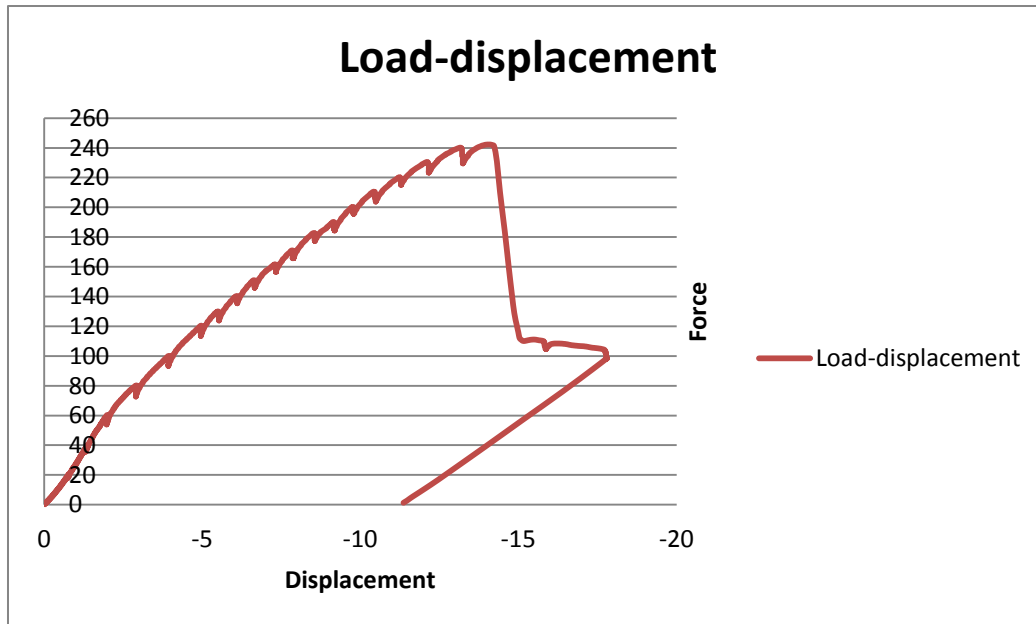


Figure 76: Load-displacement curve for beam B

Table 18: Crack registration for beam B

Load level	Force	Comment
1	20 kN	No cracking
2	40 kN	Tiny cracks along the bottom in the middle
3	60 kN	A bit more cracking, only moment cracks
4	80 kN	Development, some shear cracks
5	100 kN	More development
6	120 kN	Development, some new cracks
7	130 kN	Development
8	140 kN	Development
9	150 kN	Not much development
10	160 kN	New shear crack in the north
11	170 kN	Development
12	180 kN	Development
13	190 kN	Close to failure? Deep cracks
14	200 kN	Nothing new
15	210 kN	Development
16	220 kN	Wider cracks
17	230 kN	Development
18	240 kN	Many new cracks, big shear cracks →very close to failure

Table 18 contains the notes from the testing of beam B. Figure 77 to 80 show some of the stages of cracking and figure 81 shows the beam after failure.

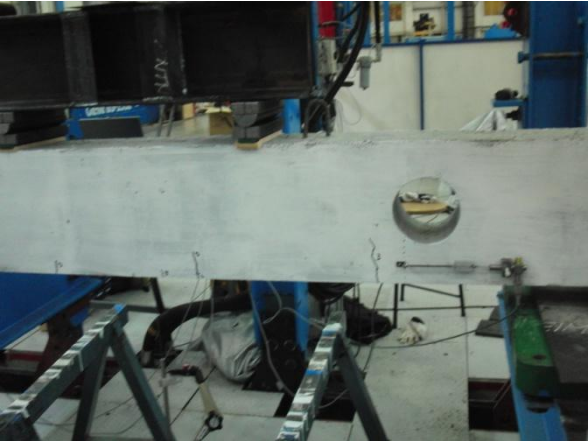


Figure 77: Initial cracking, beam B

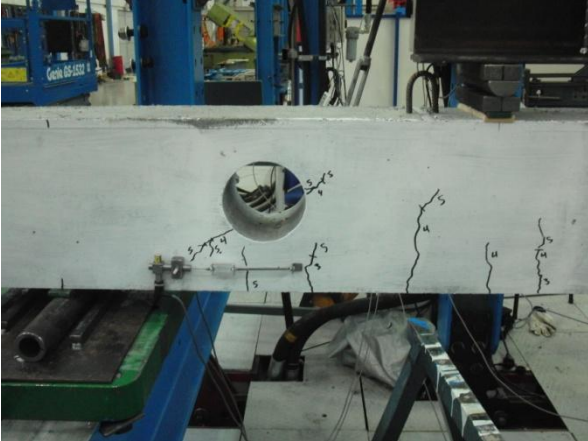


Figure 78: Crack development, beam B

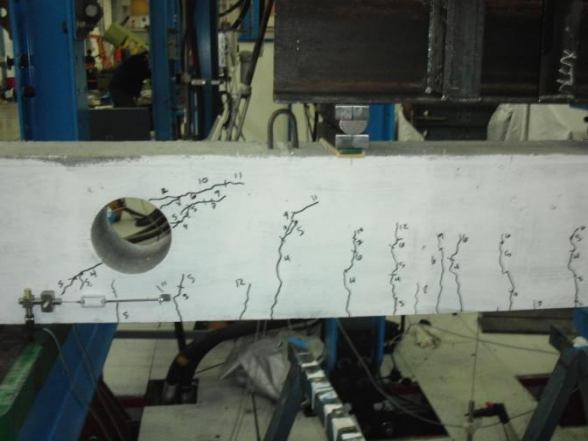


Figure 79: Crack development, beam B

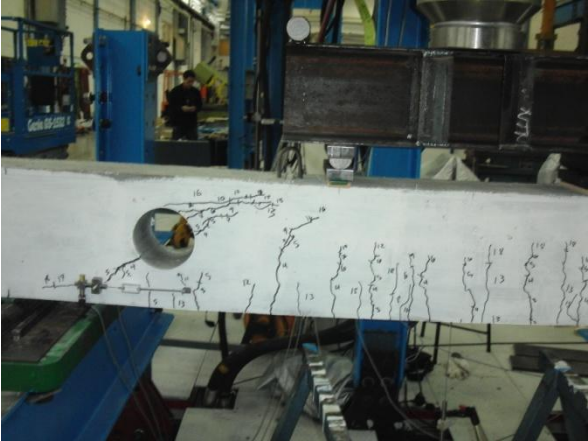


Figure 80: Close to failure, beam B

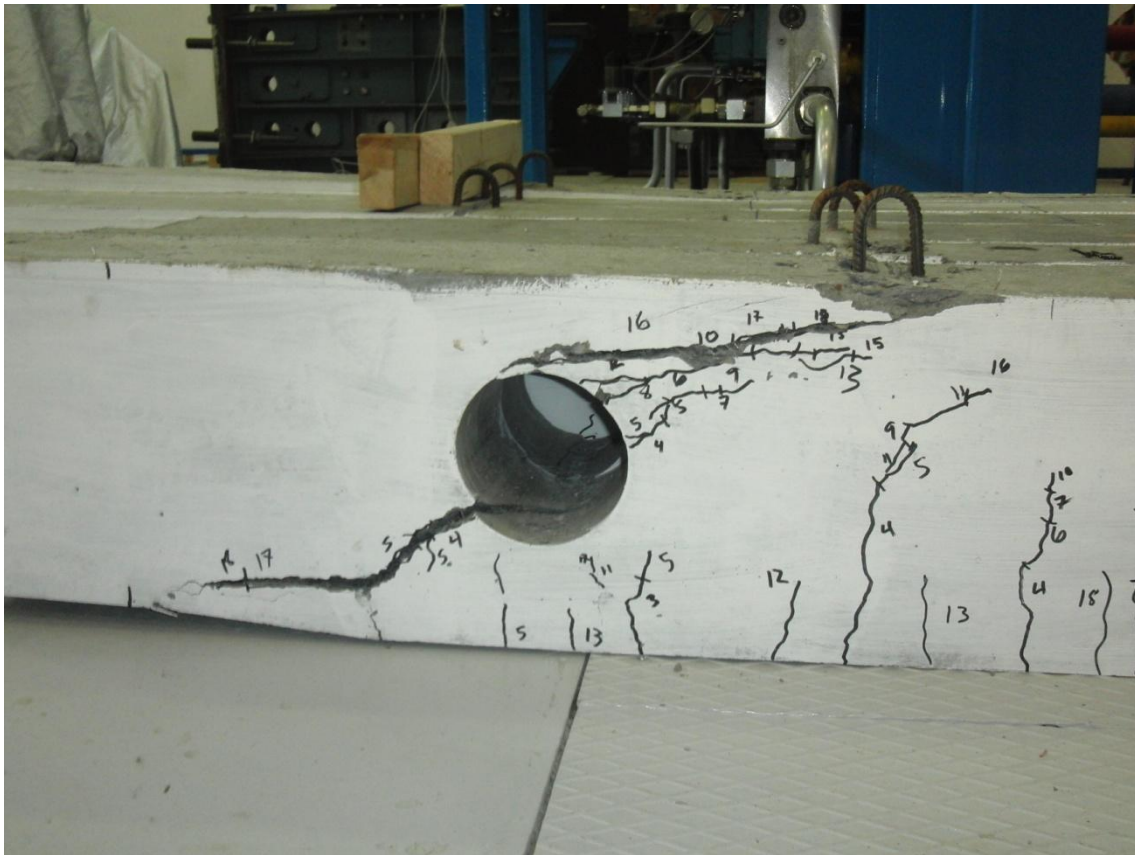


Figure 81: Beam B after failure

As for beam A there were transducers placed beneath the opening on the beams to register the shear cracking. The transformers were placed on each side of the beam as the cracking is likely to be different from one side to the other. Figure 82 and 83 show the cracking by the opening in the north and south respectively. A problem on this beam was that the failure happened outside where the transformers were placed, and these diagrams may therefore be unusable.

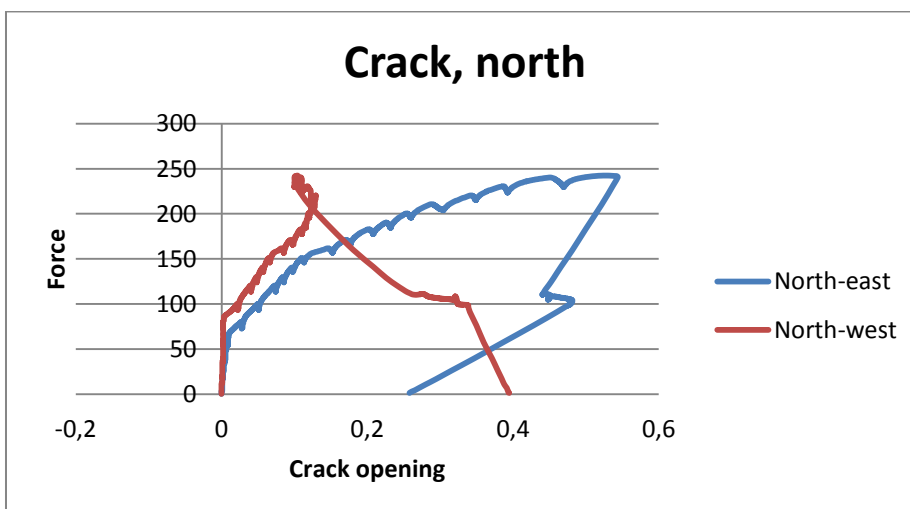


Figure 82: Crack openings for northern opening in beam B

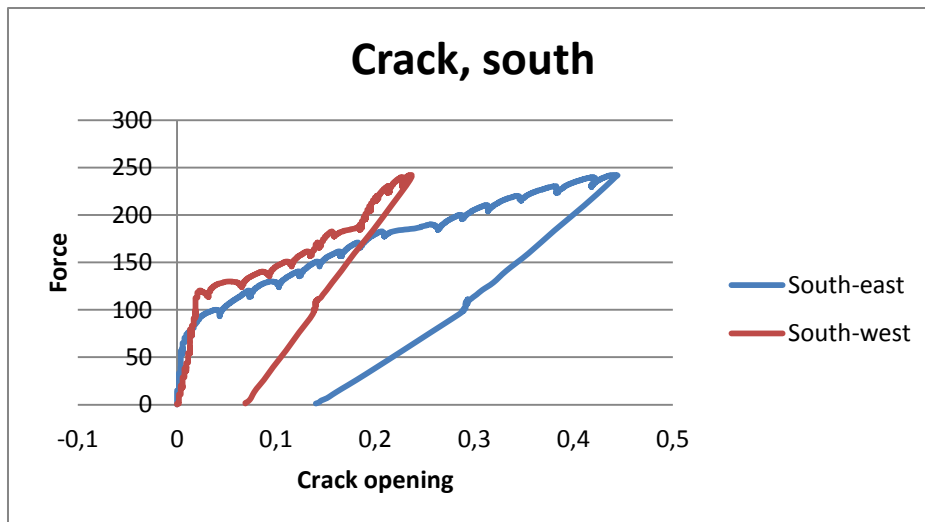


Figure 83: Crack openings for southern opening in beam B

It's quite obvious from the curve in figure 82 from the northern cracks that the red "north-west"-curve is impossible to use. The crack appeared directly behind the glued transformer, which can explain the strange form of the curve. The other curve looks good, and it seems as if the beam reached a crack width of a bit over 0.5 mm before failure. From the photo in figure 81 this seems like a bit too small. This crack reached the 0.3 mm limit at about 210 kN loading.

For the southern cracks the transformer on the west side also missed the largest shear cracks, but here the largest crack was fully outside the end of the transformer and the curve therefore looks reasonable. However, the curve doesn't describe the largest shear cracks on this side and must therefore be ignored. The south-east curve looks better and probably gives a better description on the behaviour. This shows that the crack opening around the southern opening was about 0.44 mm at failure. This seems more reasonable as the failure happened at the northern opening. The crack openings reached the 0.3 mm limit at about 206 kN loading.

#### 10.3.4 Beam C

Beam C only had fibre reinforcement as shear reinforcement, and is therefore likely to have a lower capacity than beam B. Which beam that is the strongest of beam A and C was one of the things that were interesting in this test. In beam C there are no stirrups near the openings to "lift" the shear force, and the steel fibre reinforcement alone must provide this effect.

The force-displacement curve for beam C is shown in figure 84. As for beam B the curve is almost straight all the way to failure. There is, as for both other beams, a slight change of slope at a lower level; here it occurs at about 60 kN. The definite break happens at 199.5 kN, and the capacity drops dramatically from here without much increase in displacement down to about 115 kN. Like for beam B, the curve levels out because of the fibres and the beam

has a residual capacity between 105 and 113 kN. The machine was stopped at just over 13 mm displacement and the load was removed, as can be seen in the graph.

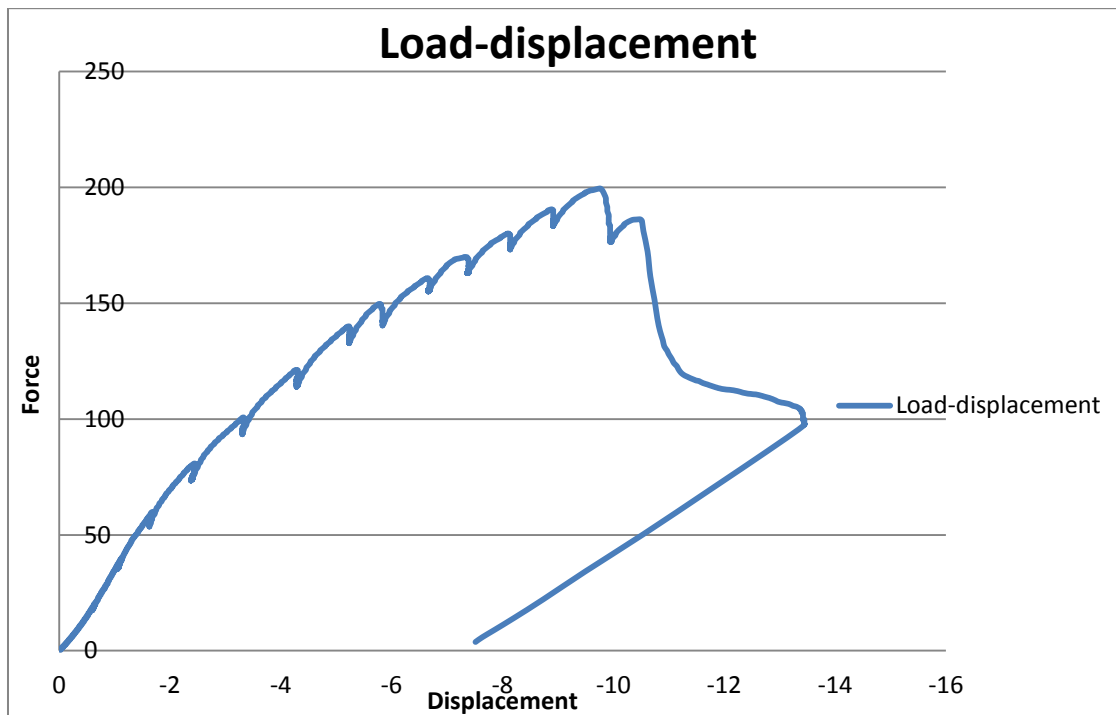


Figure 84: Load-displacement curve for beam C

Table 19: Crack registration for beam C

Load level	Force	Comment
1	20 kN	No cracking
2	40 kN	Small cracks at the bottom in the middle
3	60 kN	Development of existing cracks, a small shear crack in the north
4	80 kN	Development, commencing of shear cracks in the south
5	100 kN	Development, some new cracks
6	120 kN	Development, some new cracks
7	140 kN	Development, some new cracks
8	150 kN	Not much development
9	160 kN	Development, some new moment cracks
10	170 kN	Big shear cracks by the north opening
11	180 kN	Widening of shear cracks
12	190 kN	Widening, small cracks above the openings. Close to failure

Table 19 contains the notes from the testing of beam B. Figure 85 to 88 show some of the stages of cracking and figure 89 shows the beam after failure.



Figure 85: Initial cracking, beam C

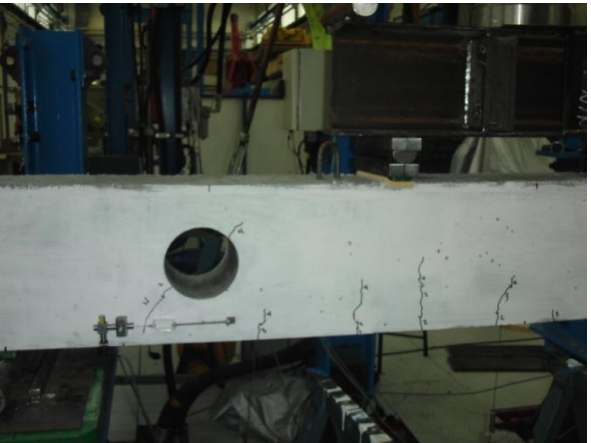


Figure 86: Crack development, beam C

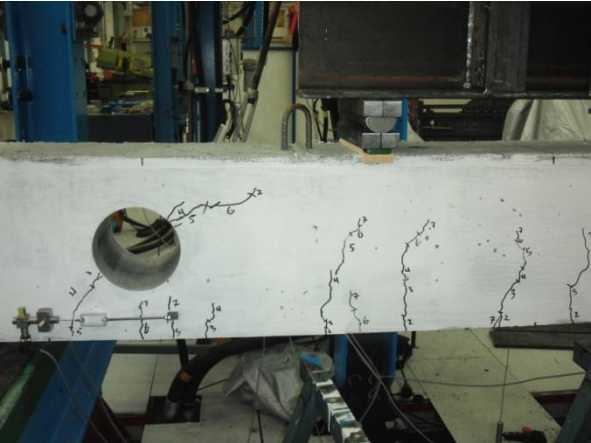


Figure 87: Crack development, beam C

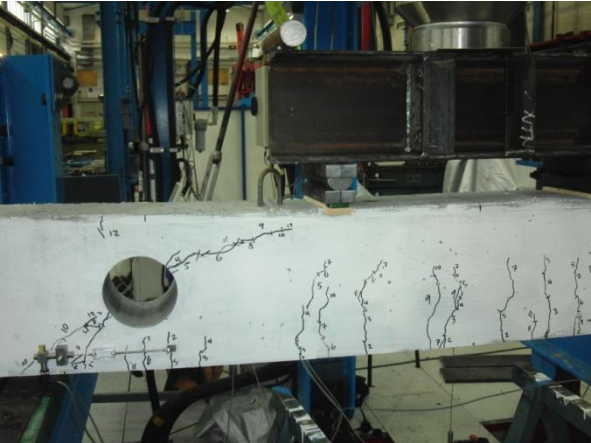


Figure 88: Close to failure, beam C

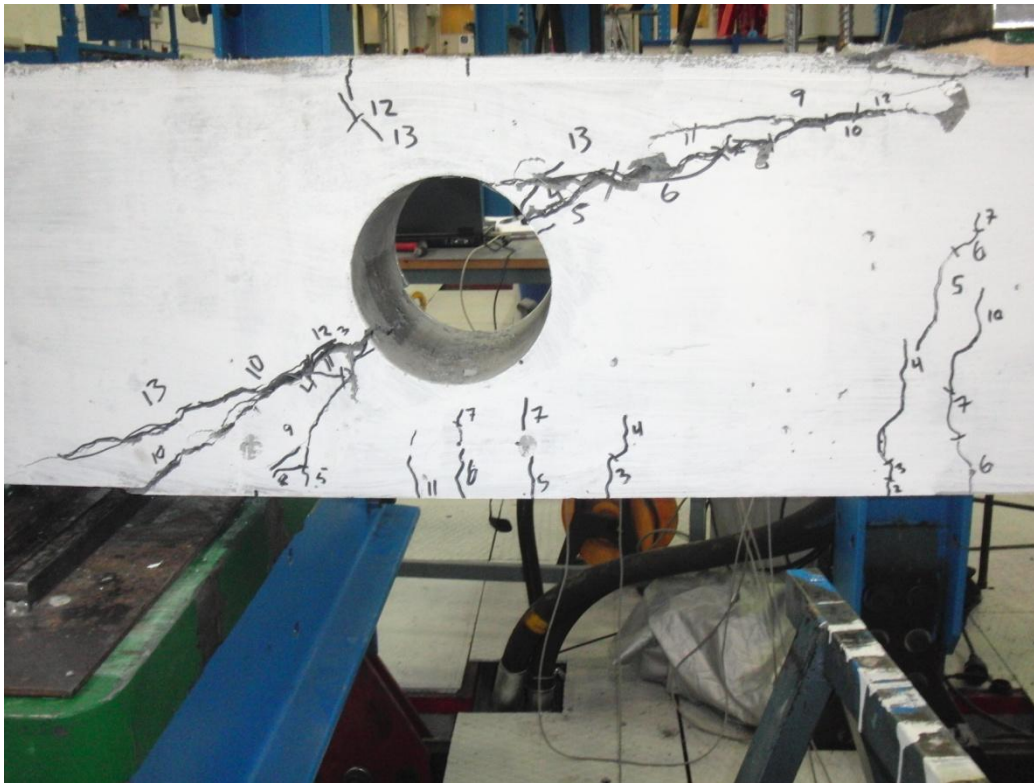


Figure 89: Beam C after failure

As for the two other beams, beam C had transformers glued beneath the openings in the beam. However, as for beam B the shear cracks and the final failure happened outside of the transformers reach as well as the largest shear cracks around the other opening, so the curves from these may be unusable. The crack opening curves from beam C can be seen in figure 90 and 91.

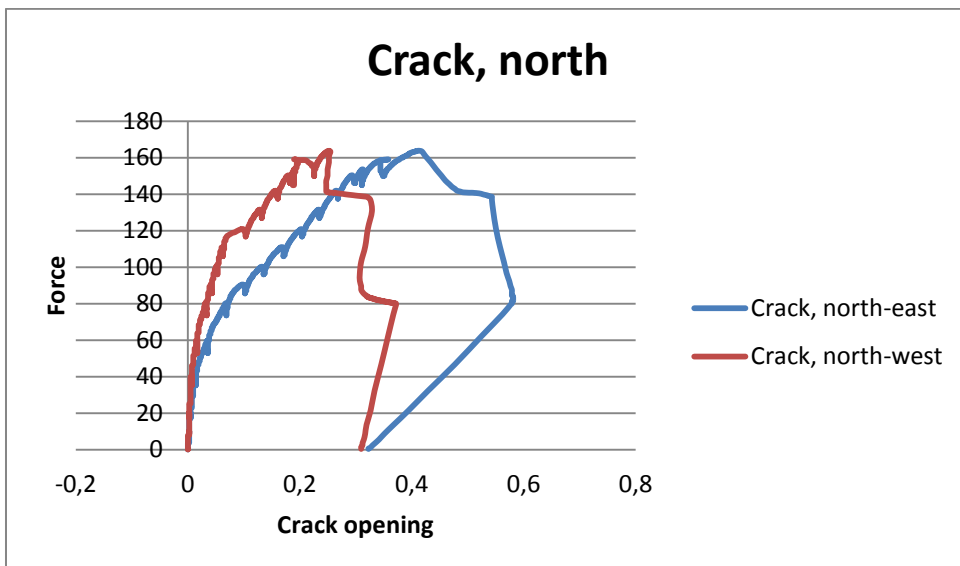


Figure 90: Crack openings for northern opening in beam C



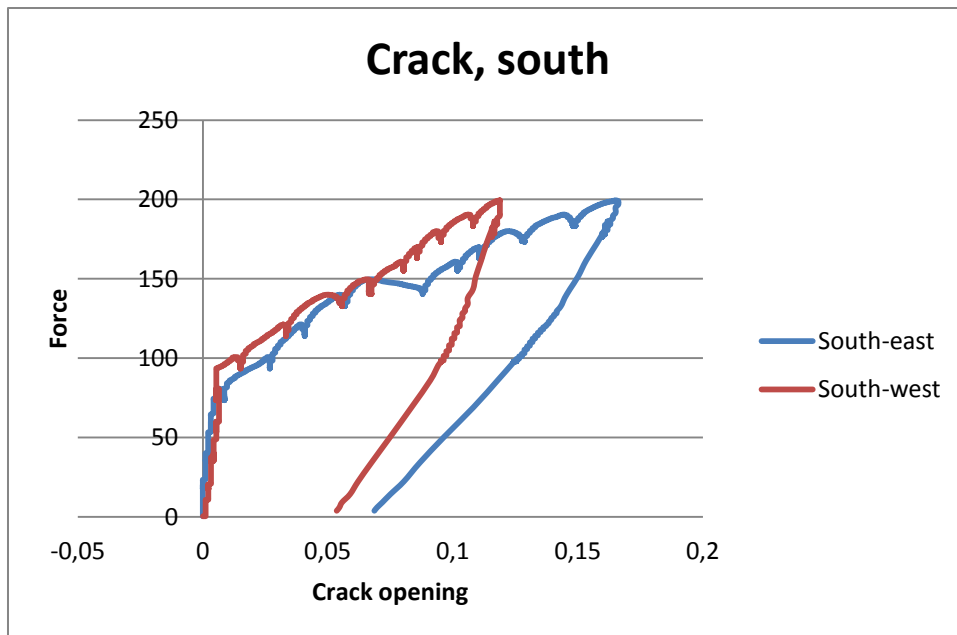


Figure 91: Crack openings for southern opening in beam C

As the figures show, the crack widths registered here are much smaller than those registered at the other beams. This is because the transformers registered other small cracks than those in the failure patterns. Therefore it is unnecessary to compare these as the curves from beam C don't give much useful information.

### 10.3.5 Reference beam

The reference beam was cast as a regular beam without openings. The reinforcement here is the same longitudinal reinforcement as the other beams, but with no functional shear reinforcement. This beam is meant to be a basis of comparison for the other beams, and is not a part of the research in this thesis per se.

The force-displacement curve for the reference beam is shown in figure 92. As for beam B and C the curve is almost straight all the way to breaking. As for all the other beams, there is a small change of slope at about 60 kN. The definite break happens at 178.8 kN, and the capacity drops dramatically from here without much increase in displacement. The machine was stopped at about 9.5 mm displacement and the load was removed, as can be seen in the graph.

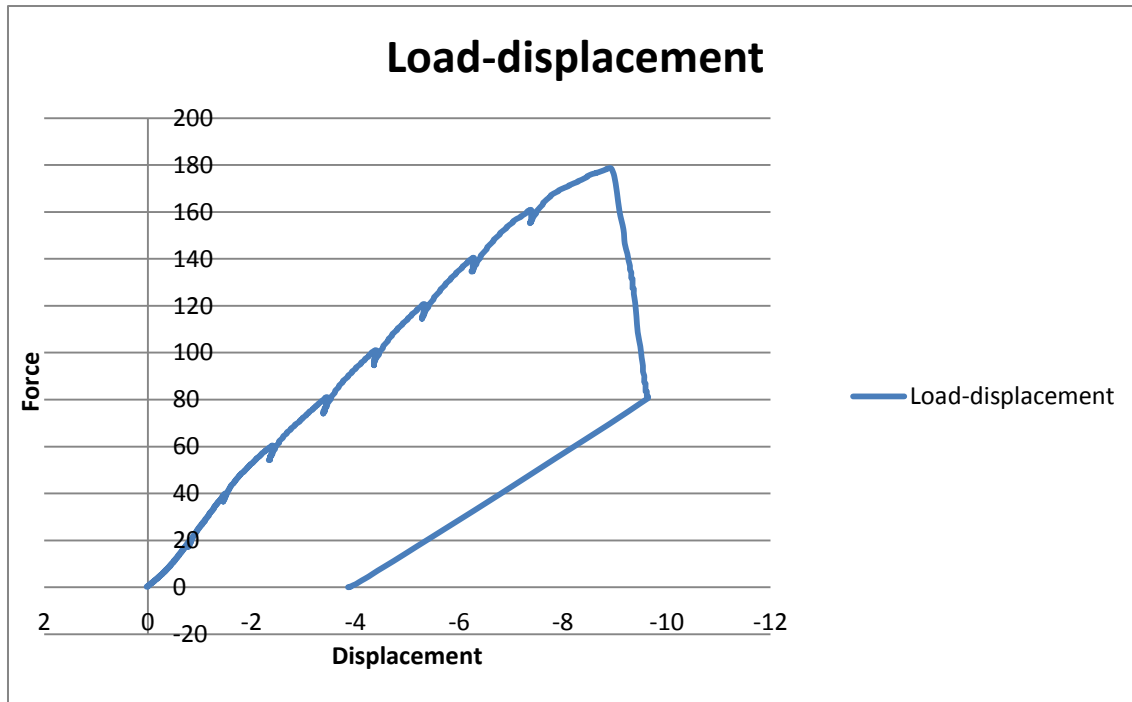


Figure 92: Load-displacement curve for the reference beam

This beam was the first beam that was tested, and the notes made are not as detailed as those of the other beams. Therefore there is no table of crack development available for this beam. The machine was stopped every 20 kN from start to failure, and cracks were drawn and numbered at each stop. The numbers go from 1 at 20 kN to 8 at 160 kN, which was the last stop before failure. There were no cracks registered until load level 3 (at 60 kN). Figure 93 and 94 show the crack development for the beam and figures 95 and 96 show the beam after failure. The 20 kN intervals seemed to be a bit inaccurate when it came to registration of cracks. Therefore the machine was stopped more often near failure for the other beams.

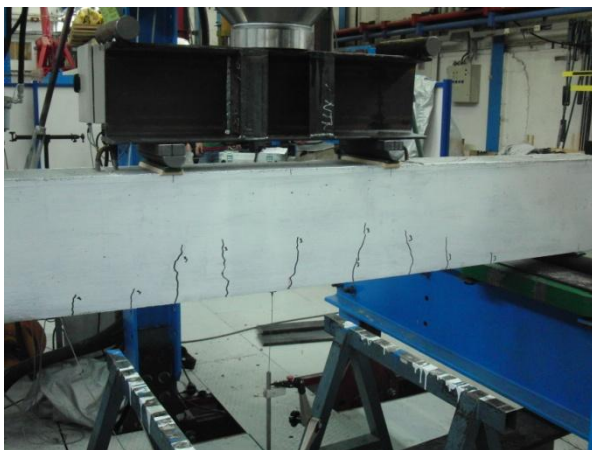


Figure 93: Initial cracking, reference beam

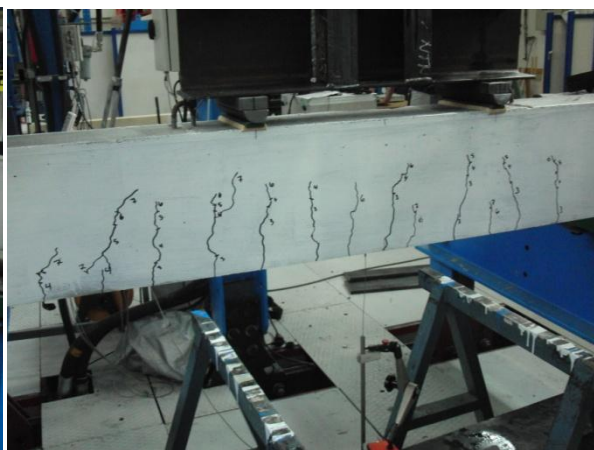


Figure 94: Crack development, reference beam

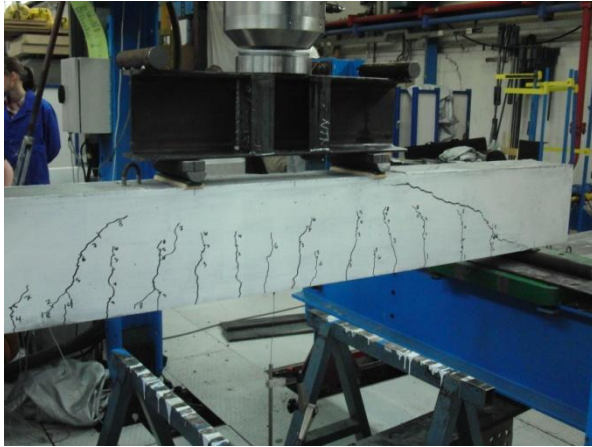


Figure 95: Close to failure, reference beam

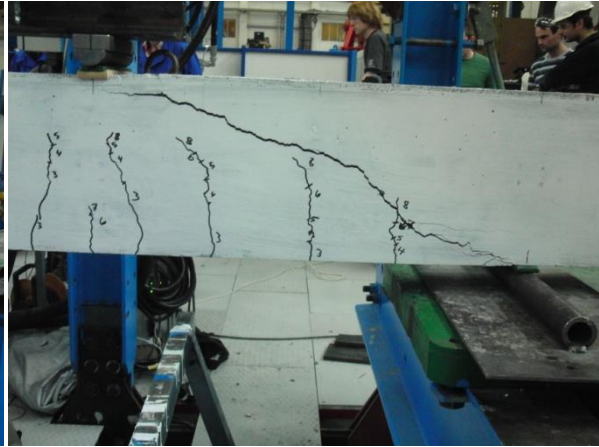


Figure 96: The reference beam after failure

As this beam had no opening it also didn't have transducer recording the crack widths for the beam. This isn't as interesting for this beam as for the others and the placement of the shear cracks were harder to foresee.

## 11 Calculations of shear capacity

### 11.1 Pre-testing calculations

The following calculations are carried out with an assumed value for the concrete's compressive strength,  $f_{ck} = 35$  MPa, and the calculated theoretical value for the residual tensile strength for the FRC,  $f_{tk,res} = 1.67$  MPa. The calculations are also done with no safety factor so as to get the answers as close to the real capacity as possible.

For all the beams the force equivalent to the capacity was high enough to reach the S-limit from the Vierendeel theory described in chapter 6.3 *Design forces*. Therefore it's assumed that the cross-section above the opening will carry all the force at failure.

Details from the calculations may be seen in annex 5.

#### 11.1.1 Reference beam

The reference beam has a regular shape and no fibre reinforcement and may therefore be calculated by the formulas found in EC2 (Standard Norge, 2004), where the assumed maximum moment is  $M_{Ed} = 37.5$  kNm.

Moment capacity:

$$M_{Rd,test} = 0.275 \cdot f_{cd} \cdot b \cdot d^2 = 0.275 \cdot 35 \cdot 200 \cdot 260^2 \cdot 10^{-6} = 130 \text{ kNm}$$

$$z = \min \left( \left( 1 - 0.17 \cdot \frac{M_{Ed}}{M_{Rd,test}} \right) \cdot d; 0.95 \cdot d \right) = 0.95 \cdot d = 0.95 \cdot 260 = 247 \text{ mm}$$

$$M_{Rd} = A_s \cdot z \cdot f_{yd} = 628.3 \text{ mm}^2 \cdot 247 \text{ mm} \cdot 500 \frac{\text{N}}{\text{mm}^2} \cdot 10^{-6} = 77.6 \text{ kNm}$$

The calculated moment capacity is almost twice the assumed maximum moment, and it is therefore likely that the shear capacity will decide the beam's capacity.

Shear capacity:

$$V_{Rd,c} = \left[ C_{Rd,c} k (100 \rho_l f_{ck})^{\frac{1}{3}} + k_1 \sigma_{cp} \right] b_w d = \left[ 0.18 \cdot 1.877 (100 \cdot 0.0121 \cdot 35)^{\frac{1}{3}} \right] \cdot 200 \cdot 260$$

$$V_{Rd,c} = 61\,211.8 \text{ N} = 61.2 \text{ kN}$$

This gives a total load capacity for the beam:

$$F_{max} = 2 \cdot V_{Rd,c} = 2 \cdot 61.2 = \underline{\underline{122.4 \text{ kN}}}$$

#### 11.1.2 Beam A

For beam A, with regular shear reinforcement, it's likely that the  $\emptyset 8$  stirrups besides the openings take most of the shear force. However, it is also possible that the concrete above the opening may take some of the force as well. Based on this the capacity may be calculated as follows:

$$A_{sv} = 2 \cdot \left(\frac{8}{2}\right)^2 \cdot \pi = 100.53 \text{ mm}^2$$

$$V_{wd} = A_{sv} \cdot f_{yk} = 100.53 \text{ mm}^2 \cdot 500 \text{ MPa} = 50\,265.48 \text{ N} = 50.3 \text{ kN}$$

The capacity contribution from the concrete cross-section above the opening is calculated from the formula for shear capacity in EC2. This formula is also described in chapter 6.2.1 *COIN-report*, here as a part of the shear capacity formula for a fibre reinforced concrete beam. The formula is the term  $V_{Rd,ct}$ . As a simplification it is assumed that the axial force caused by the moment does not contribute to the capacity. From this formula the capacity contribution is:

$$V_{Rd,c} = 10.6 \text{ kN}$$

This gives a total shear capacity of:

$$V_{Rd} = 50.3 + 10.6 = 60.9 \text{ kN}$$

And a total load capacity for the beam of:

$$F_{Max} = 2 \cdot 60.9 \text{ kN} = \underline{121.8 \text{ kN}}$$

### 11.1.3 Beam B

As for beam A the capacity is to a large degree determined by the  $\varnothing 8$  stirrups by the opening. The capacity contribution from these is the same as for beam A. For this beam there will be a larger contribution from the concrete as this is reinforced by steel fibres, which gives it a higher capacity. The capacity can therefore be calculated as follows:

$$V_{wd} = 50.3 \text{ kN}$$

The capacity contribution from the FRC is calculated from the formula described in chapter 6.2.1 *COIN-report*. Here both terms are applied as we have fibre reinforcement. Therefore the capacity becomes:

$$V_{Rd,c} = V_{Rd,ct} + V_{Rd,cf} = 10.6 + 16.0 = 26.6 \text{ kN}$$

This gives a total shear capacity of:

$$V_{Rd} = V_{Rd,c} + V_{Rd,wd} = 26.6 + 50.3 = 76.9 \text{ kN}$$

And the total load capacity for the beam is:

$$F_{Max} = 2 \cdot 76.9 \text{ kN} = \underline{153.8 \text{ kN}}$$

### 11.1.4 Beam C

For beam C there are no stirrups near the opening to carry the shear force, and the load must there for be fully carried by the steel fibre reinforcement. The load is assumed to be carried only by the cross-section over the opening as the bottom part will probably be too

cracked to carry load when failure occurs. Therefore the capacity will be as following based on these assumptions:

$$V_{Rd,c} = V_{Rd,ct} + V_{Rd,cf} = 10.6 + 16.0 = 26.6 \text{ kN}$$

And the total load capacity of the beam is:

$$F_{Max} = 2 \cdot 26.6 \text{ kN} = \underline{53.3 \text{ kN}}$$

This, however, seems a bit too low. Therefore it's logical to assume that the steel fibres in the beam will form a tensile trajectory to act in the same way as the stirrups in beam A and B. This trajectory may be either vertical or slightly angular as shown in figure 97 and 98.

$l_{\text{eff.fibre}}$  is the width of the tensile zone and  $\alpha$  is the rotation angle.

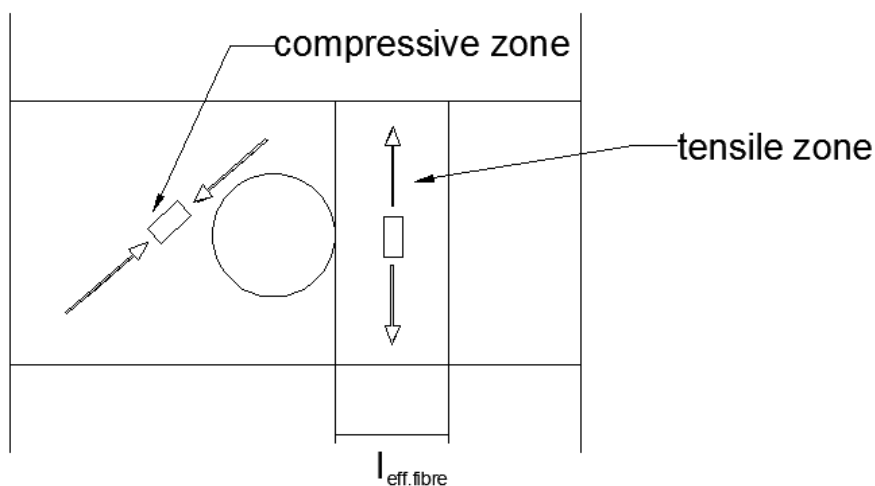


Figure 97: Vertical tensile zone near opening

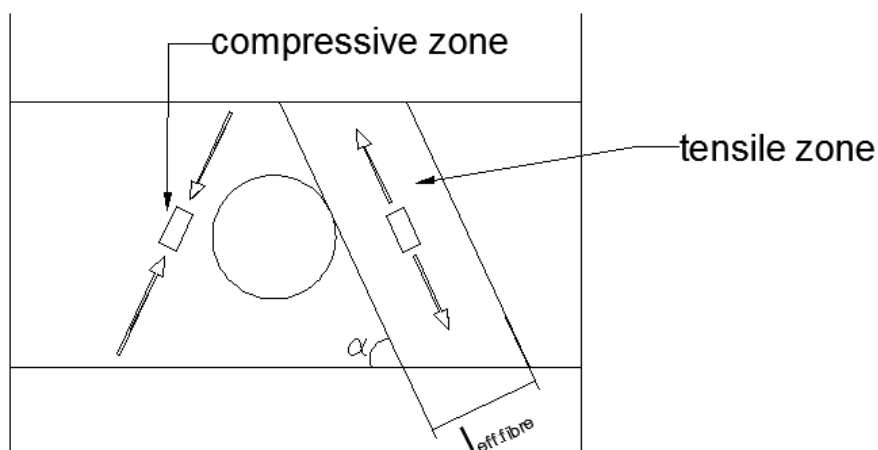


Figure 98: Angled tensile zone near opening

The width of the tensile zone is hard to estimate without any numbers for the capacity, and this calculation must be done after the testing and be based on the real capacity. The rotational angle may also be found after testing as the tensile zone will be normal to the crack angle.

## 11.2 Post testing calculations

### 11.2.1 Shear capacity

After the full-scale testing the capacities for the FRC beams were calculated once more to see whether using the measured residual tensile strength gave better results for the calculations. The measured residual tensile strength was  $f_{tk,res2.5} = 3.4 \text{ N/mm}^2$ . The calculation results are summarized in table 20.

Table 20: New capacity for beam B and C

Beam	New capacity (Maximum load)
B	187 kN
C	86.4 kN

### 11.2.2 Calculation of tensile trajectory for beam C

#### *Calculations with measured residual tensile strength*

As it turned out from the tests, the total load capacity for beam C was 199.5 kN which was quite a bit higher than what was calculated both pre- and post-testing. Based on this result the width of the assumed tensile zone for the beam may be calculated and a better way of calculating the capacity may be found.

For the model with the vertical tensile zone the formula for the width,  $l_{eff.fibre}$ , may be found from:

$$V_{Rd} = \frac{1}{2} F_{max}$$

$$V_{Rd} = b \cdot l_{eff.fibre} \cdot f_{tk,res2.5}$$

$$l_{eff.fibre} = \frac{V_{Rd}}{b \cdot f_{tk,res2.5}}$$

From the testing of cubes and standard beams cast with the FRC it became apparent that the residual tensile strength was quite a bit higher than what was assumed during the initial calculations. Therefore the  $f_{tk,res2.5}$  for these post testing calculations is set to be  $3.4 \text{ N/mm}^2$  instead of  $1.67 \text{ N/mm}^2$ .

Thus, by putting in the appropriate numbers the width of a vertical tensile trajectory will be as following:

$$l_{eff.fibre} = \frac{V_{Rd}}{b \cdot f_{tk,res2.5}} = \frac{100 \cdot 10^3 \text{ N}}{200 \text{ mm} \cdot 3.4 \frac{\text{N}}{\text{mm}^2}} = \underline{147.1 \text{ mm}}$$

For the slightly angled tensile trajectory we get the following formula:

$$V_{Rd\parallel} = V_{Rd} \cdot \sin \varphi$$

$$l_{eff.fibre} = \frac{V_{Rd} \cdot \sin \varphi}{b \cdot f_{tk,res2.5}}$$

From the pictures from the testing the crack angle ( $\theta$ ) may be found. The angle of the tensile trajectory ( $\varphi$ ) is assumed to be normal to this angle. The crack angles for the beam are shown in figure 99. As the angles above and below the opening are different, the mean value is used as the crack angle.

$$\bar{\theta} = \frac{20 + 35}{2} = 27.5^\circ$$

$$\varphi = 90 - \theta = 90 - 27.5 = 62.5^\circ$$

The width of the angled tensile trajectory then becomes:

$$l_{eff.fibre} = \frac{V_{Rd} \cdot \sin \varphi}{b \cdot f_{tk,res2.5}} = \frac{100 \cdot 10^3 \text{ N} \cdot \sin 62.5}{200 \text{ mm} \cdot 3.4 \frac{\text{N}}{\text{mm}^2}} = \underline{130.4 \text{ mm}}$$

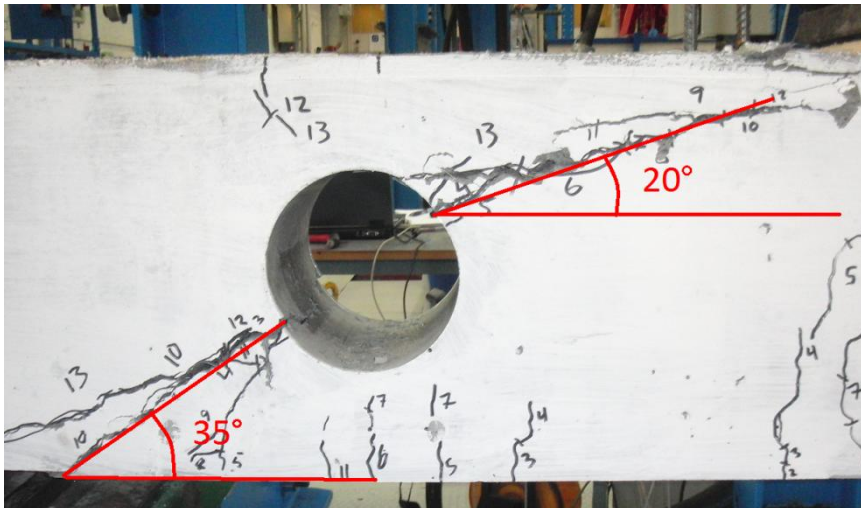


Figure 99: Crack angle for beam C

As the calculated capacity should be a bit lower than the real capacity, the tensile widths of respectively the vertical and the angled trajectory is set to 135 and 120 mm. The new capacity is calculated:

$$\text{Vertical: } V_{Rd} = l_{eff.fibre} \cdot b \cdot f_{tk,res2.5} = 135 \text{ mm} \cdot 200 \text{ mm} \cdot 3.4 \frac{\text{N}}{\text{mm}^2} = 91\,800 \text{ N} = 91.8 \text{ kN}$$

$$F_{max} = 2 \cdot V_{Rd} = 2 \cdot 91.8 \text{ kN} = \underline{183.6 \text{ kN}}$$

$$\text{Angled: } V_{Rd} = \frac{l_{eff.fibre} \cdot b \cdot f_{tk,res2.5}}{\sin \varphi} = \frac{120 \text{ mm} \cdot 200 \text{ mm} \cdot 3.4 \frac{\text{N}}{\text{mm}^2}}{\sin 62.5} = 91\,994 \text{ N} = 92.0 \text{ kN}$$

$$F_{max} = 2 \cdot V_{Rd} = 2 \cdot 92 \text{ kN} = \underline{184 \text{ kN}}$$

There should be made a standard way of calculating the width of such a trajectory for FRC, but it's hard to suggest a method after testing just one such beam. For this beam the



recommended widths are  $0.675b$  for the vertical and  $0.6b$  for the angled trajectory. This, however, may vary and further tests should be executed to create good formulae for this type of FRC beam.

### *Calculation with theoretical residual tensile strength*

It is also interesting to calculate the width of the tensile trajectory with the theoretically calculated residual tensile strength as this is what would be used in a design situation. For this calculation the residual tensile strength will therefore be set to  $f_{tk, res2.5} = 1.67 \text{ N/mm}^2$ . The calculations are carried out the same way as in last section and gives the following results.

Vertical:

$$l_{eff.fibre} = \underline{299.4 \text{ mm}}$$

Angled:

$$l_{eff.fibre} = \underline{265.6 \text{ mm}}$$

For the capacity calculations the tensile trajectory widths are chosen conservatively to be  $l_{eff.fibre} = 250 \text{ mm}$  for the vertical and  $l_{eff.fibre} = 220 \text{ mm}$  for the angled. This gives the following capacities:

Vertical:

$$V_{Rd} = 83.5 \text{ kN} \rightarrow F_{max} = \underline{167.0 \text{ kN}}$$

Angled:

$$V_{Rd} = 82.8 \text{ kN} \rightarrow F_{max} = \underline{165.6 \text{ kN}}$$

### **11.2.3 Calculation of tensile trajectory for beam B**

#### *Calculations with measured residual tensile strength*

For beam B the capacity calculated both before and after testing was a bit low. This suggests that the fibres in beam B help the shear stirrup in lifting the shear force over the opening. Based on the post testing calculated capacity it will be possible to find the width of a tensile trajectory for beam B. The tensile trajectory will only be calculated vertically as this is the way the stirrups are placed. The beam turned out to have a real capacity of 242.2 kN which is 55.2 kN more than the post-testing calculated capacity (187 kN). Based on this number the width of the tensile trajectory is calculated:

$$V_{Rd} = \frac{1}{2} F_{max} = \frac{1}{2} \cdot 55.2 \text{ kN} = 27.6 \text{ kN}$$

$$l_{eff.fibre} = \frac{V_{Rd}}{b \cdot f_{tk, res2.5}} = \frac{27.6 \cdot 10^3 \text{ N}}{200 \text{ mm} \cdot 3.4 \frac{\text{N}}{\text{mm}^2}} = \underline{40.6 \text{ mm}}$$

If we set  $l_{\text{eff, fibre}} = 30 \text{ mm}$  we get the following post testing capacity:

$$V_{Rd} = \frac{187}{2} \text{ kN} + 30 \text{ mm} \cdot 200 \text{ mm} \cdot 3.4 \frac{\text{N}}{\text{mm}^2} \cdot 10^{-3} \frac{\text{kN}}{\text{N}} = 114 \text{ kN}$$

$$F_{\text{max}} = 2 \cdot V_{Rd} = 2 \cdot 114 \text{ kN} = \underline{\underline{228 \text{ kN}}}$$

### *Calculation with theoretical residual tensile strength*

As for beam C the calculations of the tensile trajectory of beam B is carried out with the theoretical residual tensile strength as well as the measured. The differential load is 88.4 kN The calculations are done the same way as in the last section but with  $f_{\text{tk, res2.5}} = 1.67 \text{ N/mm}^2$ . The results are as follows:

$$l_{\text{eff, fibre}} = \underline{\underline{132.3 \text{ mm}}}$$

If we set  $l_{\text{eff, fibre}} = 110 \text{ mm}$  we get the following post testing capacity:

$$V_{Rd} = \frac{153.8}{2} \text{ kN} + 110 \text{ mm} \cdot 200 \text{ mm} \cdot 1.67 \frac{\text{N}}{\text{mm}^2} \cdot 10^{-3} \frac{\text{kN}}{\text{N}} = 113.64 \text{ kN}$$

$$F_{\text{max}} = \underline{\underline{227.3 \text{ kN}}}$$

## 12 Discussion

### 12.1 Comparison of calculations and test

Table 21: Summary of test and calculation results

Beam	Real capacity	Pre-test calculation	Post-test calculation	Calculation with tensile trajectory
A	163.9 kN	121.8 kN	-	-
B	242.2 kN	153.8 kN	187 kN	228 kN
C	199.5 kN	53.3 kN	86.4 kN	180 kN
Reference	178.8 kN	122.4 kN	-	-

As the calculations are very conservative compared to the real capacity the mass of the load distribution beam and cylinders in the testing rig is neglected. They only added a load of 0.5 kN. The same goes for the own weight of the concrete which only add a shear force of 1.3 kN at the openings.

#### *Beam A*

The calculated capacity for beam A was 121.8 kN while the real test capacity turned out to be 163.9 kN. This is an ok result for the calculations, as the calculated capacity should be a bit lower than the real capacity even if the safety factors are not included. This is because the assumed capacity of the concrete and the reinforcement steel often is a bit lower than the real value as there are quite high safety requirements. From this it's reasonable to assume that the calculation method used for beam A, with a combined capacity from the stirrups and the concrete cross-section above the opening, is a good method for this kind of beam.

#### *Beam B*

For beam B the calculated capacity was 153.8 kN and the real capacity was 242.2 kN. Here it is an even larger gap between the real and calculated capacity. But for FRC there might be more possible sources of error than in a regular concrete beam, for instance the flow and spread of the fibres in the beam may have a big influence on the capacity. Therefore it is good to have a bit conservative calculations for such beams. There might be that the fibres create a tensile trajectory for the combination beam that "helps" the stirrups near the opening and that this causes a larger capacity than the calculated value. The width of such a trajectory was calculated and came out at 40.6 mm. The new capacity based on a trajectory of 30 mm came out at 228 kN which may be a bit too unconservative. It may be that it's better to neglect this contribution in capacity calculations. However, when the safety factors are added the results may be a bit better. The combination of stirrup and steel fibre tensile trajectory may be interesting to investigate further in the future to make better calculation models.

### *Beam C*

The pre-testing calculated capacity for beam C was 53.3 kN which obviously is much too low as the real capacity turned out to be 199.5 kN. This capacity was difficult to determine before the tests was carried out as there is no formulas to calculate the width of the tensile trajectory created by the steel fibres. From the post-testing calculations the capacity came out at about 180 kN by using a trajectory width of 135 mm for the vertical trajectory and 120 mm for the angled, which naturally is much closer to the real capacity as the trajectory width was calculated using the real capacity. For future use of FRC in beams with openings it will be necessary to develop a set of formulas to calculate the width of the trajectory to get a reasonable calculation method for such structural elements.

### *Reference beam*

The reference beam should be easy to calculate as it is a standard beam with no openings or fibre reinforcement. The formulas for such standard structural elements are extensively tested and are used as standards in the industry today. The calculated capacity was 122.4 kN and the real test capacity was 178.8 kN. Here the calculation is also quite conservative.

## **12.2 Comparison of the beams**

From the tests it became apparent that the fibres had a very good effect on the shear capacity of the beams. The beam with the combined reinforcement was the strongest by a good margin, which was to be expected. What was the most interesting was that the beam with only fibre reinforcement as shear reinforcement was stronger than the beam with only traditional stirrup reinforcement. This suggests that fibre reinforcement as shear reinforcement in beams with openings might be an efficient design in the future.

An interesting observation was that even though beam B had the combined reinforcement of beam A and C, the capacity of the beam was quite a bit less than the sum of beam A and C's capacities ( $163.9 + 199.5 = 363.4$  kN). The reason for this might be that the reinforcements prevent each other from working fully because they both reduce the size of the cracks and therefore the effectiveness of each of the reinforcements.

## 13 Conclusions and suggestions for further work

### 13.1 Conclusions

The object of this report was to test whether it would be possible to replace traditional shear reinforcement in beams with openings with steel fibre reinforcement. Iron fixing of shear stirrups is a time consuming and hard work and finding an alternative to this would be valuable for the building industry.

The tests that were carried out during this project showed that using 1 vol. % fibres in addition to regular tensile reinforcement can give stronger beams than using regular reinforcement. In addition the beams had a clear increase in ductility which also gives the structures higher safety. As the use of fibres does not decrease the material cost for a building project the economical gain would be caused by the decrease in amount of work.

On the downside the fibres severely deteriorated the flowability of the concrete and made it hard to cast. The fresh fibre reinforced concrete required much work as it was cast so as not to flow over the edges of the formwork, and the casting therefore took longer to carry out than the casting of the regular concrete. On the other hand as the strength of the beam with only fibre reinforcement surpassed the strength of the regularly reinforced beam it might be possible to decrease the amount of fibres in the mix. With a lower fibre content the flowability should improve.

The measured residual tensile strength proved to be much higher than the theoretical value. A reason for this might be that the standard beams are smaller and has no steel bar reinforcement so the steel fibres might have gotten a better distribution than in the large beams. However, the calculations for the large beams were done with the theoretical value and were quite conservative and that suggests that it would be possible to use a higher value for the residual tensile strength.

The calculations made with the measured residual tensile strength proved to be quite good and it seems like a possible way to design such structural elements in the future.

### 13.2 Suggestions for further work

The tests done in this project gave some pointers towards the benefits of using steel fibre reinforcement in structural concrete beams with openings. However, it's hard to draw reliable conclusions from so few experiments. To better identify the properties of FRC beams with openings it will be important to do more experiments like this to know what is the trend and what is random occurrences.

It will be beneficial to develop formulas and rules for calculations of the tensile trajectory for the SFRC beams with openings. This will be possible to do after carrying through further testing of such beams with different variables (e.g. amount of fibres, geometry of cross-section, tensile reinforcement etc).

In this report the serviceability limit state has not been emphasized since the time has been limited. In a real design situation this will be an important part of the calculations, and should therefore be looked into. It would be interesting to investigate how the fibres affect the crack mouth opening displacements for shear cracks around the openings of a SFRC beam.

The measured and theoretical residual tensile strength turned out very differently (the first more than double the second). From earlier experiments this seems to be the norm (Backe-Hansen, et al., 2011) and the reasons for this should be mapped and the formulas improved.

## 13 References

- Backe-Hansen, Tore and Hamstad, Bjørnar. 2011.** *Fibre reinforced concrete structures: Testing of prefabricated beams with dapped beam end.* Trondheim : NTNU, 2011.
- Bekaert. 2005.** Direct Industry. [Online] 2005. [Cited: 10 May 2012.]  
<http://pdf.directindustry.com/pdf/bekaert/dramix-rc-80-60-bn/5919-56674.html>.
- Betongelementforeningen. 2006.** *Betongelementboken, Bind C: Elementer og knutepunkter.* Oslo : Betongelementforeningen, 2006. ISBN 82-991880-3-2.
- Brodowski, D.M., Katona, M.G. and Pope, J.A. 2010.** Application and Modeling of Steel-Fiber Reinforced Concrete for Buried Structures, SP-268-1. [book auth.] American Concrete Institute. *Fiber-Reinforced Concrete in Practice.* 2010.
- COIN. 2011.** *COIN Project Report 29-2011: Forslag til retningslinjer for dimensjonering, utførelse og kontroll av fiberarmerte betongkonstruksjoner.* Trondheim : SINTEF Building and Infrastructure, 2011. ISBN 978-82-536-1243-0.
- Destrée, X. 2010.** Steel Fiber-Reinforced Concrete in Free Suspended-Elevated Slabs. [book auth.] American Concrete Institute. *Fiber-Reinforced Concrete in Practice.* 2010.
- Døssland, Åse. 2008.** *Fibre Reinforcement in Load Carrying.* Trondheim : NTNU, 2008.
- Elasto Plastic Concrete.** Elasto Plastic Concrete. [Online] [Cited: 22 March 2012.]  
<http://www.elastoplastic.com>.
- Gjerp, Pål, Opsah, Morten and Smeplass, Sverre. 2004.** *Grunnleggende betongteknologi.* Lillestrøm : Byggenæringens forlag, 2004.
- Gossla, Prof. Dr.-Ing. Ulrich. 2005.** *Development of SFRC Free Suspended Elevated Flat Slabs.* Aachen : Aachen University of Applied Sciences, 2005.
- Löfgren, Ingemar. 2005.** *Fibre-reinforced Concrete for Industrial Construction.* Göteborg : Chalmers University of Technology, 2005.
- Mansur, M.A. and Tan, Kiang-Hwee. 1999.** *Concrete Beams With Openings - Analysis and Design.* Boca Raton, Florida : CRC Press LCC, 1999. ISBN 0-8493-7435-9.
- NTNU. 2010.** Formelsamling i betongkonstruksjoner 1, vår 2010. 2010.
- Riksantikvaren. 2009.** Riksantikvaren.no. [Internett] June 2009. [Sisert: 15 February 2012.]  
[http://www.riksantikvaren.no/filestore/363\\_Vedlikehold\\_av\\_eternitt.pdf](http://www.riksantikvaren.no/filestore/363_Vedlikehold_av_eternitt.pdf).
- Roussel, Nicolas. 2007.** *The LCPC BOX: A Cheap and Simple Technique for Yield Stress Measurements of SCC.* 2007.
- Sandbakk, Sindre. 2011.** *Fibre Reinforced Concrete - Evaluation of Test Methods and Material Development.* Trondheim : NTNU, 2011. ISBN 978-82-471-3167-1.

**Standard Norge. 2003.** *NS 3473:2003 Prosjektering av betongkonstruksjoner - Beregnings- og konstruksjonsregler.* s.l. : Standard Norge, 2003.

— **2009.** *NS-EN 12390-3:2009, Testing hardened concrete, part 3: Compressive strength of test specimens.* s.l. : Standard Norge, 2009.

— **2005.** *NS-EN 14651:2005+A1:2007 Prøvmingsmetode for betong med metalliske fibre - Måling av bøyestrekfasthet.* s.l. : Standard Norge, 2005.

— **2004.** *NS-EN 1992-1-1:2004+NA:2008, Eurocode 2: Design of Concrete Structures, Part 1-1: General Rules and Rules for Buildings.* s.l. : Standard Norge, 2004.

**The Concrete Society. 2007.** *Technical Report no. 63: Guidance for the Design of Steel Fibre Reinforced Concrete.* s.l. : The Concrete Society, 2007.

— **2007.** *Technical Report no. 65: Guidance on the Use of Macro-Synthetic-Fibre-Reinforced Concrete.* s.l. : The Concrete Society, 2007.

**The International Federation for Structural Concrete. 2010.** *Model Code. First complete draft Volume 1.* Lausanne : The International Federation for Structural Concrete, 2010.

**Thorenfeldt, E.V. et al. 2006.** *Stålfiberarmering i betong. Veiledning for prosjektering, utførelse og kontroll (Draft dokument).* 2006.



## **Annex**

Annex 1 – Results from NS-EN 14651 tests with plain concrete

Annex 2 – Results from NS-EN 14651 tests with FRC

Annex 3 – Concrete recipes from Unicon

Annex 4 – Product data sheet for Dramix 80/60

Annex 5 – Capacity calculations (from Excel)

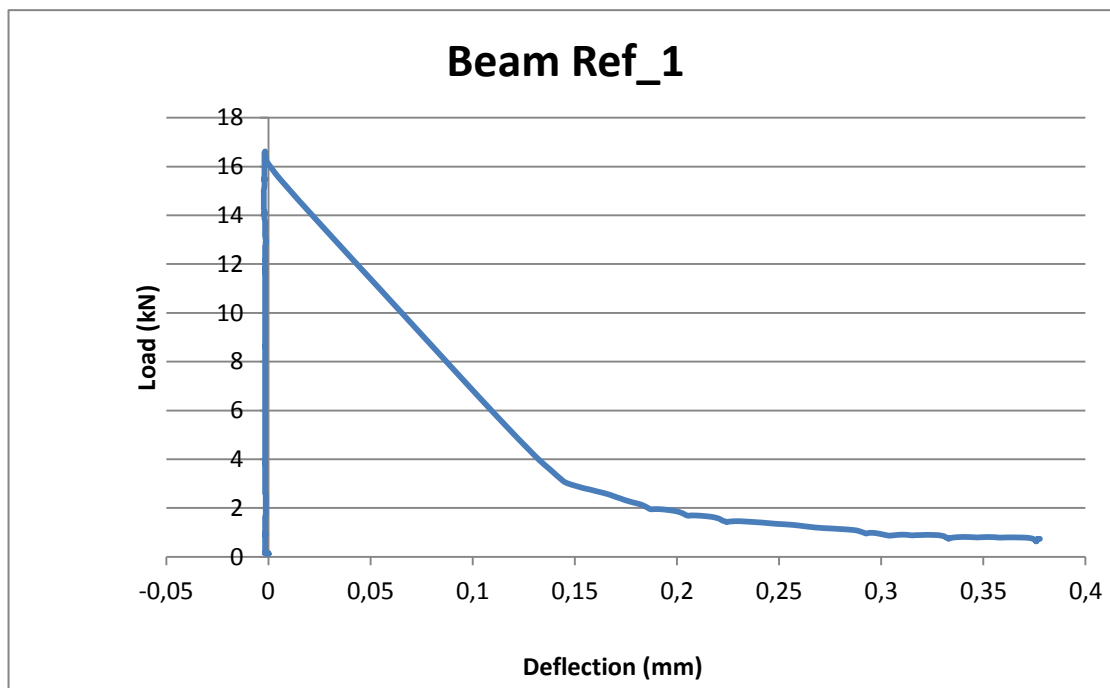
## Annex 1 – Results from NS-EN 14651 tests with plain concrete

(The tables with test results are not included as they were very large)

### Plain concrete beam 1

Dimension of the specimen	
Average Width, b	150,6 mm
Average high, $h_{sp}$	125,35 mm
Length, L	500 mm

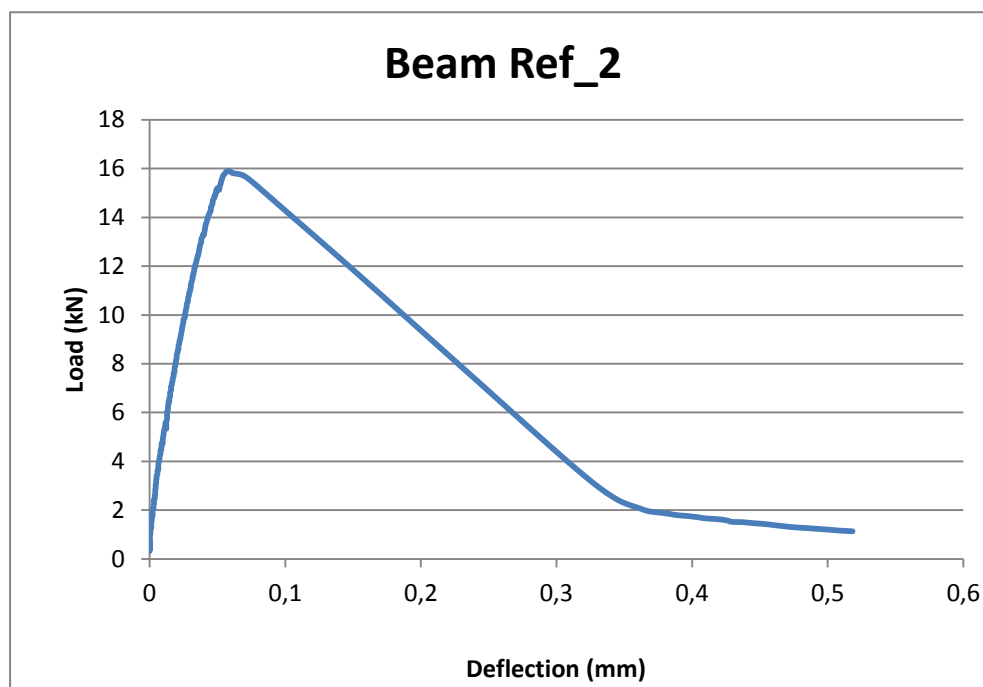
$F_L$ (maximun load)	16,6 kN
----------------------	---------



**Plain concrete beam 2**

Dimension of the specimen	
Average Width, b	150,6 mm
Average high, $h_{sp}$	125,35 mm
Length, L	500 mm

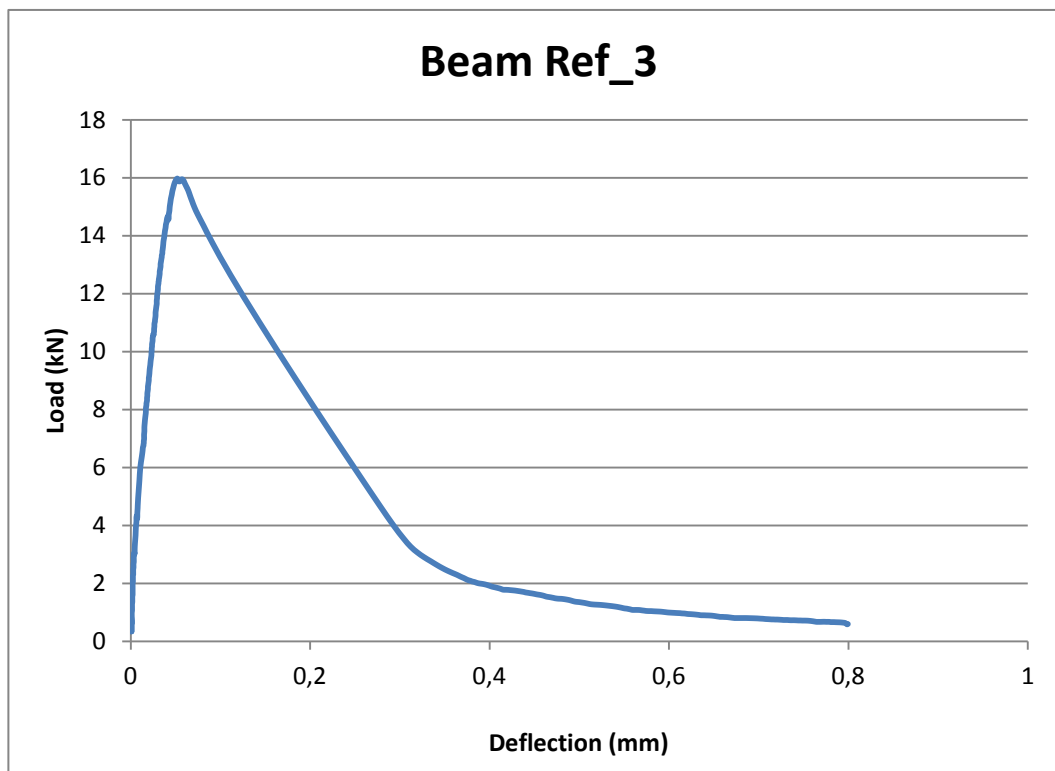
$F_L$ (maximum load)	15,9 kN
----------------------	---------



## Plain concrete beam 3

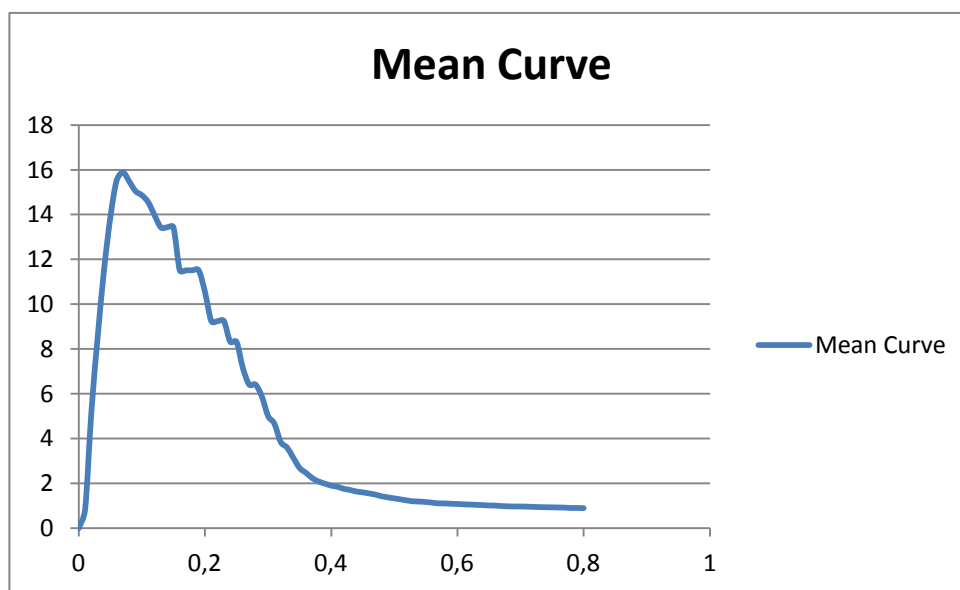
Dimension of the specimen	
Average Width, b	151,35 mm
Average high, $h_{sp}$	121,65 mm
Length, L	500 mm

$F_L$ (maximun load)	16,0 kN
----------------------	---------



## Mean values for plain concrete beams

Summarized					
	Ref_1	Ref_2	Ref_3	Mean value	CoV
Average Width, b	150,6	150,6	151,35	<b>150,9</b> mm	0,3%
Average height, h	125,35	125,35	121,65	<b>124,1</b> mm	1,7%
Length, L	500	500	500	<b>500,0</b> mm	0,0%
$F_L$	16,6	15,9	16,0	<b>16,2</b> kN	2,4%



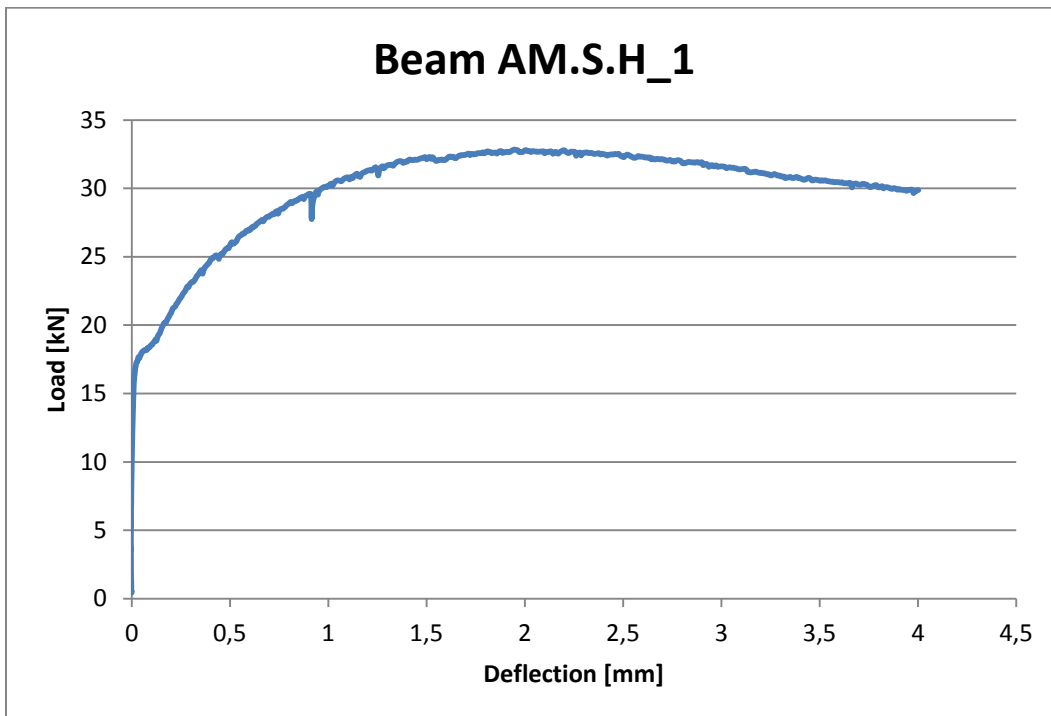
## Annex 2 – Results from NS-EN 14651 tests with FRC

### 1 % Dramix 65/60, beam 1

Dimension of the specimen	
Average Width, b	153,895 mm
Average high, $h_{sp}$	125,03 mm
Length, L	500 mm

$F_L$	18,2 kN
$f_{ct,L}^f$	5,7 N/mm <sup>2</sup>
$f_{R,1}$	7,9 N/mm <sup>2</sup>
$f_{R,2}$	9,9 N/mm <sup>2</sup>
$f_{R,3}$	10,1 N/mm <sup>2</sup>
$f_{R,4}$	9,8 N/mm <sup>2</sup>

Relationship between CMOD and $\delta$			
CMOD (mm)	$\delta$ (mm)	F <sub>j</sub>	
0,05	0,08		
0,1	0,13		
0,2	0,21		
0,5	0,47	25,36	j=1
1,5	1,32	31,71	j=2
2,5	2,17	32,54	j=3
3,5	3,02	31,55	j=4
4	3,44		

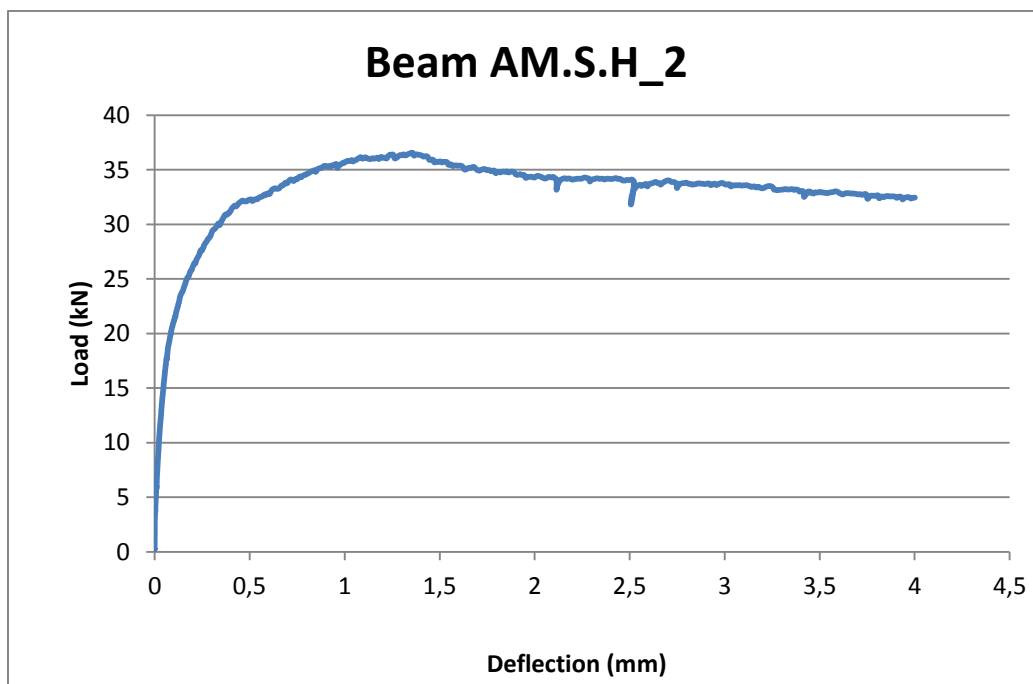


## 1 % Dramix 65/60, beam 2

Dimension of the specimen	
Average Width, b	150,865 mm
Average high, $h_{sp}$	125,65 mm
Length, L	500 mm

$F_L$	19,6 kN
$f_{ct,L}^f$	6,2 N/mm <sup>2</sup>
$f_{R,1}$	10,1 N/mm <sup>2</sup>
$f_{R,2}$	11,4 N/mm <sup>2</sup>
$f_{R,3}$	10,8 N/mm <sup>2</sup>
$f_{R,4}$	10,6 N/mm <sup>2</sup>

Relationship between CMOD and $\delta$			
CMOD (mm)	$\delta$ (mm)	F <sub>j</sub>	
0,05	0,08		
0,1	0,13		
0,2	0,21		
0,5	0,47	32,13	j=1
1,5	1,32	36,32	j=2
2,5	2,17	34,16	j=3
3,5	3,02	33,66	j=4
4	3,44		

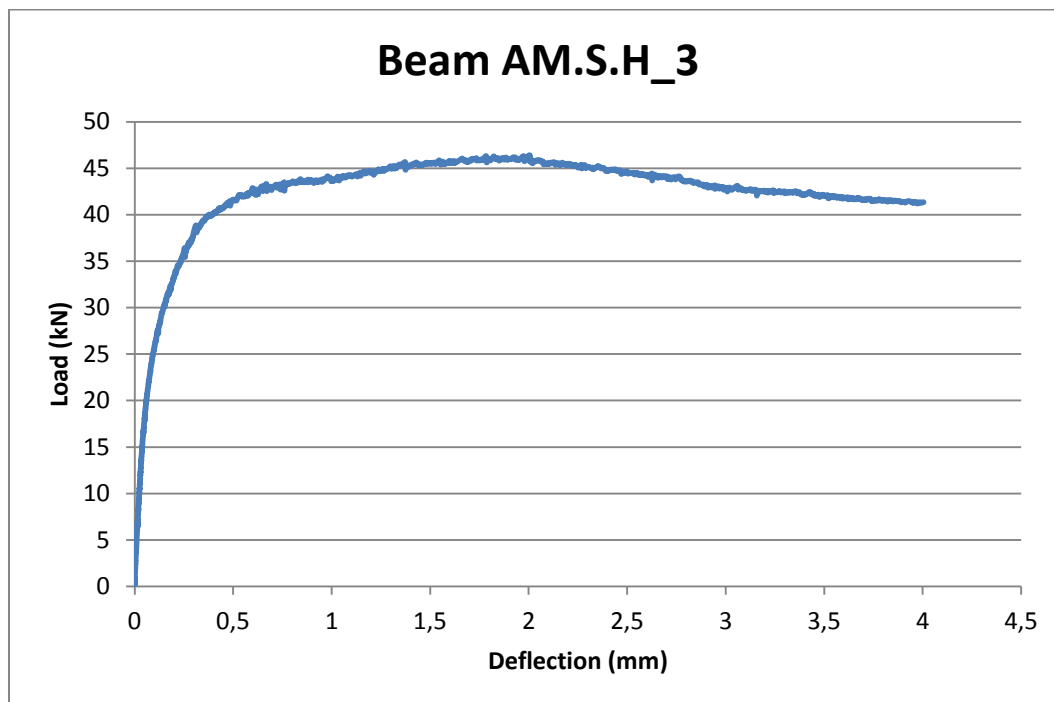


## 1 % Dramix 65/60, beam 3

Dimension of the specimen	
Average Width, b	151,225 mm
Average high, $h_{sp}$	125,965 mm
Length, L	500 mm

$F_L$	23,2 kN
$f_{ct,L}^f$	7,2 N/mm <sup>2</sup>
$f_{R,1}$	12,9 N/mm <sup>2</sup>
$f_{R,2}$	14,1 N/mm <sup>2</sup>
$f_{R,3}$	14,2 N/mm <sup>2</sup>
$f_{R,4}$	13,4 N/mm <sup>2</sup>

Relationship between CMOD and $\delta$			
CMOD (mm)	$\delta$ (mm)	F <sub>j</sub>	
0,05	0,08		
0,1	0,13		
0,2	0,21		
0,5	0,47	41,25	j=1
1,5	1,32	45,00	j=2
2,5	2,17	45,52	j=3
3,5	3,02	42,91	j=4
4	3,44		



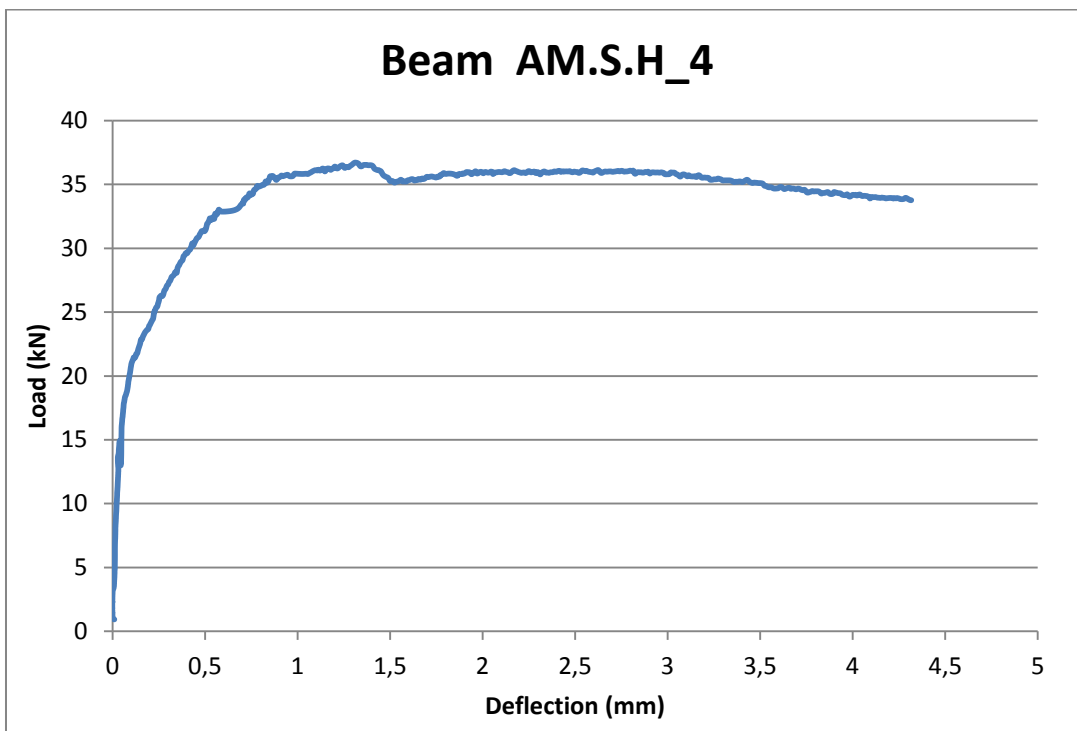


**1 % Dramix 65/60, beam 4**

Dimension of the specimen	
Average Width, b	152,495 mm
Average high, $h_{sp}$	125,415 mm
Length, L	500 mm

Relationship between CMOD and $\delta$			
CMOD (mm)	$\delta$ (mm)	F <sub>j</sub>	
0,05	0,08		
0,1	0,13		
0,2	0,21		
0,5	0,47	34,77	j=1
1,5	1,32	35,32	j=2
2,5	2,17	36,00	j=3
3,5	3,02	35,33	j=4
4	3,44		

$F_L$	29,4 kN
$f_{ct,L}^f$	9,2 N/mm <sup>2</sup>
$f_{R,1}$	10,9 N/mm <sup>2</sup>
$f_{R,2}$	11,0 N/mm <sup>2</sup>
$f_{R,3}$	11,3 N/mm <sup>2</sup>
$f_{R,4}$	11,0 N/mm <sup>2</sup>

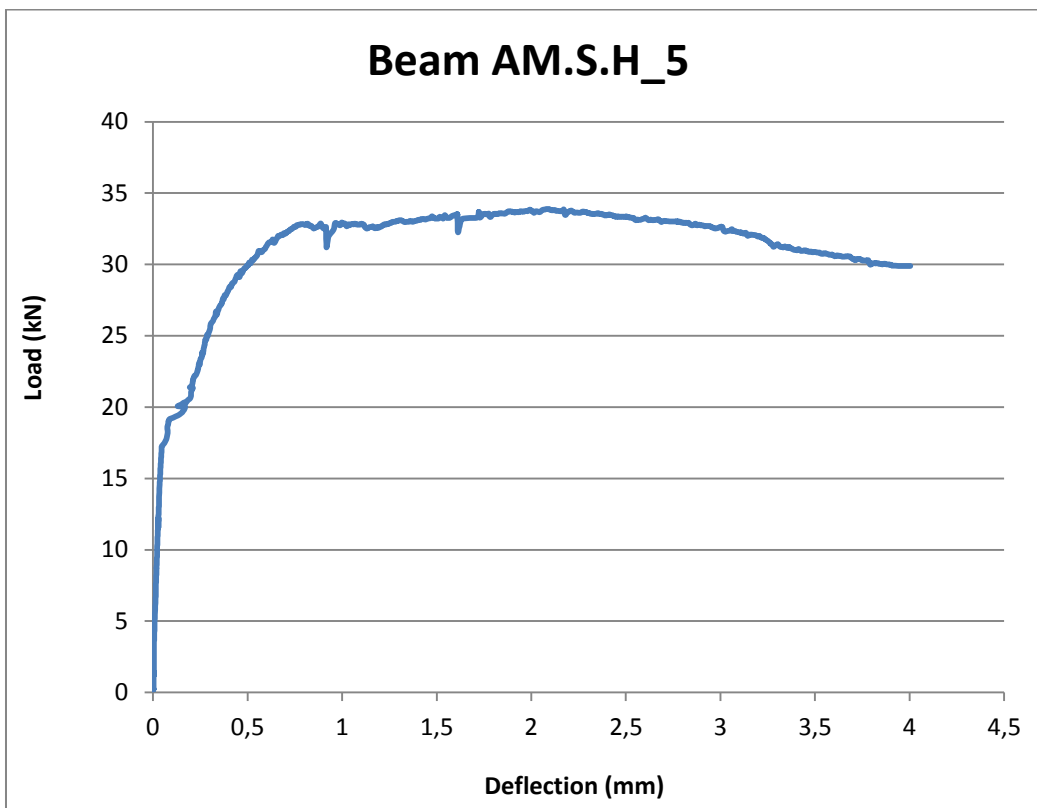


**1 % Dramix 65/60, beam 5**

Dimension of the specimen	
Average Width, b	151,925 mm
Average high, $h_{sp}$	125,73 mm
Length, L	500 mm

Relationship between CMOD and $\delta$			
CMOD (mm)	$\delta$ (mm)	F <sub>j</sub>	
0,05	0,08		
0,1	0,13		
0,2	0,21		
0,5	0,47	29,37	j=1
1,5	1,32	33,04	j=2
2,5	2,17	33,82	j=3
3,5	3,02	32,35	j=4
4	3,44		

F <sub>L</sub>	18,8 kN
$f'_{ct,L}$	5,9 N/mm <sup>2</sup>
$f_{R,1}$	9,2 N/mm <sup>2</sup>
$f_{R,2}$	10,3 N/mm <sup>2</sup>
$f_{R,3}$	10,6 N/mm <sup>2</sup>
$f_{R,4}$	10,1 N/mm <sup>2</sup>

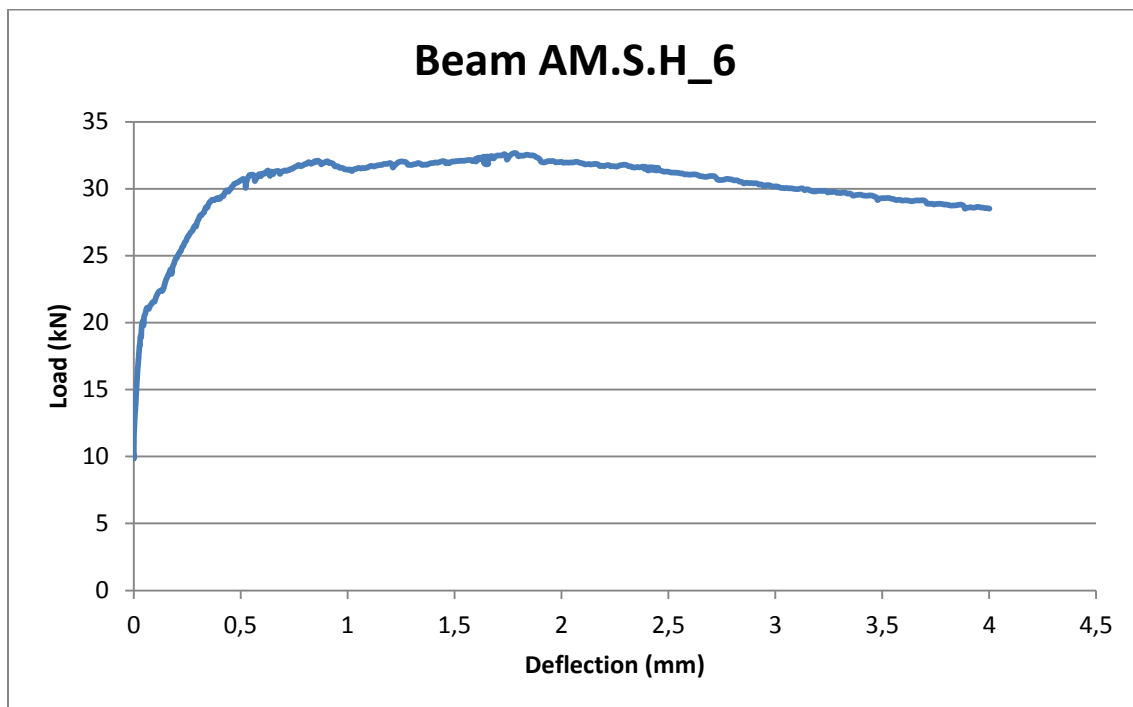


**1 % Dramix 65/60, beam 6**

Dimension of the specimen	
Average Width, b	151,32 mm
Average high, $h_{sp}$	125,285 mm
Length, L	500 mm

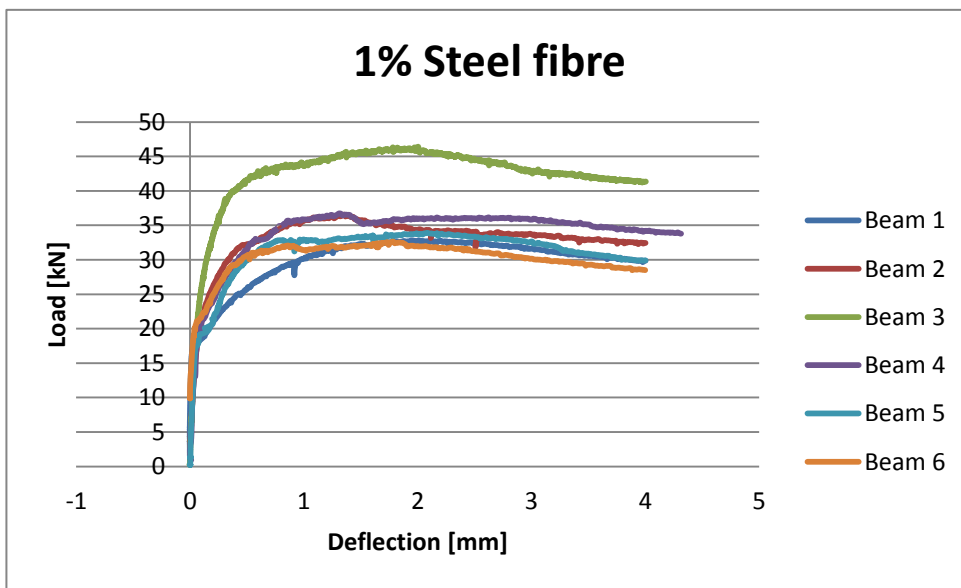
$F_L$	21,3 kN
$f_{ct,L}^f$	6,7 N/mm <sup>2</sup>
$f_{R,1}$	9,6 N/mm <sup>2</sup>
$f_{R,2}$	10,1 N/mm <sup>2</sup>
$f_{R,3}$	10,0 N/mm <sup>2</sup>
$f_{R,4}$	9,5 N/mm <sup>2</sup>

Relationship between CMOD and $\delta$			
CMOD (mm)	$\delta$ (mm)	Fj	
0,05	0,08		
0,1	0,13		
0,2	0,21		
0,5	0,47	30,34	j=1
1,5	1,32	31,83	j=2
2,5	2,17	31,81	j=3
3,5	3,02	30,09	j=4
4	3,44		




**1 % Dramix 65/60, Summarized**

Summarized									
	AM.S.H_1	AM.S.H_2	AM.S.H_3	AM.S.H_4	AM.S.H_5	AM.S.H_6	Mean value	Unit	CoV
Average Width, b	153,895	150,865	151,225	152,495	151,925	151,32	<b>152,0</b>	mm	1,1%
Average high, h	125,03	125,65	151,225	125,415	125,73	125,285	<b>134,0</b>	mm	11,2%
Length, L	500	500	151,225	500	500	500	<b>383,7</b>	mm	52,5%
$F_L$	18,2	19,6	23,2	29,4	18,8	21,3	<b>20,3</b>	kN	12,6%
$f_{ct,L}^f$	5,7	6,2	7,2	9,2	5,9	6,7	<b>6,4</b>	N/mm <sup>2</sup>	12,5%
$f_{R,1}$	7,9	10,1	12,9	10,9	9,2	9,6	<b>10,3</b>	N/mm <sup>2</sup>	24,3%
$f_{R,2}$	9,9	11,4	14,1	11,0	10,3	10,1	<b>11,8</b>	N/mm <sup>2</sup>	17,9%
$f_{R,3}$	10,1	10,8	14,2	11,3	10,6	10,0	<b>11,7</b>	N/mm <sup>2</sup>	18,8%
$f_{R,4}$	9,8	10,6	13,4	11,0	10,1	9,5	<b>11,3</b>	N/mm <sup>2</sup>	16,7%



## Annex 3 – Concrete recipes from Unicon

*Beams with carbels castings no 5, 6, 7*

**Laboratorieprotokoll**  **unicon**  
CEMENTIR HOLDING


Produksjons-ID	2012030810005	Protokoll type	Sats
Blandetidspunkt	08.03.2012 09:31:13	Tømmetid	09:29:46
Resept	UN53A-D103	B30 M60 16mm SKB	
Blander	M1	Satsstørrelse	1,50 m <sup>3</sup>
		Satsnummer	1
Miljøklasse	M60	Produsert konsistens	260
Ordrenummer	0000474468	Følgeseddelnummer	1892869
Kunde	0001014413	Unicon AS (region midt)	
Plass	NTNU	Høgskoleringen 1	
Bil	857	Bilregistreringsnummer	VT14311

Material	Enhet	Fukt %	Resept	Bør	Er	Alarm	Avvik		Er			Dens.	VOT l/m <sup>3</sup>
							%	%	VOT kg/m <sup>3</sup>	Vann kg/m <sup>3</sup>	VOT kg/m <sup>3</sup>		
Norcem Std-FA Kjøps	kg		345	518	518		0	0,0	344,4	344,4	0,0	3010	114,4
Silika ikke med i V/C	kg		13,8	20,7	20,6		-0,1	-0,5	13,7	13,7	0,0	2200	6,2
0-8 Forset	kg	4,6	1173	1840	1833		-7	-0,4	1218,8	1165,2	53,6	2700	431,5
8-16mm Vassfjell	kg	0,0	711	1067	1068		1	0,1	710,1	710,1	0,0	3040	233,6
Glenium SKY 600	kg	82,0	4,15	6,22	6,13		-0,09	-1,4	4,1	0,7	3,3	1193	0,6
Kaldt vann	kg		127	95	95		0	0,0	63,2	0,0	63,2	1000	0,0
Varmt vann	kg		59	89	88		-1	-1,1	58,5	0,0	58,5	1000	0,0
Ekstra vand	ltr		0	15	23		8	53,3	15,3	0,0	15,3	1000	0,0
<b>Total</b>	kg		2434,0	3650,9	3651,7				2428,0	2234,1	193,9		786,4

	Resept	Bør	Er	Enhet	Avvik		
					%	%	l/m <sup>3</sup>
VOT		1184,9	1182,7	1	-2,2	-0,2	786,4
Luft (2,0 %)	20,0	30,0	30,1	1	0,1	0,3	20,0
Tilsat vand		199,0	206,0	1	7,0	3,5	137,0
Total fugt		86,0	85,6	1	-0,4	-0,4	56,9
<b>Total</b>		1500,0	1504,0	1	4,0	0,3	1000,3
V/C	0,550	0,550	0,563		0,013	2,4	
Total vand/pulver tal		0,530	0,540		0,010	1,9	
Maks. vand	193	290		kg			
Vann/betong		7,8	8,0	%	0,2	2,3	
Total blandetid	60	60	222	Sek.	162	270,0	
Slutblandetid	10	10	12	Sek.	2	20,0	
Temperatur		20,0	19,8	°C	-0,2	-1,0	
Wattmeter (tabel)		56	147		91	162,5	
Wattmeter tomgang og sluttverdi		9	0				
Chlorid	0,07	0,07	0,07 % av pulver		0,00	0,0	
Mørtelindhold	332,00	497,00	504,00	1	7,00	1,4	
Fillerindhold	360,02	539,82	539,70	kg	-0,12	0,0	

Utskrevet 08.03.2012 09:35:18

Unicon Fosseorenda 1/2

*Eit END Beams* **Laboratorieprotokoll**  **unicon**  
CEMENTIR HOLDING

Produksjons-ID	2012031510051	Protokoll type	Sats
Blandetidspunkt	15.03.2012 10:13:23	Tømmetid	10:10:24
Resept	UN53A-D103	B30 M60 16mm SKB	
Blander	M1	Satsstørrelse	1,20 m <sup>3</sup>
		Satsnummer	1
Miljøklasse	M60	Produsert konsistens	260
Ordrenummer	0000474470	Følgeseddelnummer	1893075
Kunde	0001014413	Unicon AS (region midt)	
Plass	NTNU	Høgskoleringen 1	
Bil	857	Bilregistreingsnummer	VT14311

Material	Enhet	Fukt %	Resept	Bør	Er	Alarm	Avvik		Er			Dens.	VOT l/m <sup>3</sup>
							%	%	kg/m <sup>3</sup>	kg/m <sup>3</sup>	kg/m <sup>3</sup>		
Norcem Std-FA Kjøps	kg		373	448	448		0	0,0	365,1	365,1	0,0	3010	121,3
Flyveaske k=0,7	kg		75	90	88		-2	-2,2	71,7	71,7	0,0	2200	32,6
Silika ikke med i V/C	kg		17,0	20,4	20,2		-0,2	-1,0	16,5	16,5	0,0	2200	7,5
0-8 Forset	kg	4,7	1385	1740	1740		0	0,0	1418,1	1354,4	63,7	2700	501,6
8-16mm Vassfjell	kg	0,1	275	331	353		22	6,6	287,7	287,4	0,3	3040	94,5
Glenium SKY 600	kg	82,0	4,48	5,38	5,41		0,03	0,6	4,4	0,8	3,6	1193	0,7
Kaldt vann	kg		144	92	93		1	1,1	75,8	0,0	75,8	1000	0,0
Varmt vann	kg		53	63	61		-2	-3,2	49,7	0,0	49,7	1000	0,0
Dramix Ready	kg		80,00	96,00	96,00		0,00	0,0	78,2	78,2	0,0	7850	10,0
Ekstra vand	litr		0	2	23		21	1050,0	18,7	0,0	18,7	1000	0,0
<b>Total</b>	kg		2405,9	2887,8	2927,6				2386,0	2174,2	211,8		768,2

	Resept	Bør	Er	Enhet	Avvik		
					%	%	l/m <sup>3</sup>
<b>VOT</b>		936,3	942,6	1	6,2	0,7	768,2
<b>Luft (2,0 %)</b>	20,0	24,0	24,5	1	0,5	2,3	20,0
<b>Tilsat vand</b>		157,0	177,0	1	20,0	12,7	144,3
<b>Total fugt</b>		82,9	82,9	1	0,0	0,1	67,6
<b>Total</b>		1200,0	1227,0	1	27,0	2,3	1000,0
<b>V/C</b>	0,470	0,470	0,510		0,040	8,5	
<b>Total vand/pulver tal</b>		0,430	0,470		0,040	9,3	
<b>Maks. vand</b>	204	245		kg			
<b>Vann/betong</b>		8,3	8,9	%	0,6	6,9	
<b>Total blandetid</b>	60	60	292	Sek.	232	386,7	
<b>Slutblandetid</b>	10	10	26	Sek.	16	160,0	
<b>Temperatur</b>		20,0	19,3	°C	-0,7	-3,4	
<b>Wattmeter (tabel)</b>		40	91		51	127,5	
<b>Wattmeter tomgang og sluttverdi</b>		-19	216				
<b>Chlorid</b>	0,06	0,06	0,06	% av pulver	0,00	0,0	
<b>Mørtelindhold</b>	397,00	476,00	496,00	1	20,00	4,2	
<b>Fillerindhold</b>	545,76	655,37	653,17	kg	-2,19	-0,3	

Utskrevet 15.03.2012 10:20:34

Unicon Fossegrenda 1/2

# Annex 4 – Product data sheet for Dramix 80/60



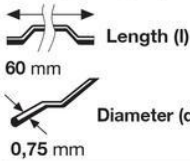
**Dramix®**



**Description:** Dramix® fibres are filaments of wire, deformed and cut to lengths, for reinforcement of concrete, mortar and other composite materials. Dramix® RC-80/60-BN is a cold drawn wire fibre, with hooked ends, and glued in bundles.

- Applications:**
- jointless floors
  - suspended ground slabs
  - jointless floors on vibrocompacted piles
  - industrial floors
  - slabs on vibro-compacted piles
  - liquid tight floors
  - overlays
  - pavements
  - segmental linings
  - compression layers
  - cellar walls
  - precast

**Geometry:**



<b>80</b>	Performance class: 80
45 65 80 / l/d	Aspect ratio (= l/d): 80
4600 fibres/kg	

- Tensile strength:**
- on the wire: minimum 1050 N/mm<sup>2</sup>
  - low carbon conforms to EN 10016-2 - C9D

**Coating:** None

**Approvals:**

Conforms to **ASTM A820**

Product  
Belgium  
**ATG 04/1857**

The Netherlands  
**22702**

Turkey  
**TS 10513**

Czech Republic  
**C.070-021415**

Quality System in  
Belgian, Brazilian, Czech,  
Turkish and Chinese plants

Product  
Poland  
**AT-15-2117/2001**

Romania  
**007-01/068-2003**

Germany  
**Z-3.71-1745**

Slovak Republic  
**1402A/02/0771/1/C/04**

**Technical data:**  
For industrial floors, floors on vibrocompacted piles, jointless floors... ask for specialized documentation.

## Recommendations - mixing

**1. General**

- ✓ preferably use a central batching plant mixer
- ✓ recommended maximum dosage:

Max. aggregate size (mm)	Dosage (kg/m <sup>3</sup> )	
	pour	pump
8	60	45
16	50	35
32	35	30

- ✓ a continuous grading is preferred
- ✓ mix until all glued fibres are separated into individual fibres. Fibres don't increase mixing time significantly.
- ✓ if special cements or admixtures are used, a preliminary test is recommended



**2. Fibre addition**

Bags are non-degradable and may not be thrown into the concrete.



**2.1. In batching plant mixer**

- ✓ never add fibres as first component in the mixer
- ✓ fibres can be introduced together with sand and aggregates, or can be added in freshly mixed concrete



**2.2. Truckmixer**

- ✓ run mixer at drum speed: 12-18 rpm
- ✓ adjust slump to a min. of 12 cm (preferably with water reducing agents or high water reducing agents)
- ✓ add fibres with maximum speed of 40 kg/min
- ✓ optional equipment: belt-hoist elevator
- ✓ after adding the fibres, continue mixing at highest speed for 4-5 min. (± 70 rotations)



**2.3. Automatic dosing**

- ✓ Fibres can be dosed from bulk at rates from 0 up to 3,5 kg/sec with a specially developed dosing equipment



## Recommendations - storage

Protect the pallets against rain

Do not stack the pallets on top of each other

**Delivered in**

non water-soluble bags of 20 kg on pallet 1200 kg  
big bag 1100 kg

N.V. Bekaert S.A. - Bekaertstraat 2 - 8550 Zwevegem - Belgium  
Tel. +32 (0) 56 / 76 69 86 - Fax +32 (0) 56 / 76 79 47  
Internet: <http://www.bekaert.com/building>

Values are indicative only. Modifications reserved. All details describe our products in general form only. For ordering and design only use official specifications and documents. N.V. Bekaert S.A. 2005

## Annex 5 – Capacity calculations (from Excel)

### Beam A

Input		Output – dimensjonerende krefter		Output - kapasitet	
M	22814625	<b>Kontroll av risstilstand</b>		<b>Utenom utsparinger</b>	
V	60839	S	106114,535	Asw	251,327412
Fo	0	grense	47328,6383	s	400
Fu	0			cotθ	2,5
N	0	<b>Tverrsnittsparmetre</b>		Vrd,ct	164933,614
eo	0	η	6,66666667		
eu	0	ρ	0,11775	<b>Ved utsparingene</b>	
d'	215	ηρ	0,785	CRd,c	0,18
ho	80	α	0,69358885	ρl	0,01413717
b	200	lu,riss	2367007,63	σp	0
hu	80	lu	8533333,33	k1	0,15
Au	16000	lo	8533333,33	k	2
fck	35			Vrd,c	10573,1071 overkant
Es	200000	<b>Fullt opprisset: S&gt;grense</b>			
Ecm	30000	Vo	60839		
As	942	Vu	0	<b>Kapasitet fra skjærbøyler</b>	
du	40			Asv	100,530965
γc	1	<b>Delvis opprisset: 0&lt;S&lt;grense</b>		Vsv	50265,4825
d	255	Vo	47627,819		
fyk	500	Vu	13211,181	<b>Tot. Kap</b>	
γs	1			VRd	60838,5896 N
do	40	<b>Urisset: S&lt;0</b>			60,8385896 kN
Aso	113,097336	Vo	30419,5		
No	0	Vu	30419,5	<b>Testkap.</b>	163,86 kN
ftd	3,2			VEd	81,93 kN



**Beam B**

Input		Output – dimensjonerende krefter		Output - kapasitet	
M	30000000	<b>Kontroll av risstilstand</b>		Asw	141,371669
V	80000	S	136363,6364	s	400
Fo	0	grense	47328,63826	cot $\theta$	2,5
Fu	0			Vrd,ct	94984,0904
N	0	<b>Tverrsnittsparmetre</b>		VRd,cf	60120
eo	0	$\eta$	6,666666667	VRd,c	155104,09
eu	0	$\rho$	0,134571429		
d'	220	$\eta\rho$	0,897142857	<b>Ved utsparingene</b>	
h	300	$\alpha$	0,715045414	CRd,c	0,18
ho	80	lu,riss	1669658,689	pl	0,01413717
b	200	lu	8533333,333	$\sigma_p$	0
hu	80	lo	8533333,333	k1	0,15
Au	16000			k	2
fck	35	<b>Fullt opprisset: S&gt;grense</b>		Vrd,c	10573,1071
Es	200000	Vo	80000	VRd,cf	16032
Ecm	30000	Vu	0	VRd,c	26605,1071
As	942				
du	35	<b>Delvis opprisset: 0&lt;S&lt;grense</b>		<b>Kapasitet fra skjærbøyler</b>	
$\gamma_c$	1	Vo	66908,47794	Asv	100,530965
d	260	Vu	13091,52206	Vsv	50265,4825
ftk,res2,5	1,67				
ftd,res2,5	1,67	<b>Urisset: S&lt;0</b>		<b>Total kap</b>	
fyk	500	Vo	40000	VRd	76870,5896 N
$\gamma_y$	1	Vu	40000		76,8705896 kN
do	40				
Aso	113,097336			<b>Testkap.</b>	242,22 kN
No	0				

*Beam C*

Input		Output – dim. krefter		Output - kapasitet	
M	15000000	<b>Kontroll av risstilstand</b>		CRd,c	0,18
V	40000	S	69767,4419	$\rho_l$	0,01231997
Fo	0	grense	47328,6383	$\sigma_p$	0
Fu	0			k1	0,15
N	0	<b>Tverrsnittparametre</b>		k	1,88561489
eo	0	$\eta$	6,66666667	Vrd,ct	60699,9395
eu	0	$\rho$	0,08975979	VRd,cf	60120
d'	215	$\eta\rho$	0,5983986	VRd,c	120819,939
h	300	$\alpha$	0,64854891		
ho	80	lu,riss	1413527,6	<b>Ved utsparingene</b>	
b	200	lu	8533333,33	CRd,c	0,18
hu	80	lo	8533333,33	$\rho_l$	0,01413717
Au	16000			$\sigma_p$	0
fck	35	<b>Fullt opprisset: S&gt;grense</b>		k1	0,15
Es	200000	Vo	40000	k	2
Ecm	30000	Vu	0	Vrd,ct	10573,1071
As	628,318531			Vrd,cf	16032
du	35	<b>Delvis opprisset: 0&lt;S&lt;grense</b>		VRd,c	26605,1071
$\gamma_c$	1	Vo	34315,6837		
d	255	Vu	5684,31632	Total kap	53210,2142 N
ftk,res2,5	1,67				
ftd,res2,5	1,67			<b>Testkap.</b>	199,5 kN
fyk	500	<b>Urisset: S&lt;0</b>			
do	40	Vo	20000		
Aso	113,097336	Vu	20000		
No	0				

*Reference beam*

Input		Output - kapasitet		
b	200	Momentkapasitet		
h	300	MRd,c	130130000	
fcd	35	z	247	
fyd	500	Mkap	77597338,5	>Mmax
d	260			
Mmax	37500000	Skjærstrekkkapasitet		
V	50000	CRd,c	0,18	
As	628,318531	k	1,87705802	
		$\rho_l$	0,01208305	
		VRd,c	61211,7884	Tot
		Tot. Kap.	122423,577	N
			122,423577	kN
		Testkap.	178,79	kN